Decentralized Robust Load-frequency Control Synthesis in Restructured Power Systems

規制緩和後の電力系統における分散型ロバスト負荷周波数制御の構成に関する研究

Hassan Bevrani

Department of Electrical Engineering
Graduate School of Engineering
Osaka University

2004

Ph.D. Dissertation

Decentralized Robust Load-frequency Control Synthesis in Restructured Power Systems

Hassan Bevrani

Department of Electrical Engineering
Graduate School of Engineering
Osaka University

2004

To Sabah, Bina and Zana

Preface

This dissertation is mainly focused on technical issues associated with load-frequency control (LFC) in restructured power systems. Operating the power system in a deregulated environment is more complex than in the past, due to the considerable degree of interconnection and the presence of technical constraints to be considered, together with the traditional requirements of system reliability. However, at present, the power system utilities participate in LFC task with simple, heuristically tuned controllers. In response to the new technical control demands, the main goal of this dissertation is to develop the robust decentralized LFC synthesis methodologies for multi-area power systems based on the fundamental LFC concepts and generalized well-tested traditional LFC scheme to meet the specified LFC objectives. The dissertation is organized as follows:

Chapter 1 gives a general introduction on load-frequency control problem and its conventional control scheme. The past achievements in the LFC literature are briefly reviewed, and the main objectives of the present dissertation are summarized.

Chapter 2 introduces modified models to adapt well-tested classical LFC scheme to the changing environment of power system operation under deregulation. The main advantage of the given strategies is the use of basic concepts in the traditional framework, and avoiding the use of impractical or untested LFC models. The introduced structures provide the base models for robust LFC synthesis in the subsequent chapters.

Chapter 3 presents two robust decentralized control design methodologies for LFC synthesis using structured singular value theory (μ). The first one describes a new systematic approach to design sequential decentralized load-frequency controllers in multi-area power systems. System uncertainties, practical constraint on control action, and desired performance are included in the synthesis procedure. The robust performance in terms of the structured singular value is used as a measure of control performance. The second control methodology addresses a control approach to the design of robust load frequency controller in a deregulated environment. In this approach, the power system is considered under the pluralistic-based LFC scheme, as a collection of separate control areas. Each control area can buy electric power from some generation companies to supply the area-load. Multi-area power system examples are presented, demonstrating the controllers' synthesis procedures and advantages of proposed strategies.

In Chapter 4, the decentralized LFC synthesis is formulated as an H_∞-based static output feedback (SOF) control problem, and is solved using an iterative linear matrix inequalities (ILMI)

algorithm to the design of robust PI controllers in multi-area power systems. Two multi-area power system examples using both traditional and bilateral based LFC schemes with a wide range of load changes are given to illustrate the proposed approach.

Chapter 5 is organized in two main sections. Firstly, the LFC problem is formulated as a multi-objective control problem and the mixed H_2/H_∞ control technique is used to synthesize the desired robust controllers for LFC system in a multi-area power system. In the second section, with regard to model uncertainties, the multi-objective LFC problem is reformulated via a mixed H_2/H_∞ control technique. Then, in order to design a robust PI controller, the control problem is reduced to a static output feedback control synthesis. Finally, the problem is easily solved using a developed ILMI algorithm. The proposed methods are applied to multi-area area power system examples under different LFC schemes. The results are compared with pure H_∞ control design.

Chapter 6 summarizes the research outcomes of this dissertation.

Hassan Bevrani
Osaka University, Osaka, Japan
July 2004

Contents

Acknowledgements

This research has been carried out during the author's tenure of Ph. D. degree (2002-2004) at the Department of Electrical Engineering, Graduate School of Engineering, Osaka University. During these years, many persons have helped me and it is my great pleasure to take this opportunity to express my gratitude to them all.

First of all, I would like to express my deepest gratitude and appreciation to Professor **Kiichiro Tsuji** for invaluable guidance, support, and encouragement throughout my study in the Department of Electrical Engineering, Osaka University.

I would like to thank my direct supervisor, Professor **Yasunori Mitani**, at the Department of Electrical Engineering, Kyushu Institute of Technology (at the first year of conducting this research, he was at the Department of Electrical Engineering, Osaka University) for allowing me the freedom to choose my research direction and for his careful advice throughout my doctoral studies. I am grateful for his friendship and guidance.

I extend my appreciation to Professor **Toshifumi Ise** in the Department of Electrical Engineering, Osaka University, for his careful review on my thesis and many useful comments and also for guidance and support me to do a marginal research on power electronic systems.

I present my sincere thanks to Professor **Takashi Sugino**, Professor **Toshimichi Ito**, Professor **Hiroaki Nishimura**, Professor **Takatomo Sasaki**, Professor **Masahiro Nakatsuka**, Professor **Sadatoshi Kumagai**, and Professor **Masayoshi Tonouchi** in the Department of Electrical Engineering, Osaka University, for serving as members of my dissertation committee.

I am also grateful for the helpful advice, encouragement, and continuous support of Assistant professor **Hideharu Sugihara**, Assistant professor **Osamu Saeki**, Dr. **Masayuki Watanabe** and Dr. **Komsan Hongesombut**.

I would like to thank Professor **Takashi Hiyama** from Department of Electrical and Computer Engineering, Kumamoto University, Professor **Masao Ikeda** from Department of Mechanical Engineering, Osaka University, Dr. **Goro Fujita** from Shibaura Institute of Technology, Dr. **Y. Y. Cao** from the University of Virginia, USA, Dr. **Dulpichet Rerkpreedapong** from Kasetsart university, Thailand, and Dr. **Vaibhav Donde** from the University of Illinois, USA, for their kind and constructive discussions.

I would like to express my sincere thanks to the Japan's government for granting me the Monbukagakusho scholarship in studying at Osaka University. I am grateful to the members of International Student Center (ISC) at Osaka University for providing a useful and enjoyable time during the Intensive Japanese Language Program (IJLP). My deep thanks go to Professor **Shinya Otani**, which his personal character with a great spirit is an example for the rest of my life.

I also thank to the members of Tsuji laboratory, Department of Electrical Engineering, Osaka University, for creating a friendship atmosphere, mutual understanding, and cooperation. A special thanks to Miss. **Akiko Iechika** the secretary of laboratory, and my colleagues especially **Tsuyoshi Ueno**, **Takuhei Hashiguchi**, **Kaewniyompanit Songpakit** and **Ken Furusawa** for their kind helps.

Thanks to our host family Dr. **Yoshino Matsunaga** and Dr. **Takaharu Matsunaga**, our family friends **Fusa Kasai** from TIFA, **Yoshimasa Yamashita** and **Makio Okamoto** for their kind attempts to make an enjoyable time for me and my family over the past two years. I feel happy that I have finished my postgraduate studies with big respect, and homage to Japan; people at the University and other places, for their great generosity and hospitality.

I would like to extend my deepest gratitude to my father, mother, brothers, sisters and their families for their deep understanding, encouragements, supports, and invaluable assistance. They have always supported me and never let me down. I also sincerely appreciate the teachers and professors of my previous study degrees.

Finally, my special thanks to my wife **Sabah** for her support and patience while we were away from our home land. Her generosity and understanding go beyond any achievement that I have been able to reach. My sons **Bina** and **Zana**, have helped me through the worst of times, and their beautiful smiles have made everything look interesting, successful, and fun.

Hassan Bevrani
Osaka University, Osaka, Japan
July 2004

Chapter 1

Introduction

In This chapter, a general introduction on load-frequency control (LFC) problem is given. The past achievements in the LFC literature are briefly reviewed, and finally, the main objectives of this dissertation are mentioned.

1.1 Load-frequency control (LFC)

1.1.1 Power system control

The objective of the control strategy in a power system is to generate and deliver power in an interconnected system as economically and reliably as possible while maintaining the frequency and voltage within permissible limits. The power system control has a hierarchical structure. The control system consists of a number of nested control loops that control different quantities in the system.

In general, the control loops on lower system levels, e.g. locally in a generator, are characterized by smaller time constants than the control loops active on a higher system level. For example, the automatic voltage regulator (AVR), which regulates the voltage of the generator terminals, responds typically in a time scale of a second or less. While, the secondary voltage control (SVC), which determines the reference values of the voltage controlling devices among which the generators, operates in a time scale of tens of seconds or minutes. That means these two control loops are virtually de-coupled.

As another example, we can consider AVR (which controls the reactive power and voltage magnitude) and LFC (which controls the real power and frequency) loops. The excitation system time constant is much smaller than the prime mover time constant and its transient decay much faster, which does not affect the LFC dynamic.

Thus, the cross-coupling between the LFC loop and the AVR loop is negligible. This is also generally true for the other control loops. As a result, a number of de-coupled control loops operating in power system in different time scales for protection, voltage control, turbine control, tie-line power and frequency control. Although the overall control system is complex, in most cases it is possible to study the different control loops individually due to the de-coupling. Depending on the loop nature, the required model, important variables, uncertainties, objectives, and possibly control strategy will be different.

A schematic diagram showing the current different time scales of the power system controllers and devices is shown in Fig. 1.1. The protection devices are in the first level. To protect the systems and other important devices they must as fast as possible. The second level is mainly related to power system stabilizers (PSS) and reactive power controllers such as AVRs, flexible ac transmission systems (FACTS), energy storages, and HVdc systems. At the highest level, the tie-line power and frequency controllers are in place.

1.1.2 LFC problem

The LFC problem in power systems has a long history. In a power system, LFC as an ancillary service acquires an important and fundamental role to maintain the electrical system reliability at an adequate level. It has gained the importance with the change of power system structure and the growth of size and complexity of interconnected systems. The well-known conventional LFC structure for a given control area (i) in a multi area power system (includes N area) is shown in Fig. 1.2, where,

Δf_i : frequency deviation,

ΔP_{gi} : governor valve position,

ΔP_{ci} : governor load setpoint,

ΔP_{ti} : turbine power,

ΔP_{di} : local load disturbance,

ΔP_{tie-i} : net tie-line power flow,

M_i : equivalent inertia constant,

D_i : equivalent damping coefficient,

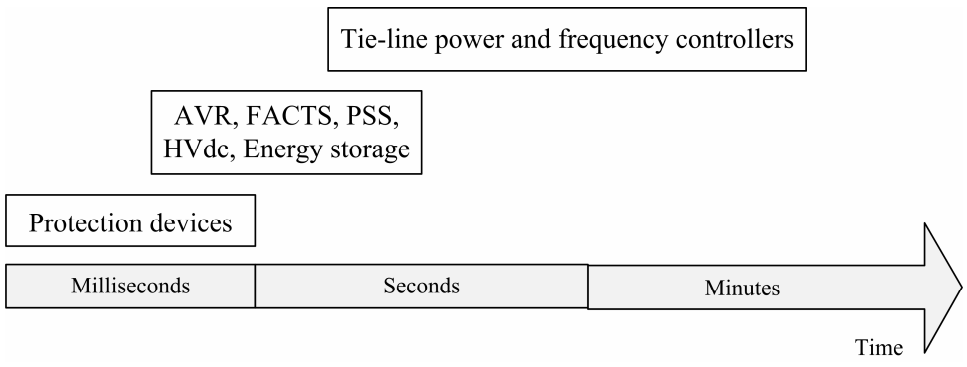

Figure 1.1: Schematic diagram of different time scales of power system controls

T_{gi} : governor time constant,

T_{ti} : turbine time constant,

T_{ij} : tie-line synchronizing coefficient between area *i* & *j*,

B_i : frequency bias,

R_i : drooping characteristic,

ACE_i : area control error (ACE).

The LFC model given in Fig. 1.2 uses three simple (first order) transfer functions for modeling the turbine, generator and power system (load and rotating mass). The effects of local load changes and interface with other areas are properly considered as two input signals. Each control area monitors its own tie-line power flow and frequency at the area control center. The area control error (ACE) which is a linear combination of tie-line and frequency errors is computed and allocated to the controller $K(s)$. Finally, the resulted control action signal or a percentage of it is applied to the turbine-governor unit. The operation objectives of the LFC are summarized to maintain system frequency close to nominal value, to control the tie-line interchange schedules, and to divide the load between generator units.

The LFC mechanism is well discussed in [1, 2]. Commonly, a simple integral or proportional-integral control law is used as controller $K(s)$ to perform LFC task. A multi-area power system is comprised of areas that are interconnected by high-voltage transmission lines or tie-lines. The trend of frequency measured in each control area is an indicator of the trend of mismatch power in the interconnection and not in the control area alone [3]. Therefore, following a load disturbance within a control area or an occurred mismatch power on tie-lines, the frequency of that control area experiences a transient change. The feedback mechanism comes into play and generates the appropriate signal to the turbine for tracking the load variation and compensate the mismatch power.

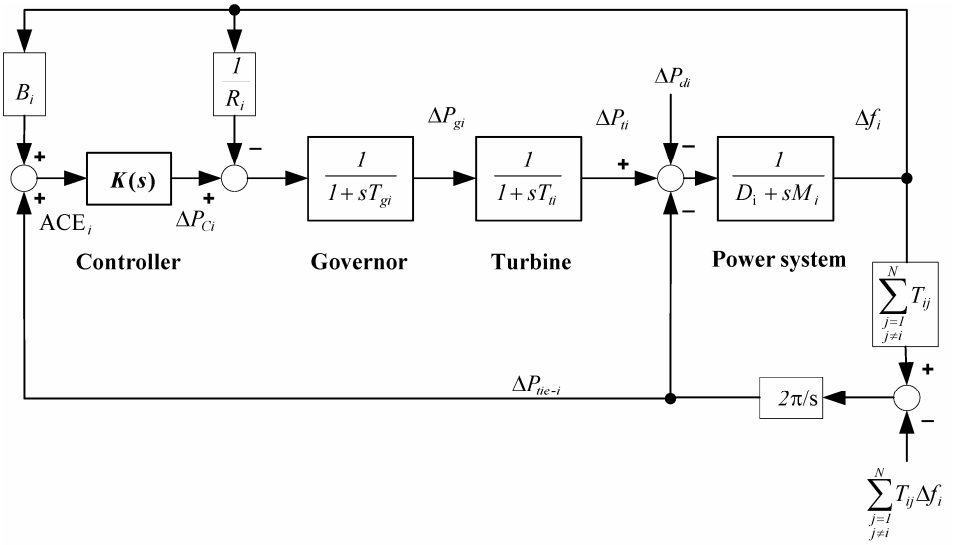

Figure 1.2: A control area equipped with LFC

Depending on the type of generating units, and constraints on their range and rate of response to the LFC signals, the actual response time (for example for a steam unit) takes a few to several tens of seconds [3]. In LFC practice, rapidly varying components of system signals are almost unobservable due to filters involved in the process. That is why further reduction in the response time of LFC is neither possible nor desired. Practically, the design and performance of an LFC system highly dependent on how generation units respond to control signal. Such control strategies are useful as they are able to maintain a sufficient level of reserved control range and a sufficient level of control rate.

In light of this fact, although the present dissertation uses some academic examples (and data) in which the assumed parameters (and in result, dynamics of the simplified models) are not completely matched to real ones, and gives the impression that the output of the models can be changed quickly, however the proposed control strategies are flexible enough to set a desired level of performance to cover the practical constraint on the control action signals.

Since the 1970s, the described LFC scheme in Fig. 1.2 is widely used by researchers for the LFC analysis and synthesis. The far reaching deregulation of the power system industry and concomitant new concepts of operation requires an evaluation and re-examination of this scheme, which is already designed to operate with large and central generating facilities to find ways to maintain, and possibly improve, their efficiency and reliability.

1.2 A brief survey on the LFC literature

The LFC scheme shown in Fig. 1.2 has evolved over the past few decades and is in use on interconnected power systems. There has been continuing interest in designing LFC with better performance to maintain the frequency and keep tie-line power flows within prespecified values using various control methodologies. The literature on LFC is voluminous. Following, a brief survey on some reported works is referred.

Since the publication of Fosha and Elgerd's paper [2], extensive research has been done on the application of modern control theory to the LFC design. References [4-24] have suggested several LFC synthesis approaches using optimal and adaptive control techniques. The efforts were usually directed towards the application of suitable linear state feedback controllers to the LFC problem. They have mainly optimized a constructed cost function to meet the LFC objectives by well-known optimization techniques or self-tuning algorithms. Several authors [5, 10, 11, 20] applied the concept of variable-structure systems to the LFC design. The discrete-type frequency regulator is also reported in some papers [7, 9, 21].

Since an important issue in the LFC design is robustness, the application of robust control theory to the LFC problem in multi-area power systems has been extensively studied during the last two decades [25-39]. The main goals have been determined as holding the robust stability, and robust performance against the system uncertainties and disturbances for a reasonable range of operating conditions. For this purpose, various robust control techniques such as H_∞ [31, 36], Linear matrix inequalities (LMI) and Riccati-equation approaches [26, 37], Kharitonov's theorem [28], Structured singular value (μ) theory [27, 38], Quantitative feedback theory [30], Lyapunove stability theory [32, 33], Pole placement technique [35], and Q-parameterization [39] have been used.

In the light of advances of intelligent control techniques during the last two decades, various intelligent-based control methodologies have been proposed to solve the LFC problem [40-53]. Artificial neural networks have been applied to the LFC problem [40, 45, 50]. The application of fuzzy logic and genetic algorithm has been reported for the same problem [42, 43, 46-48, 52, 53]. The application of fuzzy logic is mainly reported based on fuzzy scheduling of PI-based load-frequency controller parameters. A combination of the intelligent methods has also been applied to the LFC problem [41, 44, 51].

Several reports have addressed the application of special devices such as Battery energy storage, Photovoltaic power generation, Superconductivity magnetic energy storage (SMES), Solid-state phase shifter, and Capacitive energy to improve the performance of LFC system [54-60]. Furthermore, with regards to LFC analysis, modeling and modification, special applications, constraints formulation, frequency bias estimation, model identification, and performance standards, numerous reports have been published [61-77].

The above mentioned works have been done for the power systems under vertically integrated organization. Vertically integrated utilities participate in LFC with simple, classically tuned controllers. In a deregulated environment which includes separate generation, distribution, and transmission companies, generation companies may or may not participate in LFC problem. Technically, this problem will be more important as independent power producers (IPPs) penetrate the electric power markets. Therefore, the control strategies for new structure with a few number of LFC participators may not be as straight as those for vertically integrated utility structure, and, in a control area including numerous distributed generators with an open access policy and a few LFC participators, the need arises for novel control strategies based on modified dynamical models to maintain the reliability and eliminate the frequency error. Under new organization, several notable scenarios have been proposed on LFC modeling, control, and structure description [78-92].

There are various schemes and organizations for the provision of ancillary services in countries with a restructured electric industry. The type of LFC scheme in a restructured power system is differentiated by how free the market is, who controls generator units, and who has the obligation to execute LFC [78]. Several modeling and control strategies have reported to adapt well-tested classical LFC schemes to the changing environment of power system operation under deregulation [79, 80, 83, 86, 88, 89]. References [83], [84], and [89] have proposed μ and flexible neural network based load frequency controllers for a simple area with two generation companies. The effects of deregulation of the power industry on LFC and several general LFC scenarios for power system after deregulation have been addressed in [78, 81, 82, 87, 90-92].

1.3 Objectives of the present dissertation

The electric power industry is in transition from large, vertically integrated utilities providing power at regulated rates to an industry that will incorporate competitive companies selling unbundled power at lower rates. Currently, in many countries, electric systems are restructured; new market concepts were adopted to achieve the goal of better efficiency. Operating the power system in a new environment will certainly be more complex than in the past, due to the considerable degree of interconnection, and to the presence of technical constraints to be considered together with the traditional requirements of system reliability.

It is known that market power exercise affects market dynamics. In addition to various market policies, numerous generator units in distribution areas and a growing number of independent players are likely to impact on the operation and control of the power system (which is already designed to operate with large, central generating facilities). In response to the new challenges, novel modeling and control approaches are required to get a new trade off between efficiency and robustness.

At present, the power system utilities participate in LFC task with simple, heuristically tuned controllers. In response to the new technical control demands for large scale power systems in a restructured environment, the main goal of the present dissertation is to develop new LFC synthesis methodologies for multi-area power systems based on fundamental LFC concepts and generalized well-tested traditional LFC scheme, to meet all or a combination of following specifications:

- *Robustness*: Guarantee robust stability and robust performance for a wide range of operating conditions. For this purpose, robust control techniques are to be used in synthesis and analysis procedures.

- *Decentralized property*: Because of practical advantages, decentralized control design is the most common design procedure in real-world applications, while centralized design is difficult numerically/practically for large scale power system. In addition, the possibility of sequential decentralized LFC design is to be studied.

- *Simplicity of structure*: To meet the practical advantages, the robust decentralized LFC design problem is to be reduced to a synthesis of low-order or proportional-integral (PI) control problem, which is usually used in a real-world power systems.

- *Formulation of uncertainties, constraints, and contracts information*: The LFC synthesis procedure must be flexible enough to include generation rate constraints and uncertainties in power system models. The proposed approaches advocate the use of the physical understanding of the system for robust controller synthesis. Furthermore, the coupling between LFC dynamics and contract transactions is studied in order to get suitable alternatives for the future realization of decentralized LFC systems.

- *Cover all the specified LFC objectives*: The LFC objectives, i.e., frequency regulation and tracking the load changes, maintaining the tie-line power interchanges to specified values in the presence of generation constraints and model uncertainties, identify the LFC synthesis as a multi-objective control problem. Therefore, the LFC design is to be considered as a decentralized robust multi-objective control problem.

1.4 References

[1] O. I. Elgerd, C. Fosha, "Optimum megawatt-frequency control of multiarea electric energy systems," *IEEE Trans. Power Apparatus & Systems*, vol. PAS-89, no. 4, pp. 556-563, 1970.

[2] C. Fosha, O. I. Elgerd, "The megawatt-frequency control problem: a new approach via optimal control," *IEEE Trans. Power Apparatus & Systems*, vol. PAS-89, no. 4, pp. 563-577, 1970.

[3] N. Jaleeli, D. N. Ewart, L. H. Fink, "Understanding automatic generation control," *IEEE Trans. Power System*, vol. 7, no. 3, pp. 1106-1112, 1992.

[4] M. S. Calovic, "Linear regulator design for a load and frequency control," *IEEE Trans. Power Appar. Systems*, vol. 91, pp. 2271-2285, 1972.

[5] N. N. Bengiamin, W. C. Chan, "Variable stucture control of electric power generation," *IEEE Trans. Power Appar. Systems*, vol. 101, pp. 376-380, 1982.

[6] T. Hiyama, "Design of decentralised load-frequency regulators for interconnected power systems," *IEE Proc., Pt. C*, vol. 129, no. 1, pp. 17-23, 1982.

[7] T. Hiyama, "Optimisation of discrete-type load-frequency regulators considering generation-rate constraints," *IEE Proc., Pt. C*, vol. 129, no. 6, pp. 285-289, 1982.

[8] V. R. Moorthi, P. P. Aggarwal, "Suboptimal and near optimal control of a load-frequency control system," *IEE Proc., Pt. C*, vol. 129, no. 6, pp. 1635-1660, 1982.

[9] J. Kanniah, S. C. Tripathy, O. P. Malik, G. S. Hope, "Microprocessor-based adaptive load-frequency control," *IEE Proc. Gener. Transm. Distrib.*, vol. 131, no. 4, pp. 121-128, 1984.

[10] A. Y. Sivaramakrishnan, M. V. Hartiharan, M. C. Srisailam, "Design of variable structure load frequency controller using pole assignment technique," *Int. J. Control*, vol. 40, pp. 487-498, 1984.

[11] Y. Y. Hsu, W. C. Chan, "Optimal variable structure control of interconnected hydrothermal power systems," *Int. J. Electrical Power and Energy Systems*, vol. 6, pp. 221-229, 1984.

[12] M. A. Sheirah, M. M. A-el-Fattah, "Improved load-frequency self-tuning regulator," *Int. J. Control*, vol. 39, pp. 143-158, 1984.

[13] I. Vajk, M. Vajta, L. Keviczky, R. Haber, J. Hetthessy, K. Kovacs, "Adaptive load frequency control of the Hungarian power system," *Automatica*, vol. 21, pp. 129-137,1985.

[14] A. Feliachi, "Optimal decentralized load frequency control," *IEEE Trans. Power Systems*, vol. PWRS-2, no. 2, pp. 379-384, 1987.

[15] Y. M. Park, K. L. Lee, "Optimal decentralized load frequency control," *Int. J. Electrical Power and Energy Systems*, vol. 27, pp. 279-288, 1987.

[16] O. P. Malik, A. Kumar, G. S. Hope, "A load frequency control algorithm based on a generalized approach," *IEEE Trans. Power Systems*, vol. 3, no. 2, pp. 375-382, 1988.

[17] C. T. Pan, C. M. Liaw, "An adaptive controller for power system load frequency control," *IEEE Trans. Power Systems*, vol. PWRS-4, pp. 122-128, 1989.

[18] M. Aldeen, J. F. Marsh, “Decentralised proportional-plus-integral design method for interconnected power systems,” *IEE Proc., Pt. C*, vol. 138, no.4, pp. 285-289, 1991.

[19] C. M. Liaw, K. H. Chao, “On the design of an optimal automatic generation controller for interconnected power systems,” *Int. J. Control*, vol. 58, pp. 113-127, 1993.

[20] A. Z. Al-Hamouz, Y. L. Al-Magid, “Variable structure load frequency controllers for multiarea power systems,” *Electrical Power and Energy Systems*, vol. 15, pp. 293-300, 1993.

[21] A. Rubaai, V. Udo, “Self-tuning load frequency control: Multilevel adaptive approach,” *IEE Proc. Gener. Transm. Distrib.*, vol. 141, no. 4, pp. 285-290, 1994.

[22] C. M. Liaw, “Design of reduced-order adaptive load-frequency controller for an interconnected hydrothermal power system,” *Int. J. Control*, vol. 60, pp. 1051-1068, 1994.

[23] G. Ray, N. Yadaiah, G. D. Prasad, “Design of load frequency regulator based on the Schur approach,” *Electric Power Systems Research*, vol. 36, pp. 145-149, 1996.

[24] M. H. Kazemi, M. Karrari, M. B. Menhaj, “Decentralized robust adaptive-output feedback controller for power system load frequency control,” *Electrical Engineering*, no. 84, pp. 75-83, 2002.

[25] Y. Wang, R. Zhou, C. wen, “Robust load-frequency controller design for power systems,” *IEE Proc., Pt. C*, vol. 140, no. 1, pp. 11-16, 1993.

[26] K. Y. Lim, Y. Wang, R. Zhou, “Robust decentralized load-frequency control of multi-area power systems,” *IEE Proc. Gener. Transm. Distrib.*, vol. 143, no. 5, pp. 377-386, 1996.

[27] T. C. Yang, H. Cimen, Q. M. ZHU, “Decentralised load frequency controller design based on structured singular values,” *IEE Proc. Gener. Transm. Distrib.*, vol. 145, no. 1, pp. 7-14, 1998.

[28] H. Bevrani, “Application of Kharitonov's theorem and its results in load-frequency control design,” *J. Electr. Sci. Technol.-BARGH* (in Persian), no. 24, pp. 82-95, 1998.

[29] K. Y. Lim, Y. Wang, G. Guo, R. Zhou, “A new decentralized robust controller design for multi-area load-frequency control via complete state feedback,” *Optimal Control Appl. & Methods*, vol. 19, pp. 345-361, 1998.

[30] A. M. Stankovic, G. Tadmor. T. A. Sakharuk, “On robust control analysis and design for load frequency regulation,” *IEEE Trans. Power Systems*, vol. 13, no. 2, pp. 449-455, 1998.

[31] H. Bevrani, “Tracking in dispatching centers using robust controller,” *Technical Journal of Electric Power Industry San'at-e-Barg*, (in Persian), no. 26, pp. 36-39, July 1998.

[32] G. Ray, A. N. Prasad, T. K. Bhattacharyya, “Design of decentralized robust load-frequency controller based on SVD method,” *Computers and Electrical Engineering*, vol. 25, pp. 477-492, 1999.

[33] G. Ray, A. N. Prasad, G. D. Prasad, “A new approach to the design of robust load-frequency controller for large scale power systems,” *Electric Power Systems Research*, vol. 51, pp. 13-22, 1999.

[34] J. Liu, M. S. Fadali, R. Zhou, “Performance constrained stabilization of uncertain systems: application to load-frequency control,” *Computers and Electrical Engineering*, vol. 25, pp. 135-152, 1999.

[35] M. Azzam, “Robust automatic generation control,” *Energy Conversion & Management*, vol. 40, pp. 1413-1421, 1999.

[36] T. Ishi, G. Shirai, G. Fujita, "Decentralized load frequency based on H_∞ control," *Electrical Engineering in Japan*, vol. 136, no. 3, pp. 28-38, 2001.

[37] D. Rerkpreedapong, A. Hasanovic, A. Feliachi, "Robust load frequency control using genetic algorithms and linear matrix inequalities," *IEEE Trans. Power Systems*, vol. 18, no. 2, pp. 855-861, 2003.

[38] T. C. Yang, Z. T. Ding, H. Yu, "Decentralised power system load frequency control beyond the limit of diagonal dominance," *Electrical power and Energy systems*, vol. 24, pp. 173-184, 2002.

[39] M. Azzam, Y. S. Mohamed, "Robust controller design for automatic generation control based on Q-parameterization," *Energy Conversion & Management*, vol. 43, pp. 1663-1673, 2002.

[40] F. Beaufays, Y. Abdel-Magid, B. Widrow, "Application of neural networks to load-frequency control in power systems," *Neural Networks*, vol. 7, no. 1, pp. 183-194, 1994.

[41] M. Djukanovic, M. Novicevic, D. J. Sobajic, Y. P. Pao, "Conceptual development of optimal load frequency control using artificial neural networks and fuzzy set theory," *Int. J. of Engineering Intelligent Systems for Electrical Engineering & Communication*, vol. 3, no. 2, pp. 95-108, 1995.

[42] C. S. Chang, W. Fu, "Area load frequency control using fuzzy gain scheduling of PI controllers," *Electric Power Systems Research*, vol. 42, pp. 145-152, 1997.

[43] G. A. Chown, R. C. Hartman, "Design and experience with a fuzzy logic controller for automatic generation control (AGC)," *IEEE Trans. Power Systems*, vol. 13, no. 3, pp. 965-970, 1998.

[44] C. S. Chang, W. Fu, F. Wen, "Load frequency controller using genetic algorithm based fuzzy gain scheduling of PI controller," *Electric Machines and Power Systems*, vol. 26, pp. 39-52, 1998.

[45] D. K. Chaturvedi, P. S. Satsangi, P. K. Kalra, "Load frequency control: a generalised neural network approach," *Electrical power and Energy systems*, vol. 21, pp. 405-415, 1999.

[46] J. Talaq, F. Al-Basri, "Adaptive fuzzy gain scheduling for load frequency control," *IEEE Trans. Power Systems*, vol. 14, no. 1, pp. 145-150, 1999.

[47] Z. M. Al-Hamouz, H. N. Al-Duwaish, "A new load frequency variable structure controller using genetic algorithm," *Electric Power Systems Research*, vol. 55, pp. 1-6, 2000.

[48] A. Demirorem, S. Kent, T. Gunel, "A genetic approach to the optimization of automatic generation control parameters for power systems," *European Trans. Electrical Power*, vol. 12, no. 4, pp. 275-281, 2002.

[49] T. P. I. Ahmed, P. S. N. Rao, P. S. Sastry, "A reinforcement learning approach to automatic generation control," *Electric Power Systems Research*, vol. 63, pp. 9-26, 2002.

[50] H. L. Zeynelgil, A. Demirorem, N. S. Sengor, "Load frequency control for power system with reheat steam turbine and governor deadband non-linearity by using neural network controller," *European Trans. Electrical Power*, vol. 12, no. 3, pp. 179-184, 2002.

[51] Y. L. Karnavas, D. P. Papadopoulos, "AGC for autonomous power system using combined intelligent techniques," *Electric Power Systems Research*, vol. 62, pp. 225-239, 2002.

[52] M. K. El-Sherbiny, G. El-Saady, A. M. Yousef, "Efficient fuzzy logic load-frequency controller," *Energy Conversion & Management*, vol. 43, pp. 1853-1863, 2002.

[53] E. Yesil, M. Guzelkaya, I. Eksin, “Self tuning fuzzy PID type load frequency controller,” *Energy Conversion & Management*, vol. 45, pp. 377-390, 2004.

[54] S. C. Tripathy, “Improved load-frequency control with capacitive energy storage,” *Energy Conversion & Management*, vol. 38, no. 6, pp. 551-562, 1997.

[55] H. Asano, K. Yajima, Y. Kaya, “Influence of photovoltaic power generation on required capacity for load frequency control,” *IEEE Trans. Energy Conversion*, vol. 11, no. 1, pp. 188-193, 1996.

[56] I. Ngamroo, Y. Mitani, K. Tsuji, “Application of SMES coordinated with solid-state phase shifter to load frequency control,” *IEEE Trans. Applied Superconductivity*, vol. 9, no. 2, 1999.

[57] S. K. Aditya, D. Das, “Battery energy storage for load frequency control of an interconnected power system,” *Electric Power Systems Research*, vol. 58, pp. 179-185, 2001.

[58] A. Demiroren, “Application of a self-tuning to automatic generation control in power system including SMES units,” *ETEP*, vol. 12, no. 2, pp. 101-109, 2002.

[59] A. Demiroren, E. Yesil, “Automatic generation control with fuzzy logic controllers in the power system including SMES units,” Electrical Power & Energy Systems, vol. 26, pp. 291-305, 2004.

[60] T. Sasaki, T. Kadoya, K. Enomoto, “Study on load frequency control using redox flow batteries,” *IEEE Trans. Power Systems*, vol. 19, no. 1, pp. 660-667, 2004.

[61] L. D. Douglas, T. A. Green, R. A. Kramer, “New approach to the AGC non-conforming load program,” *IEEE Trans. Power Systems*, vol. 9, no. 2, pp. 619-628, 1994.

[62] R. K. Green, “Transformed automatic generation control,” *IEEE Trans. Power Systems*, vol. 11, no. 4, pp. 1799-1804, 1996.

[63] R. P. Schulte, “An automatic generation control modification for present demands on interconnected power systems,” *IEEE Trans. Power Systems*, vol. 11, no. 3, pp. 1286-1294, 1996.

[64] J. Z. Zhu, C. S. Chang, G. Y. Xu, “A new model and algorithm of secure and economic automatic generation control,” *Electric Power Systems Research*, vol. 45, pp. 119-127, 1998.

[65] N. Jaleeli, L. S. Vanslyck, “NERC’s new control performance standards,” *IEEE Trans. Power Systems*, vol. 14, no. 3, pp. 1092-1099, 1999.

[66] M. Yao, R. R. Shoults, R. Kelm, “AGC logic based on NERC’s new control performance standard and disturbance control standard,” *IEEE Trans. Power Systems*, vol. 15, no. 2, pp. 852-857, 2000.

[67] Y. Hain, R. Kulessky, G. Nudelman, “Identification-based power unit model for load-frequency control purposes,” *IEEE Trans. Power Systems*, vol. 15, no. 4, pp. 1313-1321, 2000.

[68] N. Maruejouls, T. Margotin, M. Trotignon, P. L. Dupuis, J. M. Tesseron, “Measurement of the load frequency control system service: comparison between American and European indicators,” *IEEE Trans. Power Systems*, vol. 15, no. 4, pp. 1382-1387, 2000.

[69] D. J. Trudnowski, W. L. McReynolds, J. M. Johnson, “Real-time very short-term load prediction for power system automatic generation control,” *IEEE Trans. Control Systems Technology*, vol. 9, no. 2, pp. 254-260, 2001.

[70] G. Gross, J. W. Lee, "Analysis of load frequency control performance assessment criteria," *IEEE Trans. Power Systems*, vol. 16, no. 3, pp. 520-532, 2001.

[71] N. Hoonchareon, C. M. Ong, R. A. Kramer, "Implementation of an ACE_1 decomposition method," *IEEE Trans. Power Systems*, vol. 17, no. 3, pp. 757-761, 2002.

[72] N. Hoonchareon, C. M. Ong, R. A. Kramer, "Feasibility of decomposing ACE_1 to identify the impact of selected loads on CPS1 and CPS2," *IEEE Trans. Power Systems*, vol. 17, no. 3, pp. 752-756, 2002.

[73] Y. H. Moon, H. S. Ryu, J. G. Lee, K. B. Song, M. C. Shin, "Extended integral control for load frequency control with the consideration of generation-rate constraints," Electrical Power & Energy Systems, vol. 24, pp. 263-269, 2002.

[74] J. L. R. Amenedo, S. Arnalte, J. C. Burgos, "Automatic generation control of a wind farm with variable speed wind turbines," *IEEE Trans. Energy Conversion*, vol. 17, no. 2, pp. 279-284, 2002.

[75] L. R. C. Chien, C. M. Ong, R. A. Kramer, "Field tests and refinements of an ACE model," *IEEE Trans. Power Systems*, vol. 18, no. 2, pp. 898-903, 2003.

[76] L. R. C. Chien, N. Hoonchareon, C. M. Ong, R. A. Kramer, "Estimation of β for adaptive frequency bias setting in load frequency control," *IEEE Trans. Power Systems*, vol. 18, no. 2, pp. 904-911, 2003.

[77] B. Stojkovic, "An original approach for load-frequency control-the winning solution in the second UCTE synchronous zone," *Electric Power Systems Research*, vol. 69, pp. 59-68, 2004.

[78] R. D. Chritie, A. Bose, "Load frequency control issues in power system operation after deregulation," *IEEE Trans. Power Systems*, vol. 11, no. 3, pp. 1191-1200, 1996.

[79] J. Kumar, NG. K. Hoe and G. B. Sheble, "AGC simulator for price-based operation, Part I: A model," *IEEE Trans. Power Systems*, vol. 2, no. 12, pp. 527-532, 1997.

[80] J. Kumar, NG. K. Hoe and G. B. Sheble, "AGC simulator for price-based operation, Part II: case study results," *IEEE Trans. Power Systems*, vol. 2, no. 12, pp. 533-538, 1997.

[81] B. H. Bakken, O. S. Grande, "Automatic generation control in a deregulated power system," *IEEE Trans. Power Systems*, vol. 13, no. 4, pp. 1401-1406, 1998.

[82] A. P. S. Meliopoulos, G. J. Cokkinides, A. G. Bakirtzis, "Load-frequency control service in a deregulated environment," Decision Support Systems, vol. 24, pp. 243-250, 1999.

[83] H. Bevrani, "Reduced μ-based load frequency controller in a deregulated power system environment," in *Proc. of 14th Int. Power System Conf.*, Iran, 1999.

[84] H. Bevrani, "Robust load frequency controller in a deregulated environment: A μ-synthesis approach," in *Proc. of IEEE Int. Conf. on Control applications*, pp. 616-621, 1999.

[85] H. Bevrani, M. Teshnehlab and H. Bevrani, "Load frequency controller design in a deregulated environment using flexible neural networks," in *Proc. of 15th Int. Power System Conf.*, pp. 1-6, Iran, 2000.

[86] V. Donde, M. A. Pai and I. A. Hiskens, "Simulation and optimization in a AGC system after deregulation," *IEEE Trans. Power Systems*, vol. 16, no. 3, pp. 481-489, 2001.

[87] J. M. Arroyo, A. J. Conejo, "Optimal response of a power generator to energy, AGC, and reserve pool-based markets," *IEEE Trans. Power Systems*, vol. 17, no. 2, pp. 404-410, 2002.

[88] B. Delfino, F. Fornari and S. Massucco, “Load-frequency control and inadvertent interchange evaluation in restructured power systems,” *IEE proc.-Gener. Transm. Distrib.*, vol.149, no.5, pp. 607-614, 2002.

[89] H. Bevrani, “A novel approach for power system load frequency controller design,” in *Proc. of IEEE Power Engineering Society Transmission and Distribution Conf.*, vol. 1, pp. 184-189, Yokohama, Japan, 2002.

[90] H. Bevrani, A. Rezazadeh and M. Teshnehlab, “Comparison of existing LFC approaches in a deregulated environment,” in *Proc. of 5th IEE Int. Conf. On Power System Management and Control*, pp. 238-243, London, UK, 2002.

[91] F. Liu, Y. H. Song, J. Ma, S. Mei, Q. Lu, “Optimal load-frequency control in restructured power systems,” *IEE Proc. Gener. Transm. Distrib.*, vol. 150, no. 1, pp. 377-386, 2003.

[92] S. Bhowmik, K. Tomsovic, A. Bose, “Communication models for third party load frequency control,” *IEEE Trans. Power Systems*, vol. 19, no. 1, pp. 543-548, 2004.

Chapter 2

LFC structure in a new environment

In a vertically integrated power system, it is assumed that each bulk generator unit is equipped with secondary control and frequency regulation requirements, but in an open energy market, generation companies (Gencos) may or may not participate in the LFC task. On the other hand, a distribution company (Disco) may contract individually with Gencos or independent power producers (IPPs) for power in different areas. Therefore, in a control area, including numerous distributed generators with an open access policy and a few LFC participators, the need arises for novel modeling strategies for LFC synthesis and analysis.

This chapter introduces modified models to adapt the well-tested classical LFC scheme to the changing environment of power system operation under deregulation. The main advantage of these strategies is the use of basic concepts in the traditional framework and avoiding the use of impractical or untested LFC models. The mentioned structures provide the base models for robust LFC synthesis in the subsequent chapters.

2.1 Traditional-based LFC model

Although a linearized model is usually used for LFC synthesis and analysis, power systems have a highly nonlinear and time-varying nature. A large scale power system consists of a number of interconnected control areas. Fig. 2.1 shows the block diagram of control area-*i* with *n* Gencos, in an *N*-control area power system. As usual in LFC literature, three first order transfer functions are used to model generator, turbine, and power system (rotating mass and load) units. The traditional LFC structure is discussed in [1] and [2].

In Fig. 2.1, the practical constraints on generation rate and the impacts of areas interface have been properly considered. w_{1i} and w_{2i} show local load disturbance and area interface, respectively. The other parameters are:

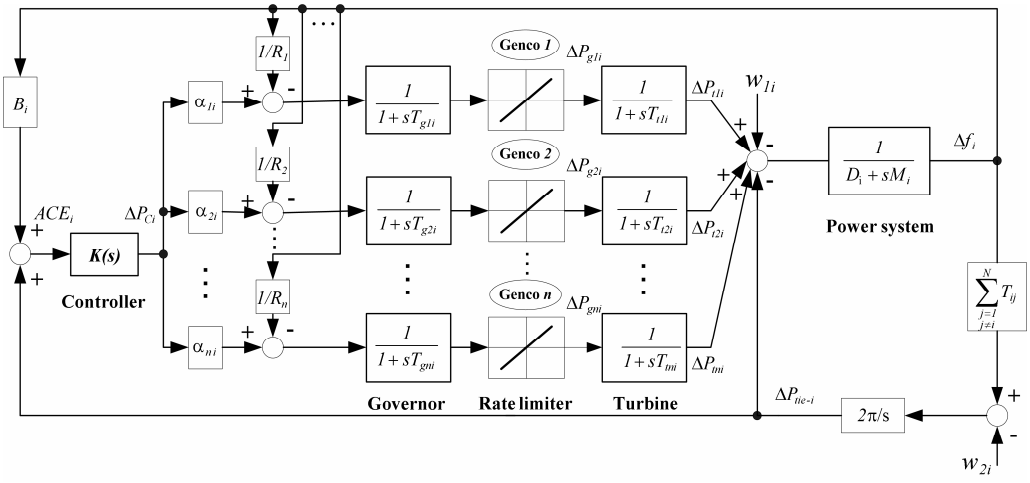

Figure 2.1: Traditional-based LFC model for a general control area

Δf_i : frequency deviation,

ΔP_{gi} : governor valve position,

ΔP_{ci} : governor load setpoint,

ΔP_{ti} : turbine power,

ΔP_{tie-i} : net tie-line power flow,

M_i : equivalent inertia constant,

D_i : equivalent damping coefficient,

T_{gi} : governor time constant,

T_{ti} : turbine time constant,

T_{ij} : tie-line synchronizing coefficient between area *i* & *j*,

B_i : frequency bias,

R_k : drooping characteristic,

ACE_i : area control error (ACE),

α_{ki} : ACE participation factors.

Following a load disturbance within the control area, the frequency of the area experiences a transient change and the feedback mechanism comes into play and generates the appropriate rise/lower signal to the participating Gencos according to their participation factors (α_{ki}) to make generation follow the load. In the steady state, the generation is matched with the load, driving the tie-line power and frequency deviations to zero. As there are many Gencos in each area, the control signal has to be distributed among them in proportion to their participation in the LFC. Hence, the ACE participation factor shows the sharing rate of each participant Genco unit in the LFC task.

$$\sum_{k=1}^{n} \alpha_{ki} = 1 \quad ; \quad 0 \le \alpha_{ki} \le 1 \tag{2.1}$$

The balance between connected control areas is achieved by detecting the frequency and tie line power deviations to generate the ACE signal, which is in turn utilized in the control strategy as shown in Fig. 2.1. The ACE for each control area can be expressed as a linear combination of tie-line power change and frequency deviation.

$$ACE_i = B_i \Delta f_i + \Delta P_{tie\text{-}i} \tag{2.2}$$

It can be shown that considering w_{1i} and w_{2i} as two input disturbance channels is useful to the design of decentralized LFC [3-4]. These signals can be defined as follows:

$$w_{1i} = \Delta P_{di} \quad , \quad w_{2i} = \sum_{\substack{j=1 \\ j \neq i}}^{N} T_{ij} \Delta f_j \tag{2.3}$$

where ΔP_{di} is area load disturbance. According to Fig. 2.1, in each control area the ACE performs the input signal of controller. Therefore, we have the following control input for the LFC system,

$$u_i = \Delta Pci = f(ACE_i) \tag{2.4}$$

where $f(\cdot)$ is a function which identifies the structure of controller. The state-space model for control area *i* is given in (2.5).

$$\begin{aligned} \dot{x}_i &= A_i x_i + B_{l_i} w_i + B_{2i} u_i \\ y_i &= C_{yi} x_i \end{aligned} \tag{2.5}$$

where

$$x_i^T = \begin{bmatrix} \Delta f_i & \Delta P_{tie-i} & x_{ti} & x_{gi} \end{bmatrix}$$

$$x_{ti} = \begin{bmatrix} \Delta P_{t1i} & \Delta P_{t2i} & \cdots & \Delta P_{tni} \end{bmatrix}, \quad x_{gi} = \begin{bmatrix} \Delta P_{g1i} & \Delta P_{g2i} & \cdots & \Delta P_{gni} \end{bmatrix}$$

$$u_i = \Delta P_{\mathrm{Ci}}, \quad y_i = \beta_i \Delta f_i + \Delta P_{tie\text{-}i}, \quad w_i^{\mathrm{T}} = \begin{bmatrix} w_{1i} & w_{2i} \end{bmatrix}$$

and,

$$A_i = \begin{bmatrix} A_{i11} & A_{i12} & A_{i13} \\ A_{i21} & A_{i22} & A_{i23} \\ A_{i31} & A_{i32} & A_{i33} \end{bmatrix}, \quad B_{1i} = \begin{bmatrix} B_{1i1} \\ B_{1i2} \\ B_{1i3} \end{bmatrix}, \quad B_{2i} = \begin{bmatrix} B_{2i1} \\ B_{2i2} \\ B_{2i3} \end{bmatrix}$$

$$A_{i11}=\begin{bmatrix} -D_i/M_i & -1/M_i \\ 2\pi\sum_{\substack{j=1\\ j\neq i}}^{N} T_{ij} & 0 \end{bmatrix},\quad A_{i12}=\begin{bmatrix} 1/M_i & \cdots & 1/M_i \\ 0 & \cdots & 0 \end{bmatrix}_{2\times n}$$

$$A_{i22}=-A_{i23}=diag\begin{bmatrix} -1/T_{t1i} & -1/T_{t2i} & \cdots & -1/T_{tni} \end{bmatrix}$$

$$A_{i33}=diag\begin{bmatrix} -1/T_{g1i} & -1/T_{g2i} & \cdots & -1/T_{gni} \end{bmatrix}$$

$$A_{i31}=\begin{bmatrix} -1/(T_{g1i}R_{1i}) & 0 \\ \vdots & \vdots \\ -1/(T_{gni}R_{ni}) & 0 \end{bmatrix},\quad A_{i13}=A_{i21}^{\mathrm{T}}=0_{2\times n},\quad A_{i32}=0_{n\times n}$$

$$B_{1i1}=\begin{bmatrix} -1/M_i & 0 \\ 0 & -2\pi \end{bmatrix},\quad B_{1i2}=B_{1i3}=0_{n\times 2}$$

$$B_{2i1}=0_{2\times 1},\ B_{2i2}=0_{n\times 1},\quad B_{2i3}^{T}=\begin{bmatrix} \alpha_{1i}/T_{g1i} & \alpha_{2i}/T_{g2i} & \cdots & \alpha_{ni}/T_{gni} \end{bmatrix}$$

Currently, most existing LFC systems in developed countries with a restructured electric industry are working with the designed controllers based on the traditional-based LFC model. Recently, several proposed LFC scenarios attempted to adapt well-tested traditional LFC scheme to the changing environment of power system operation under deregulation [5-8].

2.2 Pluralistic-based LFC model

There are several control scenarios and LFC schemes depending on the electrical system structure. However, the common goal in each control area is restoring the frequency and the net interchanges to their desired values. For example, in Europe, three different types of control are defined by the Union for the Co-ordination of Transmission of Electricity (UCTE): centralized network control, decentralized pluralistic network control, and decentralized hierarchical network control [7]. The countries with a central electricity supply system use the central network control, where LFC is operated through a single secondary controller. The other two decentralized methods consider some separate control areas and each control area has an individual controller. One or more control areas operating together for what concerns LFC can establish a “control block”, and in this case a block co-ordinator is defined as the overall control center for the LFC and for the accounting of the whole control block. This section is focused on LFC synthesis in each control area under decentralized pluralistic network control scheme. A general diagram for the pluralistic LFC is shown in Fig. 2.2.

In this scheme, each control area regulates the frequency by its own controller. If some control areas perform a control block, a separate controller (block coordinator) coordinates the whole block towards its neighbor blocks/control area by means of its own controller and regulating capacity. Consider a general control area with

N Gencos and assume that the k^{th} Genco (G_k) can generate enough power to track the load and to perform the LFC task, and other Gencos are the main suppliers for area-load. In this structure, the connection of each control area to the rest of the power system is considered as disturbance channel(s).

Although power systems are inherently non-linear, simplified and linearized models are usually used for LFC. In robust control strategies, the error caused by the simplification and linearization can be considered as parameter uncertainties and unmodeled dynamics. In this section, the modeling idea given in [9] is generalized for pluralistic-based LFC scheme. In order to build an area system model, it is assumed that each Genco has one generator unit. The linearized dynamics of the individual generators are given by:

$$\begin{aligned} &\frac{2H_i}{f_0}\frac{d\Delta f_i}{dt} = \Delta P_{ti} - \Delta P_i - d_i - D_i\Delta f_i \\ &\frac{d\Delta\delta_i}{dt} = 2\pi\Delta f_i \end{aligned} \quad ; \qquad i=1, 2, \ldots, N \tag{2.6}$$

where

H_i : constant of inertia,

δ_i : rotor angle,

f_o : nominal frequency,

ΔP_i : electrical power,

d_i : disturbance (power quantity).

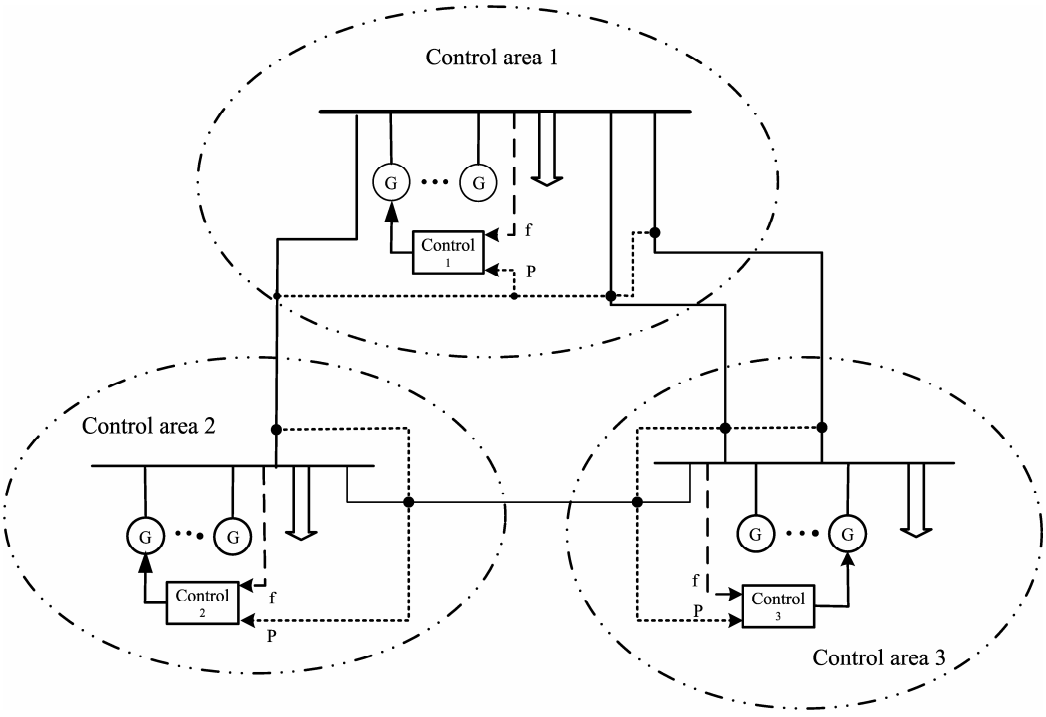

Figure 2.2: Three control area in the pluralistic-based LFC scheme

The generators are equipped with a speed governor. The simplest models of speed governors and turbines associated with generators are given by:

$$\begin{aligned}\frac{d\Delta P_{gi}}{dt} &= -\frac{1}{T_{gi}}\Delta P_{gi} + \frac{K_{gi}}{T_{gi}}(\Delta P_{ci} - \frac{1}{R_i}\Delta f_i) \\ \frac{d\Delta P_{ti}}{dt} &= -\frac{1}{T_{ti}}\Delta P_{ti} + \frac{K_{ti}}{T_{ti}}\Delta P_{gi}\end{aligned} \quad ; \qquad i=1,\ldots,N \tag{2.7}$$

where K_{ti} and K_{gi} are the gains of turbine and governor. The individual generator models are coupled to each other via the control area system. Mathematically, the local state space of each individual generator must be extended to include the system coupling variable (δ), which allows the dynamics at one point on the system transmitted to all other points.

Let bus *m* be the load bus, $V_i = |V_i| \angle \delta_i$ be the voltage at bus *i*, and assume $\Delta\delta_{ij} = \Delta\delta_i - \Delta\delta_j$. The power that flows from the Gencos to the area-load is expressed in terms of the voltages and line reactances.

$$\Delta P_i = T_i(\Delta\delta_i - \Delta\delta_m) = -T_i\Delta\delta_{ki} + T_i\Delta\delta_{km} \quad ; \qquad i=1, 2, \ldots, k-1, k+1, \ldots, N \tag{2.8}$$

and

$$\Delta P_k = T_k(\Delta\delta_k - \Delta\delta_m) = T_k\Delta\delta_{km} \tag{2.9}$$

where

$$T_i = \frac{|V_i||V_m|\cos(\delta_i^0 - \delta_m^0)}{x_i} \quad ; \quad i=1, 2, \ldots, N \tag{2.10}$$

T_i is synchronizing power coefficient of line *i* connected to the load bus (bus *m*) via a line whose reactance is x_i. The change in load is expressed by

$$\Delta P_L = \sum_{i=1}^{N}\Delta P_i = (\sum_{i=1}^{N} T_i)\Delta\delta_{km} - \sum_{\substack{i=1 \\ i\neq k}}^{N} T_i\Delta\delta_{ki} \tag{2.11}$$

$\Delta\delta_{km}$ is eliminated from Eqs. (2.8) and (2.9) using Eq. (2.11),

$$\Delta\delta_{km} = (\sum_{i=1}^{N} T_i)^{-1}[\Delta P_L + \sum_{\substack{i=1 \\ i\neq k}}^{N}(T_i\Delta\delta_{ki})] \tag{2.12}$$

Rewrite the Eqs. (2.8) and (2.9) using Eq. (2.12) as follows.

$$\Delta P_i = T_i(\sum_{j=1}^{N} T_j)^{-1}[\Delta P_L + \sum_{\substack{j=1 \\ j\neq k}}^{N}(T_j \Delta\delta_{kj})] - T_i \Delta\delta_{mi} \quad ; \quad i=1, 2, \ldots, k-1, k+1, \ldots, N \tag{2.13}$$

$$\Delta P_k = T_k(\sum_{i=1}^{N} T_i)^{-1}[\Delta P_L + \sum_{\substack{i=1 \\ i\neq k}}^{N}(T_i \Delta\delta_{ki})] \tag{2.14}$$

Rewriting Eqs. (2.6) and (2.7) with Eqs. (2.13) and (2.14), the state space model of the control area is obtained as

$$\dot{x} = Ax + Bu + Fw \tag{2.15}$$

where

$$x^T = \begin{bmatrix} X_1 & X_2 & \cdots & X_N & X_{N+1} \end{bmatrix}, \quad w^T = \begin{bmatrix} \Delta P_L & d \end{bmatrix}; \; u = \Delta P_{ck}$$

d is the disturbance vector, and

$$X_i = \begin{bmatrix} \Delta f_i & \Delta P_{ti} & \Delta P_{gi} \end{bmatrix} \quad ; \quad i=1, 2, \ldots, N$$

$$X_{N+1} = \begin{bmatrix} \Delta\delta_{k1} & \Delta\delta_{k2} & \cdots & \Delta\delta_{k(k-1)} & \Delta\delta_{k(k+1)} & \cdots & \Delta\delta_{kN} & \Delta\delta_{k} \end{bmatrix}_{1\times N}$$

Since one of the LFC objectives is known to guarantee that the frequency to returns to its nominal value following a step disturbance, Eq. (2.15) is augmented to include the rotor angle ($\Delta\delta_k$) of G_k in the state vector.

2.3 Bilateral-based LFC model

This section addresses a modified dynamical model for the analysis and synthesis of bilateral-based LFC scheme in a new environment versus a traditional one, following the ideas presented in [8]. The proposed LFC model uses all information required in a vertically operated utility industry plus the contract data information. Based on the bilateral transactions, a distribution company (Disco) has the freedom to contract with any available generation company (Genco) in its own or another control area. Therefore, the concept of physical control area is replaced by virtual control area (VCA). The boundary of a VCA is flexible and encloses the Gencos and the Disco associated with the contract. In a full bilateral LFC framework, it is assumed that each Disco is responsible for tracking its own load and honoring tie-line power exchange contracts with its neighbors by securing as much transmission and generation capacity as needed.

Analogously to the traditional LFC, the physical control area boundaries are assumed for each Disco, its distribution area and local Gencos as before. But, a Disco may have a contract with a Genco in another control area out of its distribution area boundaries. Similar to [10], the general theme in this work is that the loads (the Discos) are responsible for purchasing the services they require. Each control area has its own LFC and is responsible for tracking its own load and honoring tie-line power exchange contracts with its neighbors. Currently, these transactions are done under the supervision of the independent system operator (ISO), independent contract administrator (ICA), or other responsible organizations. There can be various combinations of contracts between each Disco and available Gencos. On the other hand, each Genco can contract with various Discos. Similar to the Disco participation matrix in [8], let us define the "generation participation matrix (*GPM*)" concept to visualize these bilateral contracts in the generalized model conveniently.

The *GPM* shows the participation factor of each Genco in the considered control areas and each control area is determined by a Disco. The rows of a *GPM* correspond to Gencos and the columns correspond to control areas that contract power. For example, for a large scale power system with *m* control area (Discos) and *n* Gencos, the *GPM* has the following structure:

$$GPM = \begin{bmatrix} gpf_{11} & gpf_{12} & \cdots & gpf_{1(m-1)} & gpf_{1m} \\ gpf_{21} & gpf_{22} & \cdots & gpf_{2(m-1)} & gpf_{2m} \\ \vdots & \vdots & \vdots & \vdots & \vdots \\ gpf_{(n-1)1} & gpf_{(n-1)2} & \cdots & gpf_{(n-1)(m-1)} & gpf_{(n-1)m} \\ gpf_{n1} & gpf_{n2} & \cdots & gpf_{n(m-1)} & gpf_{nm} \end{bmatrix} \tag{2.16}$$

Here, gpf_{ki} refers to "generation participation factor" and shows the participation factor of Genco *k* in the load following of area *i* (based on a specified bilateral contract). The sum of all the entries in a column in this matrix is unity, i.e.

$$\sum_{k=1}^{n} gpf_{ki} = 1 \tag{2.17}$$

Based on the above explanations, the modified LFC block diagram for control area-*i* in a contract-based environment is obtained, as shown in Fig. 2.3. New information signals due to various possible contracts between Disco *i* and other Discos and Gencos are shown as dashed-line inputs. v_{1i} includes the sum of local contracted demand and area load disturbances. v_{2i} includes the interface effects between each control area and other areas. This signal is defined the same as w_{2i} in the traditional-based LFC structure which is expressed in Eq. (2.3).

$$v_{1i} = \Delta P_{Loc\text{-}i} + \Delta P_{di} \tag{2.18}$$

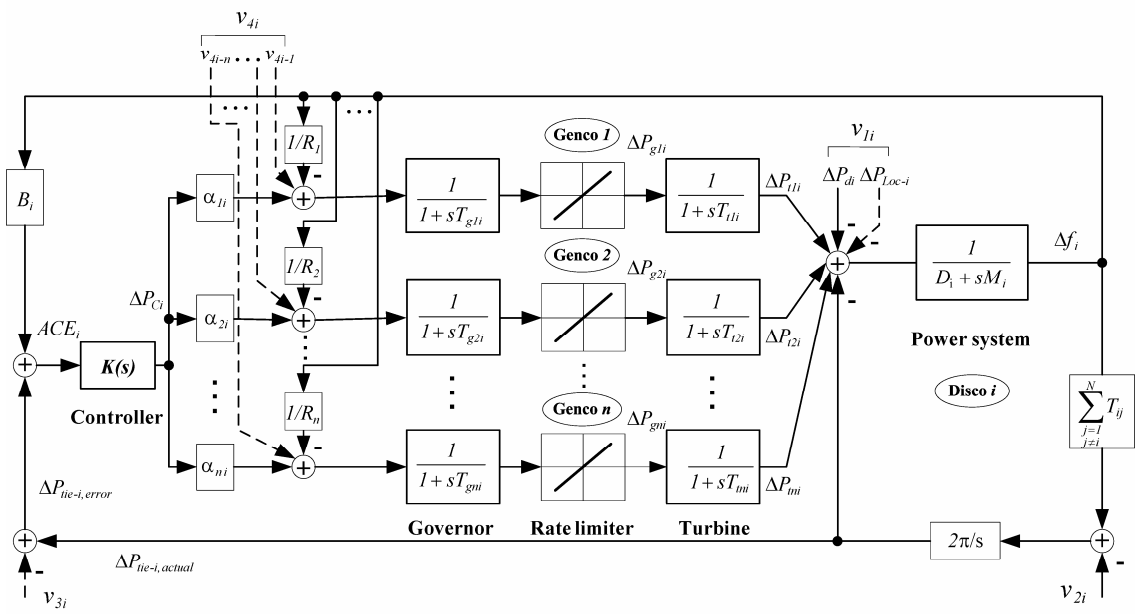

Figure 2.3: Bilateral-based LFC scheme

$$v_{2i} = \sum_{\substack{j=1 \\ j\neq i}}^{N} T_{ij}\Delta f_j \tag{2.19}$$

Using the given idea in [8], the scheduled tie-line power v_{3i} can be generalized for *N* control areas as follows,

$$\begin{aligned} v_{3i} &= \sum (Total\ export\ power - Total\ import\ power) \\ &= \sum_{\substack{j=1 \\ j\neq i}}^{N} (\sum_{k=1}^{n} gpf_{kj}\ )\Delta P_{Lj} - \sum_{k=1}^{n} (\sum_{\substack{j=1 \\ j\neq i}}^{N} gpf_{jk}\ )\Delta P_{Li} \end{aligned} \tag{2.20}$$

and,

$$\Delta P_{tie\text{-}i,error} = \Delta P_{tie\text{-}i,actual} - w_{3i} \tag{2.21}$$

The input signal v_{4i} shows a vector includes contracted demands of various Discos from Gencos of area *i* ,

$$v_{4i} = \begin{bmatrix} v_{4i\text{-}1} & v_{4i\text{-}2} & \cdots & v_{4i\text{-}n} \end{bmatrix} \tag{2.22}$$

where,

$$\begin{aligned} v_{4i\text{-}1} &= \sum_{j=1}^{N} gpf_{1j}\Delta P_{Lj} \\ &\vdots \\ v_{4i\text{-}n} &= \sum_{j=1}^{N} gpf_{nj}\Delta P_{Lj} \end{aligned} \tag{2.23}$$

and,

N: number of control areas,

ΔP_{Li} : contracted demand of area *i*,

$\Delta P_{Loc\text{-}i}$: total local demand (contracted and uncontracted) in area *i*,

$\Delta P_{tie\text{-}i,actual}$: actual $\Delta P_{tie\text{-}i}$.

The generation of each Genco must track the contracted demands of Discos in steady state. The desired total power generation of a Genco *i* in terms of GPM entries can be calculated as

$$\Delta P_{mi} = \sum_{j=1}^{N} gpf_{ij}\Delta P_{Lj} \tag{2.24}$$

In order to take the contract violation cases into account, as given in [6] and [8], the excess demand by a distribution area (Disco) is not contracted out by any Genco and the load change in the area appears only in terms of its ACE and is shared by all Gencos of the area (in which the contract violation occurs). The simulation results (chapters 4 and 5) for various cases demonstrate the effectiveness of the proposed model as a suitable dynamical model for LFC analysis and synthesis in a bilateral-based large scale power system.

2.4 A comparison of LFC models

The introduced LFC models in previous sections give suitable schemes to adapt a well-tested classical LFC model to the changing environment of power system operation under deregulation. The common and main advantage of these models is the use of fundamental concepts in the traditional framework and avoiding the use of impractical or untested LFC models. The mentioned models are successfully used in the design of robust decentralized LFC in the following chapters.

The traditional-based LFC model introduces the well-known conventional LFC scheme using some new concepts; e. g. “Genco” and “ACE participation factor”. In a restructured power system, the principle objectives for LFC system remain, i.e., restoring the frequency and the net interchanges to their desired values for each control area. Therefore, the traditional-based LFC model holds its suitability for LFC synthesis in a new environment as well. Currently, most existing LFC systems in developed countries with restructured electric industry are working with the designed controllers based on the traditionally-based LFC model.

Pluralistic-based LFC model gives a new idea for the reformulation of traditional-based LFC schemes, which is useful to LFC synthesis for control areas with pluralistic policy or autonomous condition. In this model, the individual generation units are coupled to each other via the control area system, and mathematically, the local state space of each individual generation unit is extended to include the system coupling variable (δ). This

allows the dynamics at one point on the system transmit to all other points of related area, such that the frequency deviation value at all generation units terminals, for both open-loop and closed-loop systems, converges to a fixed value at steady state.

In the pluralistic-based LFC scheme, each control area regulates the frequency by its own controller. In a control area, one (or more) Genco with enough capacity is responsible for tracking the load and to perform the LFC task, and other Gencos are the main suppliers for area-load. In this modeling strategy, the connection of each control area to the rest of the power system is considered as a disturbance channel.

In a traditional power system, generation, transmission, and distribution are owned by a single entity called vertically integrated utility (VIU), which supplies power to the customers at regulated rates. Usually, the definition of a control area is determined by the physical boundaries of a VIU. All such control areas are interconnected by tie lines. In a new environment, Gencos submit their ramp rates (Megawatts per minute) and bids to the market operator. After a bidding evaluation, those Gencos selected to provide regulation service must perform their functions according to the ramp rates approved by the responsible organization.

Bilateral-based LFC model provides an appropriate model to adapt well-tested traditional LFC schemes to the changing environment of power system operation under deregulation and open access policy. The difference between bilateral-based LFC structure and other models (traditional and pluralistic-based LFC schemes) is in the existence of contract data information. Any entry in a *GPM* that corresponds to a contracted load by a Disco, demanded from the corresponding Genco, is reflected to the control area system. This introduces new information signals that were absent in the traditionally-based LFC structure (Fig. 2.1). These signals identify which Genco has to follow a load demanded by a specified Disco. The scheduled flow over the tie lines must be adjusted by demand signals of those distribution control areas having a contract with Gencos outside its boundaries. The difference between scheduled and current (actual) tie-line power flows gives a tie-line power error which is used to compose an ACE signal.

The associated expressions and the place of new input signals in the bilateral-based LFC model were selected in such a way that: 1) the model covers all possible contract combinations given by *GPM*; 2) the calculation results from Eqs. (2.20) and (2.24) are completely matched to the corresponding simulation results for a given set of bilateral contracts.

We can review the pluralistic and bilateral based LFC schemes from a more general point of view. In both mentioned schemes, it is assumed that Discos are responsible for tracking the load variation and perform the LFC task. Each Disco must purchase LFC from one or more Gencos. Control is highly decentralized. Each load matching contract requires a separate control process, yet this control processes must cooperatively interact to maintain system frequency and minimize time error. In these structures, a separate control process exists for each control area. The boundary of control area encloses the Gencos and the Disco associated with the contracts. The Disco is responsible for buying power from Gencos and getting it directly or through transmission companies (Transcos) to its load. Such a configuration is shown conceptually in Fig. 2.4. Control area will be interconnected to each other either through Transco or Gencos.

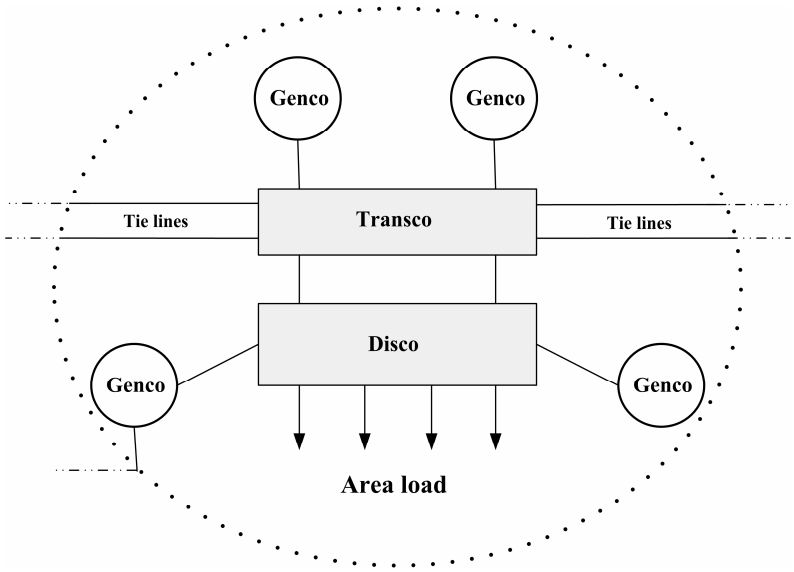

Figure 2.4: A (virtual) control area in a deregulated environment

Since, ultimately, the Genco must adjust the governor setpoint(s) of its generator(s) for the LFC, the control algorithm for each control area is executed at the Genco end (which is equipped with a proper controller). In this scheme, the Gencos are responsible for inadvertent interchange due to insufficient generator response, because in a load matching contract, they assume the responsibility of matching the Disco's load.

Several numerical examples on using the above introduced LFC models in the robust decentralized load-frequency control synthesis are given in Chapters 3, 4, and 5. In the proposed simulations, wide ranges of load variation with various contract scenarios are considered.

2.5 Summary

Technically, the basic concepts of conventional LFC structure are not changed, and therefore it is possible to adapt a well tested conventional LFC scheme to the changing environment of power system operation under deregulation. In light of this fact, three LFC modeling strategies including traditional, pluralistic, and bilateral based models are introduced. Based on these models, overall power system can be considered as a collection of distributed Discos or separate control areas interconnected through high voltage transmission lines or tie-lines.

The modeling idea presented in [8] is generalized to obtain the dynamical model for LFC analysis and synthesis in a bilateral-based restructured power system. In each control area, the effect of bilateral contracts is taken into account as a set of new input signals. It is assumed that each distribution company is responsible for tracking its own load and honoring tie-line power exchange contracts with its neighbors by securing as much transmission and generation capacity as needed.

2.6 References

[1] O. I. Elgerd, C. Fosha, "Optimum megawatt-frequency control of multiarea electric energy systems," *IEEE Trans. Power Apparatus & Systems*, vol. PAS-89, no. 4, pp. 556-563, 1970.

[2] C. Fosha, O. I. Elgerd, "The megawatt-frequency control problem: a new approach via optimal control," *IEEE Trans. Power Apparatus & Systems*, vol. PAS-89, no. 4, pp. 563-577, 1970.

[3] H. Bevrani, Y. Mitani, K. Tsuji, "Sequential design of decentralized load-frequency controllers using μ-synthesis and analysis," *Energy Conversion & Management*, vol. 45, no. 6, pp. 865-881, 2004.

[4] D. Rerkpreedapong, A. Hasanovic, A. Feliachi, "Robust load frequency control using genetic algorithms and linear matrix inequalities," *IEEE Trans. Power Systems*, vol. 18, no. 2, pp. 855-861, 2003.

[5] J. Kumar, NG. K. Hoe, G. B. Sheble, "AGC simulator for price-based operation, Part I: A model," *IEEE Trans. Power Systems*, vol.2, no.12, pp. 527-532, 1997.

[6] J. Kumar, NG. K. Hoe, G. B. Sheble, "AGC simulator for price-based operation, Part II: case study results," *IEEE Trans. Power Systems*, vol.2, no.12, pp. 533-538, 1997.

[7] B. Delfino, F. Fornari, S. Massucco, "Load-frequency control and inadvertent interchange evaluation in restructured power systems," *IEE proc. Gener. Transm. Distrib.*, vol.149, no.5, pp. 607-614, 2002.

[8] V. Donde, M. A. Pai and I. A. Hiskens, "Simulation and optimization in a AGC system after deregulation," *IEEE Trans. Power Systems*, vol. 16, no. 3, pp. 481-489, 2001.

[9] A. Feliachi, "On load frequency control in a deregulated environment," in Proc. *IEEE Int. Conf. on Control Application*, Dearborn, pp. 437-441, 1996.

[10] R. D. Chritie, A. Bose, "Load frequency control issues in power system operation after deregulation," *IEEE Trans. Power Systems*, vol. 11, no. 3, pp. 1191-1200, 1996.

Chapter 3

Structured singular value based robust decentralized LFC design

This chapter presents two robust decentralized control methodologies for LFC synthesis using structured singular value theory (μ) and is organized in two sections. The first section describes a new systematic approach to the design of sequential decentralized load-frequency controllers in a multi-area power system. System uncertainties, practical constraint on the control action and the desired performance are included in the synthesis procedure. Robust performance is used as a measure of control performance in terms of structured singular value. A 4-control area power system example is presented demonstrating the procedure of synthesis and the advantages of the proposed strategy.

The second section addresses a robust control approach to design decentralized load frequency control for large scale power systems in a deregulated environment. In this approach, the power system is considered as a collection of separate control areas under the pluralistic-based LFC scheme. Each control area can buy electric power from available generation companies to supply its load. The control area is responsible for performing its own LFC by buying enough power from prespecified generation companies that are equipped with robust load frequency controllers. A 3-control area power system example is given to illustrate the proposed control approach. The resulting controllers are shown to minimize the effect of disturbances and achieve acceptable frequency regulation in the presence of uncertainties and load variation.

3.1 Sequential decentralized LFC design

Simultaneous design for a fixed controller structure is used in all reported decentralized LFC scenarios. This approach is numerically difficult for a large scale power system and does not provide some of the advantages of using decentralized control, e.g., the ability to bring the system into service by closing one loop at a time, and the guarantee of stability and performance in the case of failures. In addition, some proposed methods might not work properly and do not guarantee performance when the operating points vary.

In this section, based on structured singular value theory (μ), a new systematic approach to sequential decentralized LFC design in a multi-area power system is described. Because of the advantages it provides, the sequential control design is the most common design procedure in real applications of decentralized synthesis methods. Sequential design involves closing and tuning one loop at a time. This method is less conservative than independent decentralized design because at each design step one utilizes the information about the controller specified in the previous step [1]. It is more practical in comparison with common decentralized methods.

After introducing the μ based sequential control framework and pairing inputs and outputs, a single-input single-output (SISO) controller is designed for each loop (control area). In the LFC design for each control area, the structured singular value [2], is used as a synthesis tool and a measure of performance robustness. This work shows that μ-synthesis can be successfully used for the sequential design of multi-area power system load frequency controllers that guarantee robustness in stability and performance for a wide range of operating conditions.

3.1.1 Model description

The traditional-based LFC model is used for each control area of a multi-area power system. Referring to the simplified traditional-based LFC model which is shown in Fig. 3.1 for control area 1, the state space realization of area *i* (from *m*-control area power system) is given as follows.

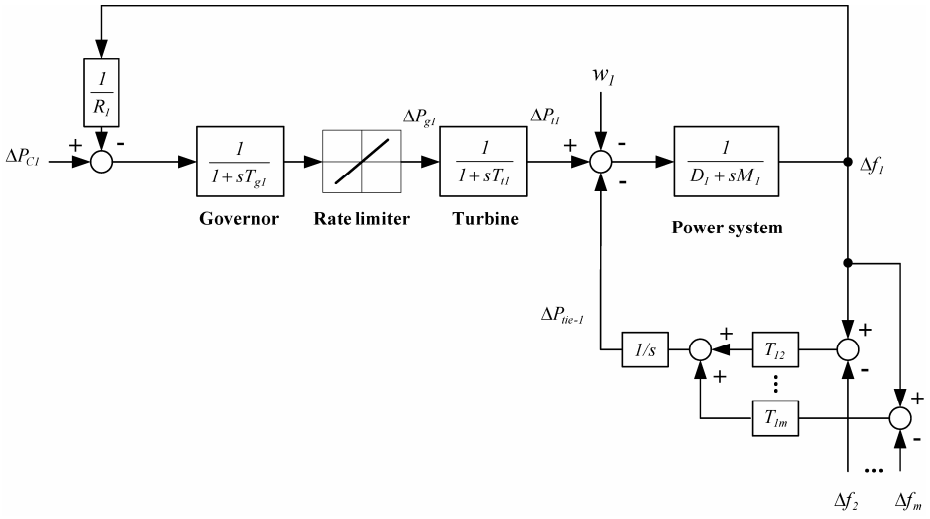

Figure 3.1: Block diagram of control area-1

$$\begin{aligned} \dot{x}_i &= A_i x_i + B_i u_i + F_i w_i \\ y_i &= C_i x_i \end{aligned} \tag{3.1}$$

The state vector x_i, control input u_i, disturbance input w_i and measured output y_i are defined by

$$x_i = \left[\Delta f_i \;\; \Delta P_{ti} \;\; \Delta P_{gi} \;\; \Delta P_{tie-i}\right]^T, \;\; u_i = \Delta P_{Ci}, \;\; w_i = \Delta P_{di}, \;\; y_i = \beta_i \Delta f_i + \Delta P_{tie-i} \tag{3.2}$$

The total real power imported to area-*i* equals the sum of all inflowing line powers P_{tie-ij} from adjoining areas, i.e.,

$$P_{tie-i} = \sum_{\substack{j=1 \\ j \neq i}}^{m} P_{tie-ij} \tag{3.3}$$

The real power in per unit transmitted across a lossless line of reactance X_{ij} is

$$P_{tie-ij} = \frac{|V_i||V_j|}{X_{ij} P_{ri}} sin(\delta_i - \delta_j) \tag{3.4}$$

Here P_{ri} is the rated power of area-*i*, and

$$V_i = |V_i| e^{j\delta_i} \tag{3.5}$$

where $|V_i|$ and δ_i are the amplitude and the angle of the terminal voltage in area-*i*.

3.1.2 Synthesis procedure

3.1.2.1 Methodology The main goal in each control area is to maintain the area frequency and tie-line power interchanges close to specified values in the presence of model uncertainties and disturbances. To achieve our objectives and to meet the μ-synthesis requirements, the control area model can be modified as shown in Fig. 3.2. In comparison with Fig. 3.1, the inter-area connections are removed, and it is considered by ΔP_{tie-i} that it is properly weighted by inter-area connecting coefficients, and is obtained from an integrator block. This figure shows the synthesis strategy for area-*i*.

It is notable that for each control area, there are several uncertainties because of parameter variations, linearization and unmodeled dynamics which are due to the approximation of the rest of the power system. Usually, the uncertainties in the power system can be modeled as multiplicative and/or additive uncertainties [3]. However, to keep the complexity of the controllers reasonably low, it is better to focus on the most important uncertainty. Sensitivity analysis of frequency stability due to parameter variation is a well known method for this purpose. In Fig. 3.2, the Δ_{Ui} models the structured uncertainty set in the form of a multiplicative type and W_{Ui}

includes the associated weighting function.

According to performance requirements and practical constraints on control action, two fictitious uncertainties W_{P1i} and W_{P2i} are added to the area model. The W_{P1i} on the control input sets a limit on the allowed control signal to penalize fast change and large overshoot in the control action. The weight W_{P2i} at the output sets the performance goal, for example, tracking/regulation error on the output deviation frequency. Furthermore, it is worth noting that in order to reject disturbances and to assure a good tracking property, W_{P1i} and W_{P2i} must be selected in such a way that the singular value of sensitivity transfer function from u_i to y_i in the related area can be reduced at low frequencies [4]. Δ_{Ui}, Δp_{1i} and Δp_{2i} are the uncertainty blocks associated with W_{Ui}, W_{P1i} and W_{P2i}, respectively.

The synthesis starts with setting the desired level of stability and performance for the first loop (control area) with a set of (u_i , y_i) and chosen uncertainties to achieve robust performance. In order to maintain adequate performance in the face of tie-line power variation and load disturbances, the appropriate weighting functions must be used. The inclusion of uncertainties adequately allows for maximum flexibility in designing the closed loop characteristics, and the demands placed on the controller will increase. We can redraw Fig. 3.2 as shown in Fig. 3.3. g_{1i} and g_{2i} are transfer functions from the control input (u_i) and input disturbance (ΔP_{di}) to the control output, respectively.

Fig. 3.4 shows M-Δ configuration for area-*i*. G_{i-1} includes a nominal model for area-*i*, associated weighting functions and scaling factors. As previously mentioned, the blocks Δp_{1i} and Δp_{2i} are the fictitious uncertainties added to assure robust performance, while the block Δ_{Ui} models the important multiplicative uncertainty associated with the area model.

Now, in step *i*, the synthesis problem is reduced to design a robust controller K_i. Based on the μ-synthesis, the robust performance holds for a given M-Δ configuration if and only if,

$$\inf_{K_i} \sup_{\omega \in R} \mu[M_i(j\omega)] < 1 \tag{3.6}$$

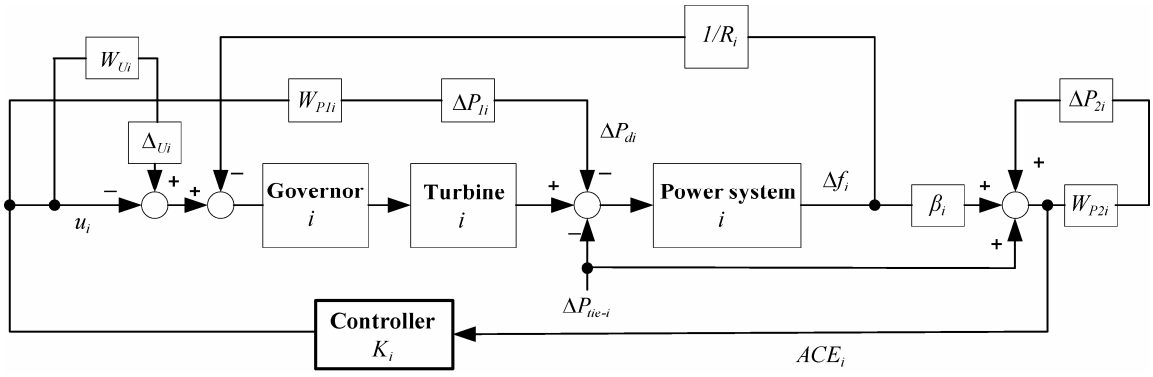

Figure 3.2: Proposed strategy for LFC synthesis in area-*i*

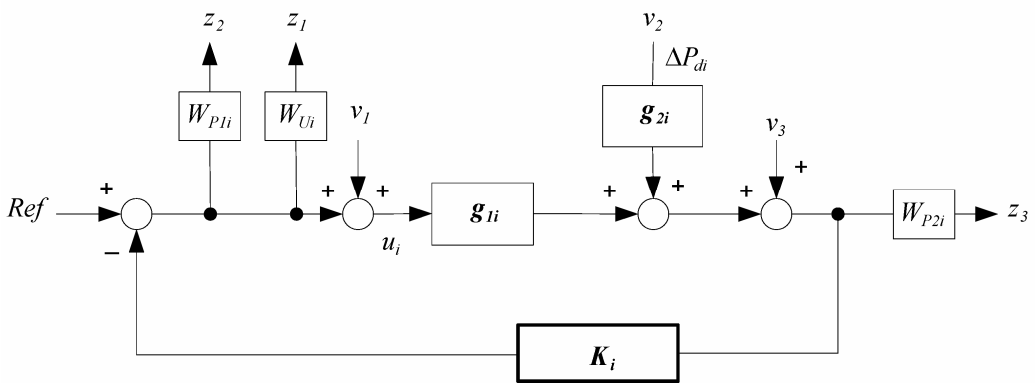

Figure 3.3: Synthesis framework for area-*i*

Here, according to Fig. 3.3, M_i for loop *i* (control area-*i*), is given by (3.7).

$$M_i = \begin{bmatrix} -T_{0i}W_{Ui} & -g_{2i}g_{1i}^{-1}T_{0i}W_{Ui} & -g_{1i}^{-1}T_{0i}W_{Ui} \\ -T_{0i}W_{P1i} & -g_{2i}g_{1i}^{-1}T_{0i}W_{P1i} & -g_{1i}^{-1}T_{0i}W_{P1i} \\ g_{1i}S_{0i}W_{P2i} & g_{2i}S_{0i}W_{P2i} & S_{0i}W_{P2i} \end{bmatrix} \tag{3.7}$$

T_{0i} and S_{0i} are complementary sensitivity and sensitivity functions of the nominal model of control area-*i* and are given by

$$T_{0i} = g_{1i}K_i(1 + g_{1i}K_i)^{-1} \tag{3.8}$$

$$S_{0i} = 1 - T_{0i} = (1 + g_{1i}K_i)^{-1} \tag{3.9}$$

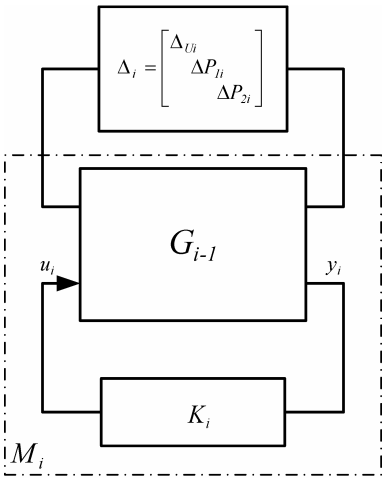

Figure 3.4: M-Δ configuration for area-*i*

Using the performance robustness condition and the well known upper bound for μ, the robust synthesis problem (3.6) is reduced to determine

$$\min_{K_i} \inf_{D} \sup_{\omega} \bar{\sigma}(D M_i(j\omega) D^{-1}) \tag{3.10}$$

or equivalently

$$\min_{K_i, D} \left\| D M_i(G_{i-1}, K_i)(j\omega) D^{-1} \right\|_\infty \tag{3.11}$$

by iteratively solving for D and K_i (D-K iteration algorithm). Here, D is any positive definite symmetric matrix with appropriate dimension and $\bar{\sigma}(.)$ denotes the maximum singular value of a matrix.

When the controller synthesis has been completed, another robust controller is designed for the second control area with its set of variables and this procedure continues until all the areas are taken into account. During the design of each controller, the effects of previously designed controllers are taken into consideration. The overall framework of the proposed strategy is given in Fig. 3.5. It is noteworthy that the block G_0 is assumed to contain a nominal open-loop model, the appropriate weighting functions and scaling factors according to Δ_1. The block G_{m-1} includes G_0 and all decentralized controllers K_1, K_2, …, K_{m-1} designed in previous iterations *1, 2, …, (m-1)* and related uncertainty blocks. The nominal open loop state-space representation of the power system is as follows:

$$\begin{aligned} \dot{x} &= Ax + Bu + Fw \\ y &= Cx \end{aligned} \tag{3.12}$$

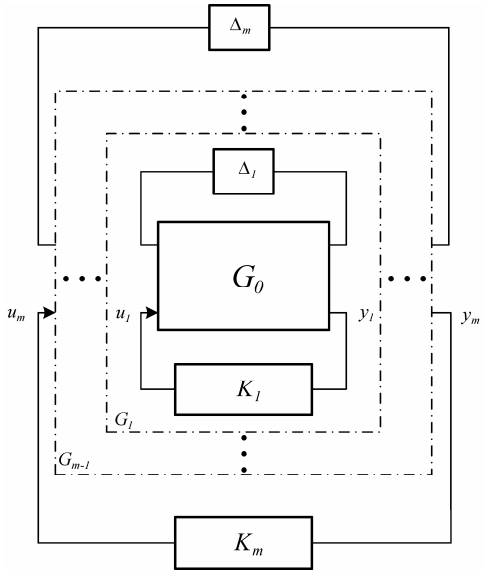

Figure 3.5: Framework for μ-synthesis

where *B* corresponds to the control input, *F* to the disturbance inputs and *C* to the output measurement which is the input to load frequency controller, and

$$\begin{aligned} &x = \left[\Delta f_1 \;\; \Delta P_{t1} \;\; \Delta P_{g1} \;\; \Delta P_{tie-1} \;\; \ldots \;\; \Delta f_m \;\; \Delta P_{tm} \;\; \Delta P_{gm} \;\; \Delta P_{tie-m}\right]^T \\ &u = \Delta P_{C1} = u_1 \; ; \;\; y = \beta_1 \Delta f_1 + \Delta P_{tie-1} = y_1 \end{aligned} \tag{3.13}$$

It should be noted that the above equations for the open loop system, in each synthesis, must be augmented by including controllers synthesized in the previous steps. In each step, a μ-controller is designed for one set of input and output variables. When this synthesis has been successfully completed, the next μ-controller is designed for another set of input-output variables and so on. In every step, the effects of previously designed controllers are taken into account. Therefore, by adding one new loop at a time, the closed loop system remains stable at each step.

3.1.2.2 Synthesis steps In summary, the proposed method consists of the following steps:

Step 1. Identify the order of loop synthesis.

The important problem with sequential design is that the final control performance achieved may depend on the order in which the controllers in the individual loops are synthesized. In order to overcome this problem, the fast loops must be closed first, because the loop gain and phase in the bandwidth region of the fast loops is relatively insensitive to the tuning of the lower loops. In other words, for cases where the bandwidths of the loops are quite different, the outer loops should be tuned so that the fast loops are contained in the inner loops. This causes a lower number of iterations during the re-tuning procedure to obtain the best possible performance [5].

Obtaining an estimation of interactions on each control area behavior to determine the effects of undesigned loops is the other important issue in the sequential synthesis procedure. Methods for determining performance relative gain array (PRGA) and closed-loop disturbance gain (CLDG) which are given in [6] are useful for this purpose.

Step 2. Identify the uncertainty blocks and associated weighting functions according to the first control area input-output set, depending on the dynamic model, practical limits and performance requirements. It is should be noted that there is no obligation to consider the uncertainty within only a few parameters. In order to consider a more complete model, the inclusion of additional uncertainties is possible and causes less conservatism in the synthesis. However, the complexity of computations and the order of obtained controllers will increase.

Step 3. Isolate the uncertainties from nominal area model, generate the Δp_{1i}, Δp_{2i}, Δ_{Ui} blocks and perform the M-$\triangle$ feedback configuration (formulate the desired stability and performance).

Step 4. Start the *D-K* iteration using the μ-synthesis toolbox ([7]) to obtain the optimal controller, which provides desirable robust performance such that

$$\max_{\omega \in R} \mu[M(j\omega)] < 1 \tag{3.14}$$

ω denotes the frequency range for which the structured singular value is computed. This procedure determines the first robust controller.

Step 5. Reduce the order of the resulting controllers by utilizing the standard model reduction techniques and then apply μ-analysis to closed loop system with reduced controller to check whether or not the upper bound of μ remains less than one.

It is notable that the controller found by this procedure is usually of a high order. To decrease the complexity of computation, appropriate model reduction techniques might be applied both to the open-loop system model and to the H_∞ controller model within each *D-K* iteration.

Step 6. Continue this procedure by applying the above steps to other loops (control area input-output sets) according to the specified loop closing order in Step 1.

Step 7. Retune the controllers which have been obtained to achieve the best performance and check if the overall power system satisfies the robust performance condition using μ analysis. If the objective is the achievement of the best possible performance, the controller that was designed first, must be removed and then re-designed. However, this must now be done with controllers that have been synthesized in successive steps, because the first synthesis was according to the more conservative state.

The proposed strategy guarantees robust performance for multi-area power systems when the design of load frequency controllers is followed according to the above sequential steps. The advantage of the procedure is it ensures that by closing one loop for a special control area at a time, this control area achieves robust performance, while at the same time the multi-area power system holds its stability at each step. Similarly, during startup, the system will at least be stable if the loops are brought into service in the same order as they have been designed [6, 8].

3.1.3 Application to a 4-control area power system

The proposed control approach is applied to a 4-control area power system example shown in Fig. 3.6. The nominal parameter values are given in Table 3.1, [9-11]. The nominal state-space model for this system as a multi-input multi-output (MIMO) system can be constructed as given in Eq. (3.12), where $A \in R^{16\times16}$, $B \in R^{16\times4}$, $F \in R^{16\times4}$ and

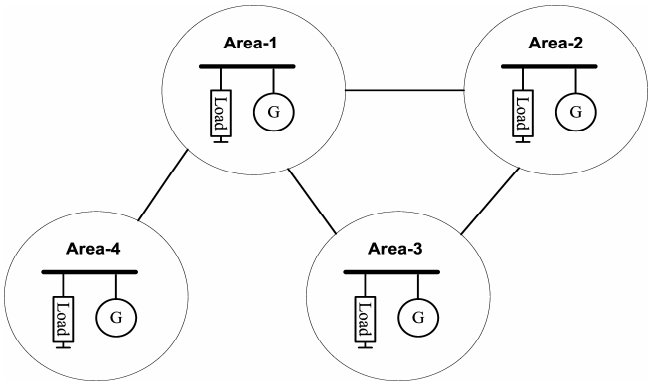

Figure 3.6: 4-control area power system

$$x = \left[\Delta f_1 \;\; \Delta P_{t1} \;\; \Delta P_{g1} \;\; \Delta P_{tie-1} \;\; \Delta f_2 \;\; \Delta P_{t2} \;\; \Delta P_{g2} \;\; \Delta P_{tie-2} \;\; \Delta f_3 \;\; \Delta P_{t3} \;\; \Delta P_{g3} \;\; \Delta P_{tie-3} \;\; \Delta f_4 \;\; \Delta P_{t4} \;\; \Delta P_{g4} \;\; \Delta P_{tie-4}\right]^T$$

$$u = \left[u_1 \; u_2 \;\; u_3 \;\; u_4 \;\right]^T,\; w = \left[\Delta P_{d1} \; \Delta P_{d2} \;\; \Delta P_{d3} \;\; \Delta P_{d4} \;\right]^T,\; y = \left[y_1 \; y_2 \;\; y_3 \;\; y_4 \;\right]^T \tag{3.15}$$

$$A = \begin{bmatrix} A_{11} & A_{12} & A_{13} & A_{14} \\ A_{21} & A_{22} & A_{23} & A_{24} \\ A_{31} & A_{32} & A_{33} & A_{34} \\ A_{41} & A_{42} & A_{43} & A_{44} \end{bmatrix} \tag{3.16}$$

$$A_{ii} = \begin{bmatrix} -\frac{D_i}{M_i} & \frac{1}{M_i} & 0 & -\frac{1}{M_i} \\ 0 & -\frac{1}{T_{ti}} & \frac{1}{T_{ti}} & 0 \\ -\frac{1}{R_i T_{gi}} & 0 & -\frac{1}{T_{gi}} & 0 \\ \sum_j T_{ij} & 0 & 0 & 0 \end{bmatrix} \tag{3.17}$$

$$A_{ij}(i \neq j) = \begin{bmatrix} 0 & 0 & 0 & 0 \\ 0 & 0 & 0 & 0 \\ 0 & 0 & 0 & 0 \\ -T_{ij} & 0 & 0 & 0 \end{bmatrix} \tag{3.18}$$

$$B = \begin{bmatrix} 0 & 0 & \frac{-1}{T_{g1}} & 0 & 0 & 0 & 0 & 0 & 0 & 0 & 0 & 0 & 0 & 0 & 0 & 0 \\ 0 & 0 & 0 & 0 & 0 & 0 & \frac{-1}{T_{g2}} & 0 & 0 & 0 & 0 & 0 & 0 & 0 & 0 & 0 \\ 0 & 0 & 0 & 0 & 0 & 0 & 0 & 0 & 0 & 0 & \frac{-1}{T_{g3}} & 0 & 0 & 0 & 0 & 0 \\ 0 & 0 & 0 & 0 & 0 & 0 & 0 & 0 & 0 & 0 & 0 & 0 & 0 & 0 & \frac{-1}{T_{g4}} & 0 \end{bmatrix}$$

$$F = \begin{bmatrix} \frac{-1}{M_1} & 0 & 0 & 0 & 0 & 0 & 0 & 0 & 0 & 0 & 0 & 0 & 0 & 0 & 0 & 0 \\ 0 & 0 & 0 & 0 & \frac{-1}{M_2} & 0 & 0 & 0 & 0 & 0 & 0 & 0 & 0 & 0 & 0 & 0 \\ 0 & 0 & 0 & 0 & 0 & 0 & 0 & 0 & \frac{-1}{M_3} & 0 & 0 & 0 & 0 & 0 & 0 & 0 \\ 0 & 0 & 0 & 0 & 0 & 0 & 0 & 0 & 0 & 0 & 0 & 0 & \frac{-1}{M_4} & 0 & 0 & 0 \end{bmatrix}$$

Table 3.1: Power system parameters

Parameter	*Area-1*	*Area-2*	*Area-3*	*Area-4*
D_i (p.u.MW/Hz)	0.0083	0.0088	0.0080	0.0088
M_i (p.u.MW)	0.166	0.222	0.16	0.13
T_{ti} (s)	0.3	0.33	0.35	0.375
T_{gi} (s)	0.08	0.072	0.07	0.085
R_i (Hz/p.u.MW)	2.4	2.7	2.5	2.0
T_{ij} (p.u.MW/Hz)	$T_{12}= T_{13}= T_{14}= T_{21}= T_{23}= T_{31}= T_{32}= T_{41}= 0.545$			

The nominal open loop MIMO system is stable and includes one oscillation mode. Simulation results show that the open-loop system performance is affected due to changes in equivalent inertia constants M_i and synchronizing coefficient T_{ij}, and these are more significant than changes of other parameters within a reasonable range. Eigenvalue analysis shows that the considerable change in these parameters leads to an unstable condition for the power system.

Therefore, to demonstrate the capability of the proposed strategy for the problem at hand, from the viewpoint of uncertainty, our focus is concentrated on the variations of the M_i and T_{ij} parameters of all control areas, that are the most important from a control viewpoint. Hence, for the given power system, LFC objectives have been set to assure robust stability and performance in the presence of specified uncertainties and load disturbances, that is,

1- Hold stability and robust performance for the overall power system and each control area in the presence of 40% uncertainty for M_i and T_{ij}, which are assumed the sources of uncertainty associated with the given power system model.

2- Minimize the effectiveness of step load disturbances (ΔP_{di}) on the output signals.

3- Maintain acceptable overshoot and settling time on frequency deviation signal in each control area.

4- Set a reasonable limit on the control action signal in the viewpoint of change speed and amplitude.

In the following section, the proposed strategy is separately applied to each control area of the given power system to meet the objectives. Because of similarities and for brevity, the first controller synthesis is described in detail, whereas only the final result for the other control areas is shown. As the bandwidths of the four loops are similar, the order of closing the loops is not important in regard to the problem at hand. Therefore, the synthesis procedure is started with control area 1.

3.1.3.1 Uncertainty weight selection As mentioned, the specified uncertainty in each control area can be considered as a multiplicative uncertainty (W_{Ui}) associated with nominal model. Corresponding to an uncertain parameter, let the $\hat{G}(s)$ denotes the transfer function from the control input u_i to the control output y_i at operating points other than the nominal point. Following a practice common in robust control, this transfer function will be represented as

$$\hat{G}(s) = G_0(s)(1 + \Delta_u(s) W_u(s)) \tag{3.19}$$

$\Delta_u(s)$ shows the uncertainty block corresponding to uncertain parameter, $W_u(s)$ is the associated weighting function and $G_0(s)$ is the nominal transfer function model. Then, the multiplicative uncertainty block can be expressed as

$$\left|\Delta_u(s) W_u(s)\right| = \left|[\hat{G}(s) - G_0(s)] G_0(s)^{-1}\right| \;;\; G_0(s) \neq 0 \tag{3.20}$$

$W_u(s)$ is a fixed weighting function containing all the information available on the frequency distribution of the uncertainty, where $\Delta_u(s)$ is stable transfer function representing the model uncertainty. Furthermore, without loss of generality (by absorbing any scaling factor into $W_u(s)$ where necessary), it can be assumed that

$$\left\|\Delta_u(s)\right\|_\infty = sup_\omega \left|\Delta_u(s)\right| \leq 1 \tag{3.21}$$

Thus, $W_u(s)$ is such that its respective magnitude Bode plot covers the Bode plot of all possible plants. Using Eq. (3.20), some sample uncertainties corresponding to the different values of M_i and T_{ij} are obtained and shown in Fig. 3.7. It can be seen that the frequency responses of parametric uncertainties are close to each other. Hence, to keep the complexity of the obtained controller at a low level, the uncertainties due to both sets of parameters variations can be modeled by using a single norm bonded multiplicative uncertainty to cover all possible plants and this is obtained as follows

$$W_{U1}(s) = \frac{0.15(s^2 + 0.004)}{s^2 + 0.1s + 18} \tag{3.22}$$

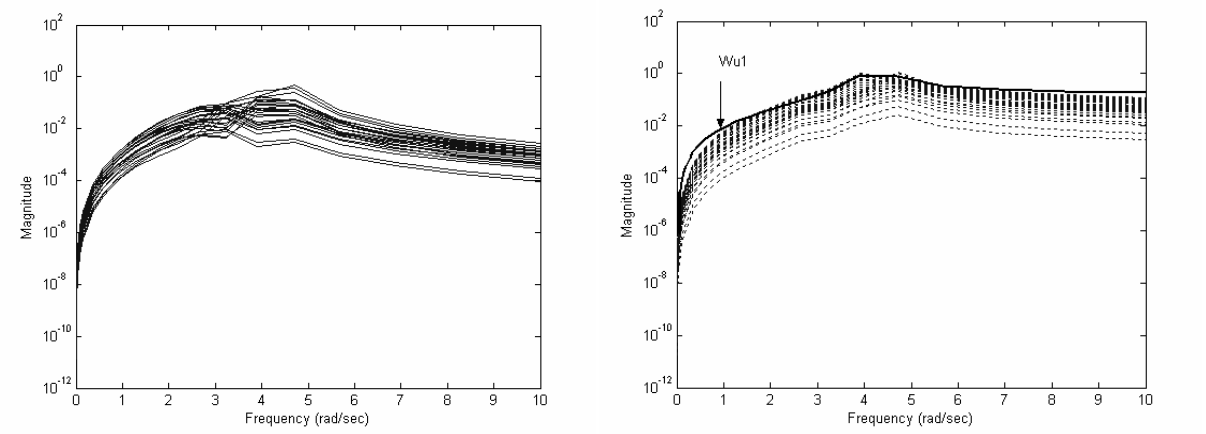

(a) (b)

Figure 3.7: Uncertainty plot due to change of a) M_i ; b) dotted (T_{ij}) and solid ($W_{U1}(s)$)

The frequency response of $W_{U1}(s)$ is also shown in Fig. 3.7b. This figure clearly shows that attempting to cover the uncertainties at all frequencies and finding a tighter fit using higher order transfer function will result in an high-order controller. The weight (3.22) used in our design provides a conservative design at low and high frequencies, but it gives a good trade-off between robustness and controller complexity.

3.1.3.2 Performance weight selection As discussed in section 3.1.2, in order to guarantee robust performance, adding a fictitious uncertainty block associated with the control area error minimization and control effort is required along with the corresponding performance weights W_{P11} and W_{P21}. In fact, an important issue regarding to the selection of these weights is the degree to which they can guarantee the satisfaction of the design performance objectives. Based on the following discussion, a suitable set of performance weighting functions that offer a good compromise among all the conflicting time-domain specifications for control area 1 is

$$W_{P11}(s)=\frac{0.5s}{0.01s+1},\quad W_{P21}(s)=\frac{s+0.75}{150s+1} \tag{3.23}$$

The selection of W_{P11} and W_{P21} entails a trade off among the different performance requirements. The weight on the control input W_{P11} was chosen close to a differentiator to penalize fast change and large overshoot in the control input. The weights on output error (W_{P21}) were chosen close to an integrator at low frequencies in order to get disturbance rejection, good tracking and zero steady-state error. Additionally, as pointed out in the previous section, the order of the selected weights should be kept low in order to keep the controller complexity low. Finally, it is well known that to reject disturbances and to track command signal properties, it is necessary for the singular value of sensitivity function to be reduced at low frequencies, and W_{P11} and W_{P21} must be selected to satisfy this condition [12]. Our next task is to isolate the uncertainties from the nominal plant model and redraw the system in the standard M-Δ configuration (Fig. 3.8).

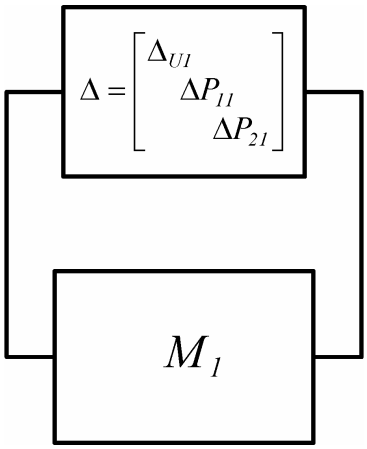

Figure 3.8: Standard M-Δ block

By using the uncertainty description and already developed performance weights, an uncertainty structure Δ, with a scalar block (corresponding to the uncertainty) and a 2×2 block (corresponding to the performance) is resulted. Having setup our robust synthesis problem in terms of the structured singular value theory, the μ-analysis and synthesis toolbox [7] is used to achieve a solution.

The controller $K_1(s)$ is found at the end of the three *D-K* iterations, yielding the value of about *0.893* on the upper bound on μ, thus guaranteeing robust performance. Since, the resulted controller has a high order (21*th*), it is reduced to a fourth-order with no performance degradation (μ *<0.998*), using the standard Hankel Norm approximation. The Bode plots of the full-order controller and the reduced-order controller are shown in Fig. 3.9. The transfer function of the reduced order controller is given as $K_1(s)=\frac{N_1(s)}{D_1(s)}$ with

$$\begin{aligned} N_1(s) &= 6.3905\,s^3 + 0.10604s^2 + 44.3998s + 37.994 \\ D_1(s) &= s^4 + 18.9617\,s^3 + 182.1594s^2 + 739.3578s + 0.7393 \end{aligned} \tag{3.24}$$

Using the same procedure and setting the similar objectives, as already discussed, achieves us a set of suitable weighting functions for the remaining loop synthesis as shown in Table 3.2. The order of the other obtained controllers without model reduction was 29 (K_2), 37 (K_3) and 45 (K_4). These controllers can be approximated by lower order controllers as follows.

$$K_2(s)=\frac{N_2(s)}{D_2(s)},\ K_3(s)=\frac{N_3(s)}{D_3(s)},\ K_4(s)=\frac{N_4(s)}{D_4(s)} \tag{3.25}$$

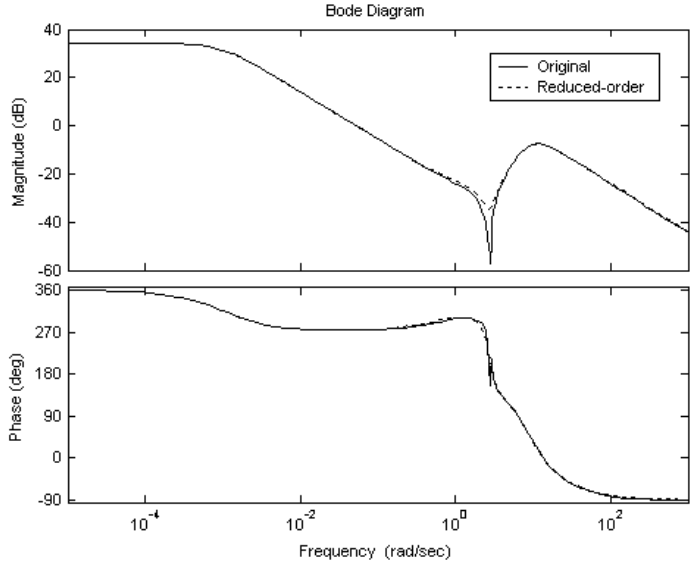

Figure 3.9: Bode plots comparison of full-order (original) and reduced-order controller $K_1(s)$

Table 3.2: Weighting functions for control area loops 2, 3 and 4

Area-2	Area-3	Area-4
$W_{u2}(s)=\frac{0.1s^2+0.001}{s^2+0.2s+21}$	$W_{u3}(s)=\frac{0.5s^2+0.005}{s^2+0.05s+10}$	$W_{u4}(s)=\frac{0.11s^2+0.004}{s^2+0.11s+15}$
$W_{p12}(s)=\frac{0.005s}{10^{-5}s+4.5}$	$W_{p13}(s)=\frac{0.01s}{10^{-4}s+1}$	$W_{p14}(s)=\frac{0.009s}{10^{-6}s+15}$
$W_{p22}(s)=\frac{s+0.1}{93(s+0.001)}$	$W_{p23}(s)=\frac{s+1.1}{100(s+0.1)}$	$W_{p24}(s)=\frac{s+0.22}{83(s+0.02)}$

where,

$$N_2(s)=140.756s^5+164530.87s^4+194365.253s^3+98449.36s^2+546138.32s+723970.37$$

$$D_2(s)=s^6+387.75s^5+35235.403s^4+67819.44s^3+2742801.2s^2+626558.42s+126075.23$$

$$N_3(s)=526.29\,s^5+1287.18\,s^4-1416.26\,s^3+6371.23\,s^2+12698.7s+633.53$$

$$D_3(s)=s^6+7229.77\,s^5+6809.8\,s^4+93877.3\,s^3+101675.4\,s^2+4632.21s+23.39$$

$$N_4(s)=560.94s^6+8329.72\,s^5+4783.48\,s^4+1246.86\,s^3+19675.43\,s^2+2638.25s+93.49$$

$$D_4(s)=s^7+18945.33\,s^6+12511.83\,s^5+76432.43\,s^4+836228.94\,s^3+42388.23s^2+1612.47s+532$$

3.1.4 Simulation results

In order to demonstrate the effectiveness of the proposed control method, some simulations were performed. In these simulations, the proposed control scenario described in section 3.1.2 was applied to the 4-control area power system as shown in Fig. 3.6. To test the system performance, a step load disturbance of $\Delta P_{di}=0.01pu$ is applied to each control area, using the nominal plant parameters and those with uncertain parameters by different percentage uncertainties.

Since the system parameters for the given four control areas are identical and the ΔP_{tie} between the two neighboring areas *k* and *j* is caused by $\Delta f_k-\Delta f_j$, the system performance can be mainly tested by applying the disturbance ΔP_{di} in the presence of the parameters uncertainties and observing the time response of Δf_i in each control area. Some selected time response simulation results are given in Figs. 3.10 and 3.11.

Fig. 3.10 shows the frequency deviation and control action signal in control areas 1 and 2, following the simultaneous step load disturbances of $\Delta P_{d1}=0.01pu$ and $\Delta P_{d2}=0.01pu$. Fig. 3.11 shows the frequency deviation following a step load disturbance of $\Delta P_{d1}=\Delta P_{d2}=0.01pu$, and a 40% increase M_i and T_{ij} in all areas, simultaneously.

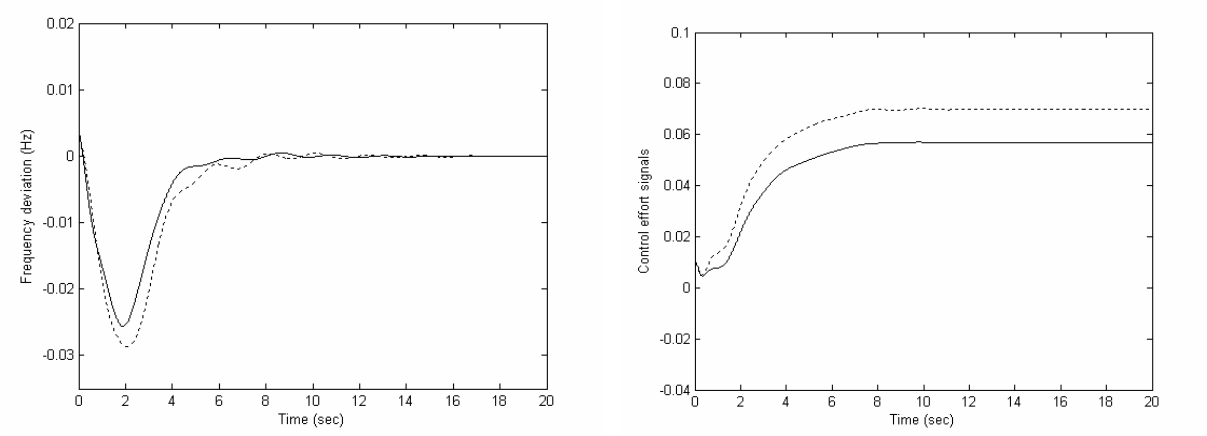

(a) (b)

Figure 3.10: a) Frequency deviation; b) Control signals, in area 1 (solid) and area 2 (dotted), following a *0.01 pu* step load disturbance in both areas

Fig. 3.12 shows the similar simulation result for control areas 3 and 4 ($\Delta P_{d3} = 0.01 pu$, $\Delta P_{d4} = 0.01 pu$ and a 40% increase in M_i and T_{ij} in all areas). Finally, Fig. 3.13 shows the power system response for the assigned possible worst case, i.e., a step load disturbance in each area and 40% decrease in uncertain parameters, simultaneously.

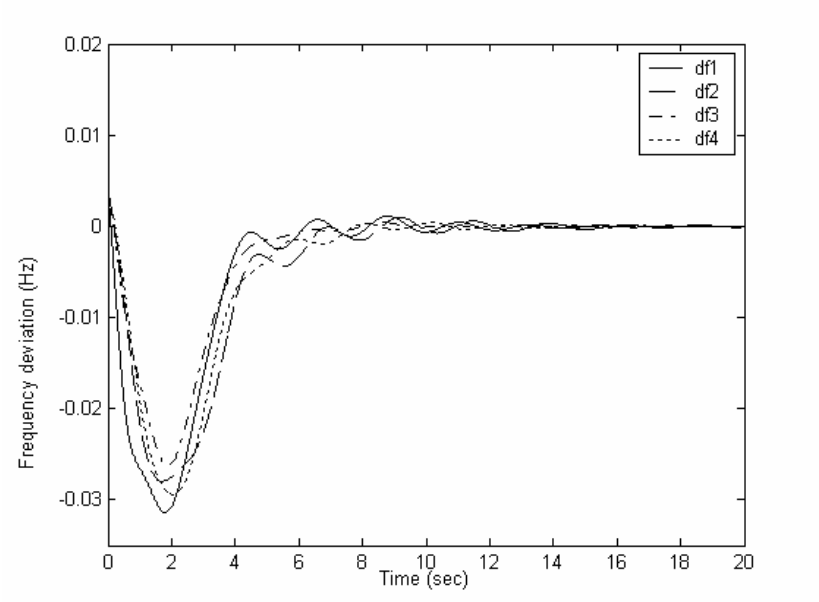

Figure 3.11: Frequency deviation in the presence of $\Delta P_{d1} = \Delta P_{d2} = 0.01 pu$ and 40% increase M_i and T_{ij}

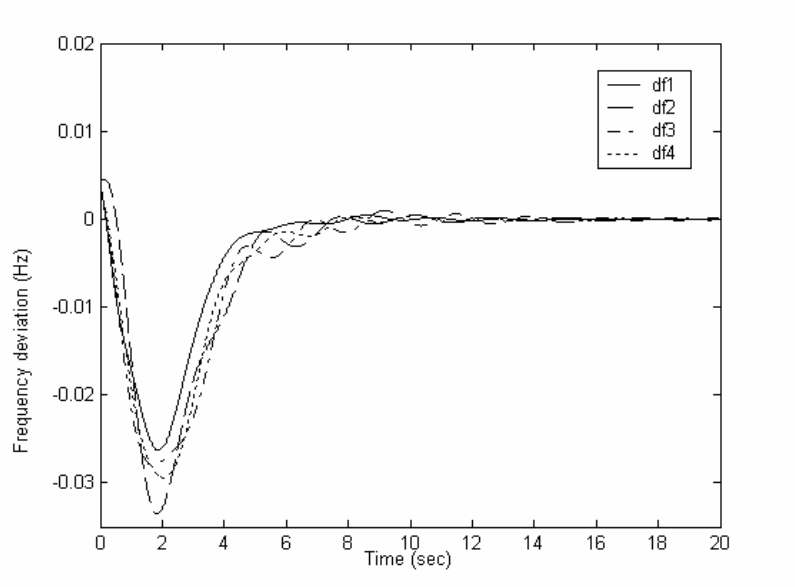

Figure 3.12: Frequency deviation in the presence of $\Delta P_{d3} = \Delta P_{d4} = 0.01pu$ and +40% change in uncertain parameters

These simulation results demonstrate the effectiveness of the proposed strategy to provide robust frequency regulation in multi-area power systems. Because of our tight design objectives which take into consideration several simultaneous uncertainties and input disturbances, the order of the resulting robust load frequency controllers are relatively high. However, the proposed method gives a good performance from the view point of disturbance rejection and frequency error minimization in the presence of model uncertainties.

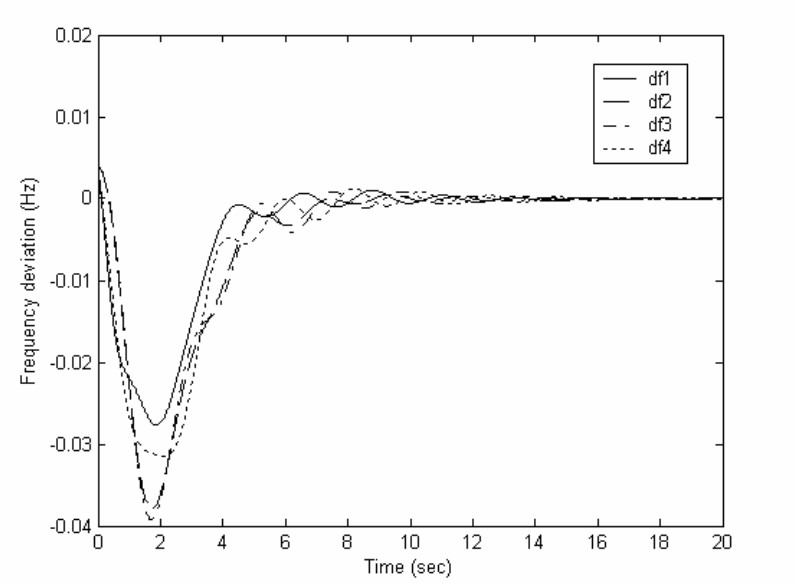

Figure 3.13: Frequency deviation following a step load disturbance $\Delta P_{di} = 0.01pu$ in each area and -40% changes in uncertain parameters

3.2 Pluralistic based decentralized LFC design

This section addresses a new design of robust load frequency controller based on the structured singular value theory for interconnected electric power systems in a competitive environment from the UCTE perspective for the pluralistic LFC scheme (Fig. 2.2). The power system structure is considered as a collection of control areas interconnected through high voltage transmission lines or tie-lines. Each control area has its own load frequency controller and is responsible for tracking its own load and honoring tie-line power exchange contracts with its neighbors. The proposed strategy is applied to a 3-control area example. The results obtained show that the controllers guarantee robust stability and robust performance for a wide range of operating conditions.

3.2.1 Synthesis methodology

The objective is to formulate the LFC problem in each control area based on the structured singular value method, independently. The general scheme of the proposed control system for a given area is shown in Fig. 3.14. β_i and λP_i are properly setup coefficients of the secondary regulator. The robust controller acts to maintain area frequency and total exchange power close to the scheduled value by sending a corrective signal to the assigned Gencos. This signal, which is weighted by the ACE participation factor α_{ij}, is used to modify the set points of generators. Consider the state space model (2.15) and analogously to the traditional area control error, let the output system variable be defined as follows:

$$y = Cx + Ew \tag{3.26}$$

where,

$$C = \begin{bmatrix} C_1 & C_2 & \cdots & C_N & C_{N+1} \end{bmatrix},\ C_i = \begin{bmatrix} \beta_i & 0 & 0 \end{bmatrix},\ C_{N+1} = [1]_{1\times N} \quad ;\quad i=1, 2, \ldots, N$$

and

$$E = [1 \quad \theta],\ w^T = \begin{bmatrix} \Delta P_L & d \end{bmatrix}.$$

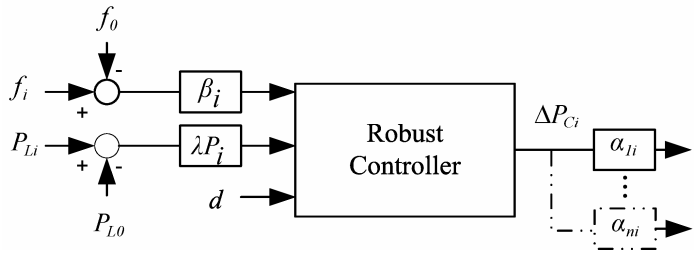

Figure 3.14: General scheme for the proposed control system

θ is a zero vector with the same size as disturbance vector (d). To achieve the LFC objectives in accordance with to the structured singular value theory requirements, a control strategy applicable for each control area is proposed as shown in Fig. 3.15. Δ_U models the structured uncertainty set in the form of multiplicative type and W_U includes the associated weighting function(s).

According to performance requirements and practical constraints on control action, three fictitious uncertainties W_{P1}, W_{P2} and W_{P3} are added to the power system model. The W_{P1} on the control input sets a limit on the allowed control signal to penalize fast changes and large overshoot in the control action. This is necessary to guarantee the feasibility of the proposed controller. At the output, the weights W_{P2} and W_{P3} set the performance goal e.g., tracking/regulation of the output area control signal. Δ_P is a diagonal matrix that includes the uncertainty blocks $\Delta p_1, \Delta p_2$ and Δp_3 associated with W_{P1}, W_{P2} and W_{P3}, respectively.

Fig. 3.15 can be redrawn as a standard M-Δ configuration, which is shown in Fig. 3.16. G includes the nominal model of the control area power system, associated weighting functions and scaling factors. The block labeled M, consists of G and controller K. Based on the μ-synthesis, robust stability and performance will be satisfied for a given M-Δ configuration, if and only if

$$\inf_{K} \sup_{\omega \in R} \mu[M(j\omega)] < 1 \tag{3.27}$$

The well-known upper bound for μ can be determined by using Eq. 3.10 or 3.11. In summary, the proposed method for each control area consists of the following steps:

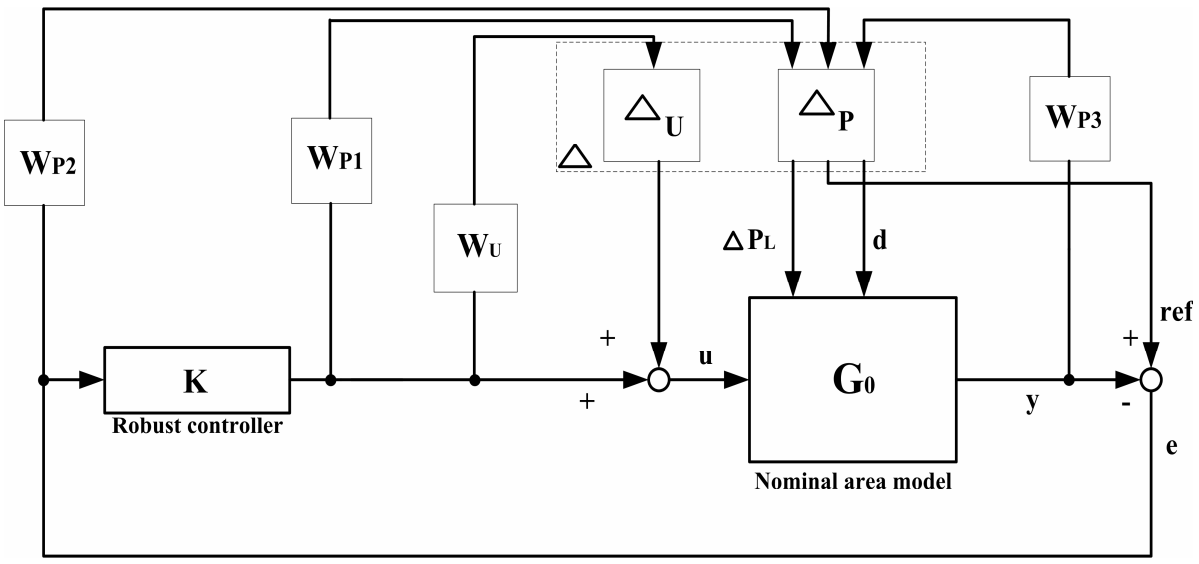

Figure 3.15: The synthesis framework

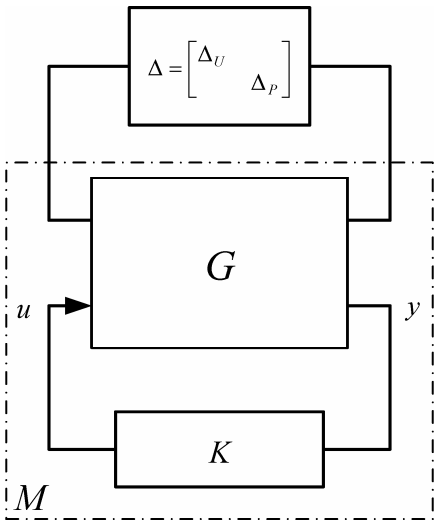

Figure 3.16: M-Δ configuration

Step 1. Identify the uncertainty blocks and associated weighting functions for the given control area, according to the dynamic model, the practical limits and performance requirements as shown in Fig. 3.15.

Step 2. Isolate the uncertainties from the nominal control area model, generate Δp_1, Δp_2, Δp_3 and Δ_U blocks and perform *M*-Δ feedback configuration (formulate the robust stability and performance).

Step 3. Start the *D-K* iteration by using μ-synthesis toolbox [7], in order to obtain the optimal controller.

Step 4. Reduce the order of the resulting controller by utilizing the standard model reduction techniques and apply μ-analysis to the closed loop system with the reduced controller to check whether or not the upper bound of μ remains less than one.

The proposed strategy guarantees robust performance and robust stability for the closed-loop system.

3.2.2 Application to a 3-Control area power system

A sample power system with three control areas under the pluralistic LFC scheme is shown in Fig. 3.17. Each control area has some Gencos and each Genco is considered as a generator unit (Gunit). It is assumed that one generator unit with enough capacity is responsible to regulate the area-load frequency.

A control area may have a contract with a Genco in the other control area. For example, control area 3 buys power from G_{11} in control area 1 to supply its load. The power system data is given in Table 3.3. Next, the synthesis procedure in control area 1 is described in detail, and the final results are presented for other two areas.

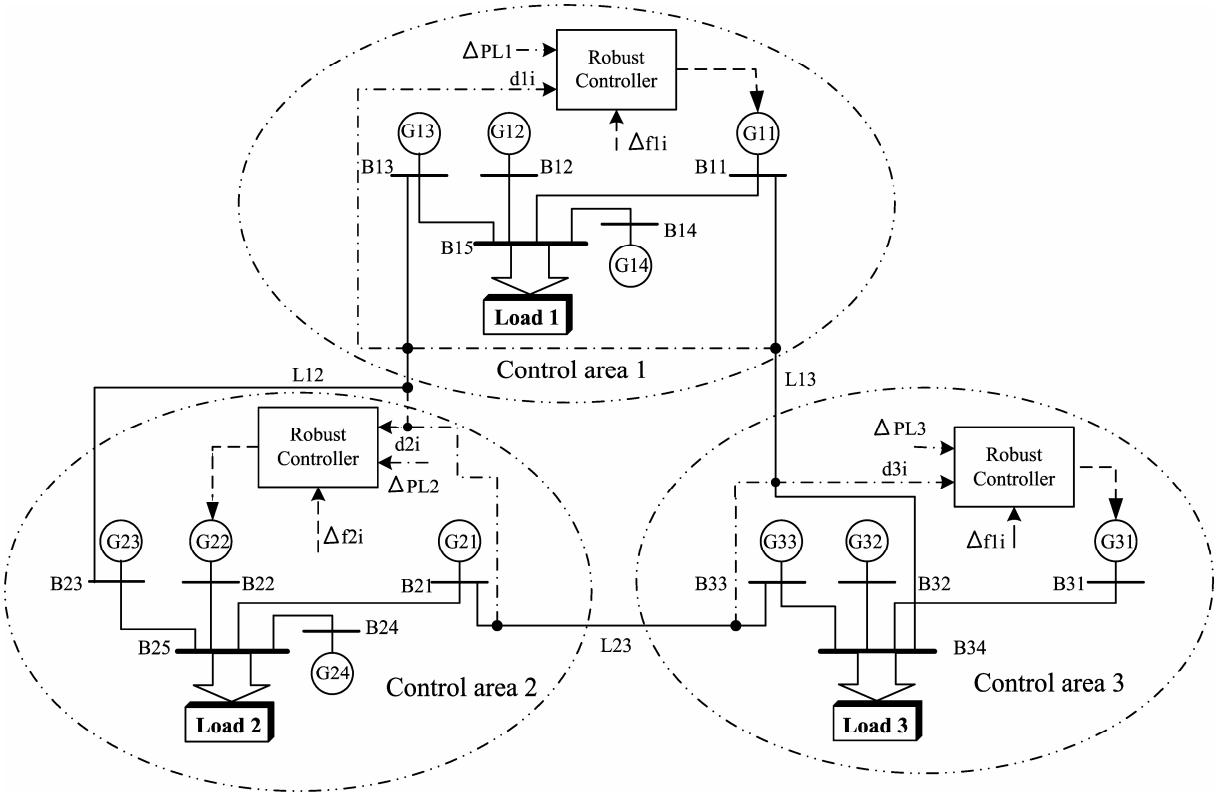

Figure 3.17: 3-control area power system

Table 3.3: Applied data for simulation

Quantity	*G11*	*G12*	*G13*	*G14*	*G21*	*G22*	*G23*	*G24*	*G31*	*G32*	*G33*
Rating (*MW*)	1600	600	800	800	600	1200	800	1000	1400	600	600
H_i (*sec*)	5	4	4	5	4	5	4	5	5	4	4
D_i (*pu MW/Hz*)	0.02	0.01	0.01	0.015	0.01	0.02	0.01	0.015	0.02	0.01	0.01
R_i (%)	4	5.2	5.2	5	5.2	4	5.2	5	4	5.2	5.2
$M_i = 2H_i/f_0$	0.167	0.134	0.134	0.167	0.134	0.167	0.134	0.167	0.167	0.134	0.134
T_{ti}	0.5	0.5	0.5	0.5	0.5	0.5	0.5	0.5	0.5	0.5	0.5
T_{gi}	0.2	0.1	0.15	0.1	0.1	0.2	0.15	0.1	0.2	0.1	0.1
K_{ti}, K_{gi}	1	1	1	1	1	1	1	1	1	1	1
T_i	0.2	0.1	0.1	0.2	0.1	0.2	0.1	0.2	0.2	0.1	0.1
T_{ij} (*MW/rad*)	T_{12} = 60		T_{13} = 60		T_{23} = 100						

According to Eq. (2.15), the state space model of control area 1 is obtained as

$$\dot{x} = Ax + Bu + Fw \tag{3.28}$$

where

$$x^T = \lfloor X_1 \quad X_2 \quad X_3 \quad X_4 \quad X_5 \rfloor$$

$$X_i = \left[\Delta f_i \quad \Delta P_{ti} \quad \Delta P_{gi} \right], \; i=1,\ldots,4; \quad X_5 = \lfloor \Delta\delta_{12} \quad \Delta\delta_{13} \quad \Delta\delta_{14} \quad \Delta\delta_1 \rfloor$$

3.2.2.1 Design objectives Control area 1 delivers enough power from G_{11} and firm power from other Gencos to supply its load and support the LFC task. In the case of a load disturbance, G_{11} must adjust its output to track the load changes and maintain the energy balance.

Simulation results show that the open-loop system performance is affected by individual changes of H_1 and H_3 (constants of inertia), which are more significant than changes to the other parameters of the control areas within a reasonable range. Eigenvalue analysis shows that a considerable change in these parameters leads the power system to an unstable condition. Therefore, from the aspect of uncertainty, our focus is concentrated on the variations of H_1 and H_3 parameters, these are the sources of uncertainty associated with the control area model and important parameters from the aspect of control.

Next, these uncertainties are modeled as an unstructured multiplicative uncertainty block that contains all the information available about H_1 and H_3 variations. It is notable that we are not under obligation to consider the uncertainty in only a few parameters.

The objectives are considered as follows for the control area 1:

1- Hold robust stability and robust performance in the presence of 75% uncertainty for H_1 and H_3 (This variation range leads the control area system to an unstable condition).
2- Hold robust stability and desired reference tracking for a 10% demand load change in control area ($0 \le \Delta P_L(\%) \le 10$).
3- Minimize the impacts of step disturbance from outside areas (*d*) through the L_{12} and L_{13}.
4- Maintain acceptable overshoot and settling time on the area frequency deviation and power changing signals.
5- Set a reasonable limit on the control action signal with regard to changes in speed and amplitude.

3.2.2.2 Uncertainty weight selection The related uncertainty weighting function in each control area is easily determined using the method described in the section 3.1.3.1. Some sample uncertainties corresponding to different values of H_1 and H_3 are shown in Fig. 3.18. This figure shows that the frequency responses of parametric uncertainties are close to each other. Hence to keep the complexity of the obtained controller at a low

level, according to the above result, the uncertainties due to H_1 and H_3 variation can be modeled by using a single norm bonded multiplicative uncertainty to cover all possible plants as follows (The frequency response of $W_U(s)$ is also shown in Fig. 3.18).

$$W_U(s) = \frac{-10(s+0.04)}{s+15} \tag{3.29}$$

3.2.2.3 Performance weight selection The performance weight selection in a μ-based LFC synthesis is explained in the section 3.1.3.2 in detail. Here, the weight on the control input W_{P1} is chosen to penalize fast change and large overshoot in the control input. The weights on the input disturbance from other areas (W_{P3}) and output error (W_{P2}) are chosen to get disturbance rejection, good tracking and zero steady-state error. In order to reject disturbances and track command signal property, it is required that the singular value of sensitivity function be reduced at low frequencies, W_{P2} and W_{P3} must be selected so that this condition is satisfied. For the problem at hand, a suitable set of performance weighting functions that offers a good compromise among all the conflicting time-domain specifications is

$$W_{p1}(s) = \frac{0.1s}{0.01s+1},\ W_{p2}(s) = \frac{0.005s+1}{35.7s+0.04},\ W_{p3}(s) = \frac{0.9s+0.9}{100s+1} \tag{3.30}$$

The next task is to isolate the uncertainties from the nominal plant model and redraw the system in the standard M-Δ configuration. Using the uncertainty description and performance weights that have been developed, an uncertainty structure Δ with a scalar block (corresponding to the uncertainty) and a 3×3 block (corresponding to the performance) is obtained.

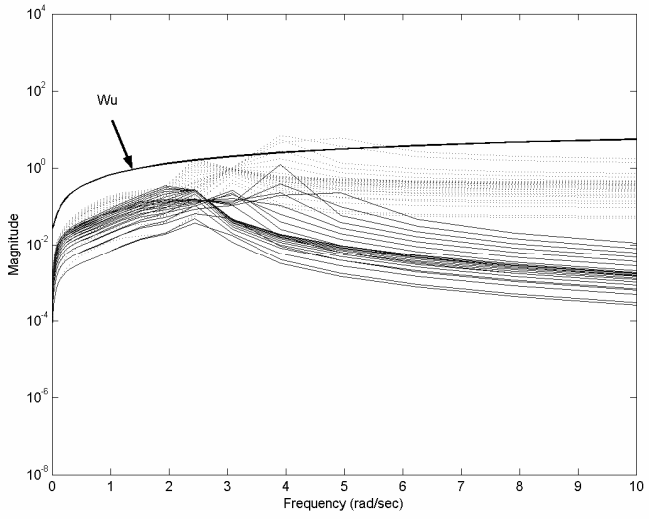

Figure 3.18: Uncertainty plot due to change of H_1 (dotted) and H_3 (solid)

The controller $K_1(s)$ is found at the end of the 3rd *D-K* iteration, yielding the value of 0.994 on the upper bound on μ, thus guaranteeing robust performance. The resulting controller has a high order (29*th*). It is reduced to a 7th order with no performance degradation using the standard Hankel Norm approximation. The Bode plots of the full-order controller and the reduced-order controller are shown in Fig. 3.19. The transfer function of the reduced order controller is given as $K_1(s) = N_1(s)/D_1(s)$ with

$$\begin{aligned} N_1(s) &= 226.28\ s^6 + 23024.16\ s^5 + 20719\ s^4 + 153700\ s^3 + 245730 s^2 + 162930\,s + 844 \\ D_1(s) &= s^7 + 3240\ s^6 + 70777\ s^5 + 710490\ s^4 + 362130\ s^3 + 3853000 s^2 + 24901\,s + 21 \end{aligned} \tag{3.31}$$

Using the same procedure and setting similar objectives, as already discussed, gives us the desired robust load frequency controllers for control areas 2 and 3. The associated polynomials with $K_2(s)$ and $K_3(s)$ are:

$$\begin{aligned} N_2(s) &= 145s^5 + 1445267s^4 + 178943657s^3 + 96405249s^2 + 274613248s + 323019700 \\ D_2(s) &= s^6 + 288s^5 + 20235s^4 + 767219s^3 + 17402801s^2 + 226558154s + 226075 \end{aligned} \tag{3.32}$$

$$\begin{aligned} N_3(s) &= 226.3\,s^5 + 22873\,s^4 - 1616\,s^3 + 137110\,s^2 + 126934s + 533 \\ D_3(s) &= s^6 + 3239.8\,s^5 + 68092\,s^4 + 638727\,s^3 + 3016725\,s^2 + 16332.2s + 13.3 \end{aligned} \tag{3.33}$$

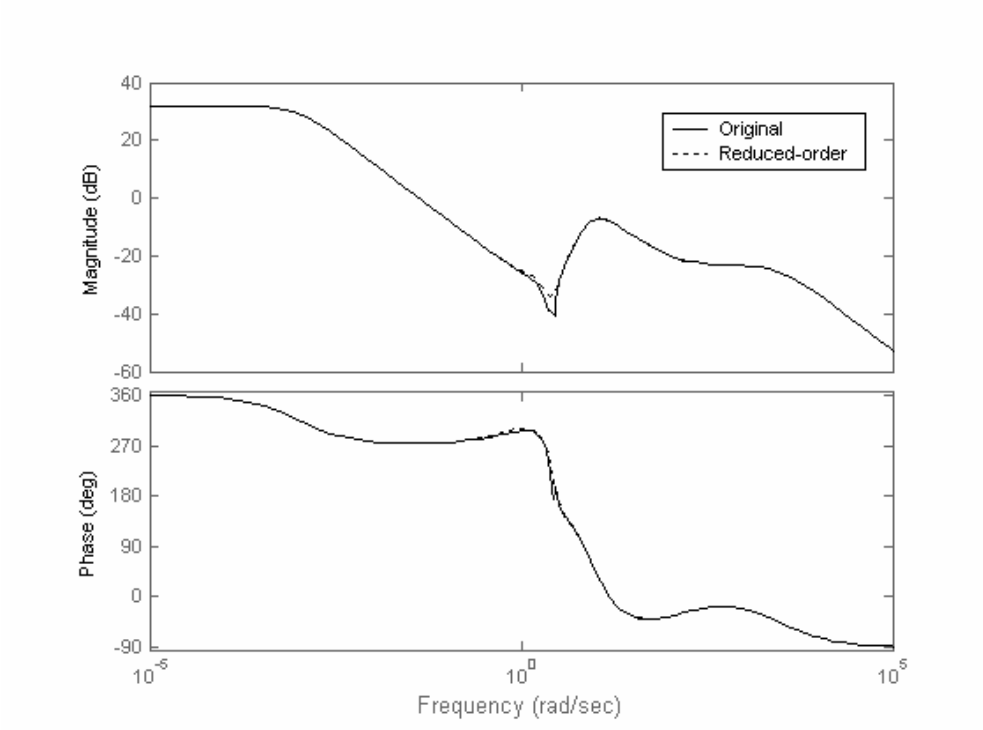

Figure 3.19: Bode plots comparison of the original and reduced-order controllers

3.2.3 Simulation results

The proposed load frequency controllers are applied to a 3-control area power system described in Fig. 3.17. Fig. 3.20 shows the frequency deviation in control area 1, following a 10% increase in the area-load. $\Delta f_{11},\cdots,\Delta f_{14}$ display the frequency deviation at Gencos G_{11}, …, G_{14}, respectively. At steady-state, the frequency in each control area reaches its nominal value. Fig. 3.21 shows the changes in power which comes to control area 1 from its Gencos. It is seen that the power is initially coming from all Gencos to respond to the load increase and will result in a frequency drop that is sensed by the speed governors of all machines. After a few seconds and at steady-state, the additional power comes only from G_{11} and the other Gencos do not contribute to the LFC task.

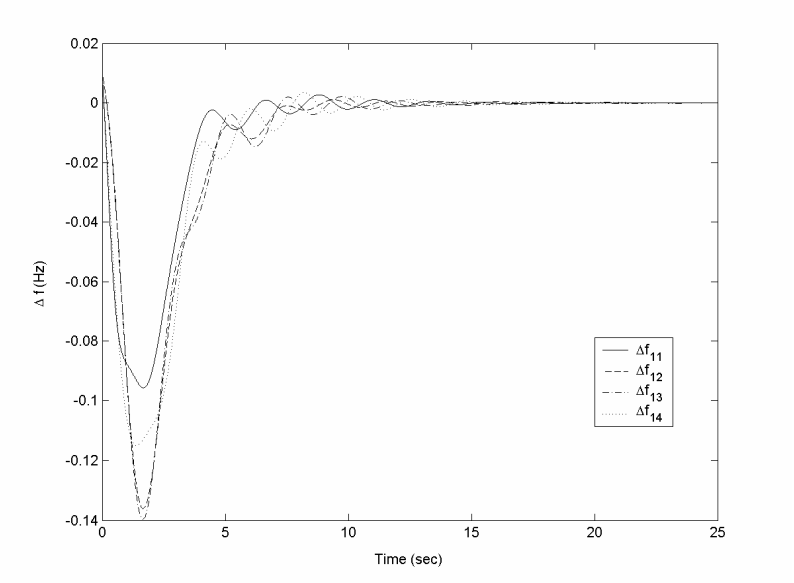

Figure 3.20: Frequency deviation in control area 1, following a 10% load increase

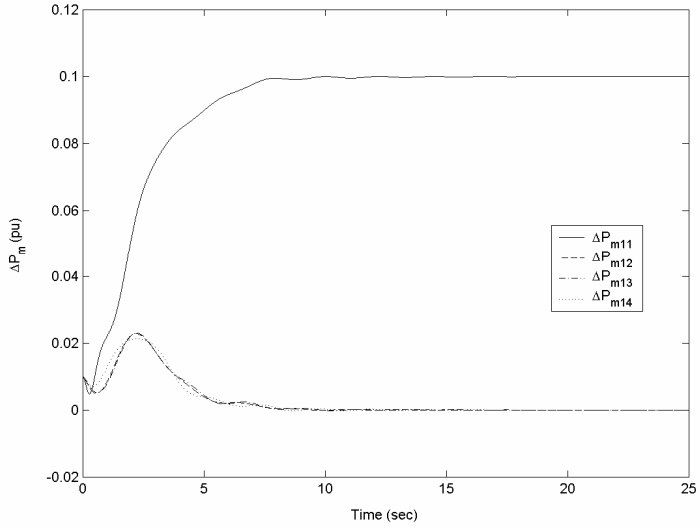

Figure 3.21: Change in supplied power in control area 1, following a 10% load increase

Fig. 3.22 demonstrates the disturbance rejection property of the closed loop system. This figure shows the frequency deviation at generation units in control area 1, following a step disturbance of *0.1 pu* on area interconnection lines L_{12} and L_{13} at *t=17s*. The power system is already started with a 10% load increase in each area. Fig. 3.23 shows the frequency deviation in control area 2 and 3, following a 10% load increase in each control area. Fig. 3.24 presents the frequency deviation and corresponding control action signals, following a large step disturbance *0.1 pu* on each interconnection line (L_{12}, L_{13} and L_{23}) in the presence the worst case of H_1 and H_3 uncertainties in three area, simultaneously. For the last simulation case, a random demand load signal shown in Fig. 3.25a, which represents the expected area demand load fluctuations, is applied to control area 1. The frequency deviations are shown in Figs. 3.25b to 3.25c. Power changes and control signals are given in Figs. 3.25d to 3.25e. These figures show that the controller tracks the load fluctuations effectively.

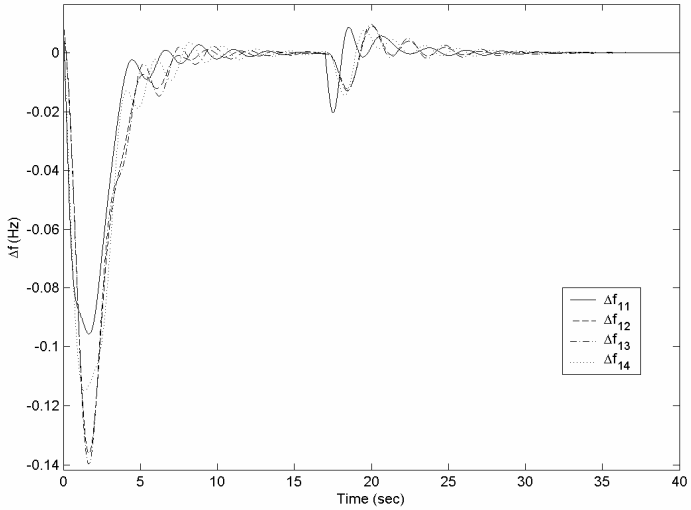

Figure 3.22: Frequency deviation in control area 1, following a *0.01 pu* step disturbance on interconnection lines at *t=17s* and 10% load increase at *t=0 s*

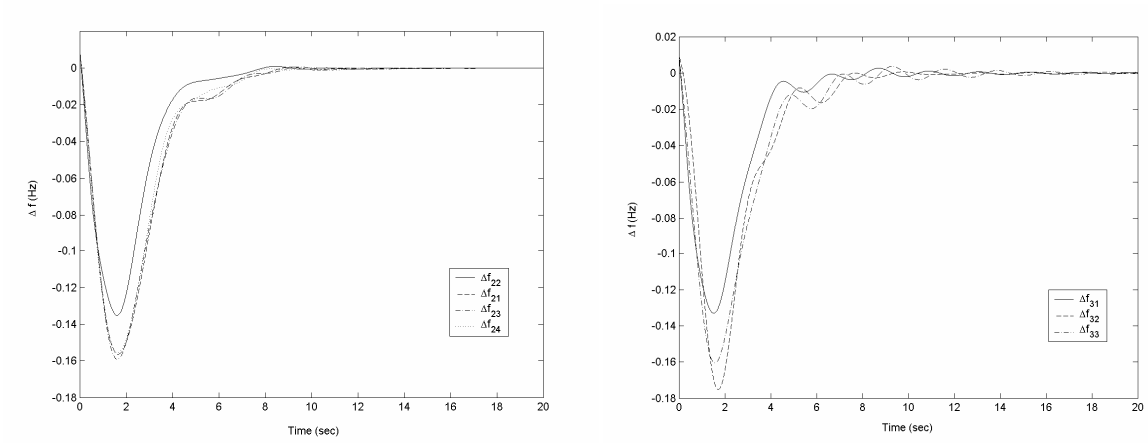

(a) (b)

Figure 3.23: Frequency deviation at Gencos in (a) control area 2, (b) control area 3, following a 10% load increase in each area

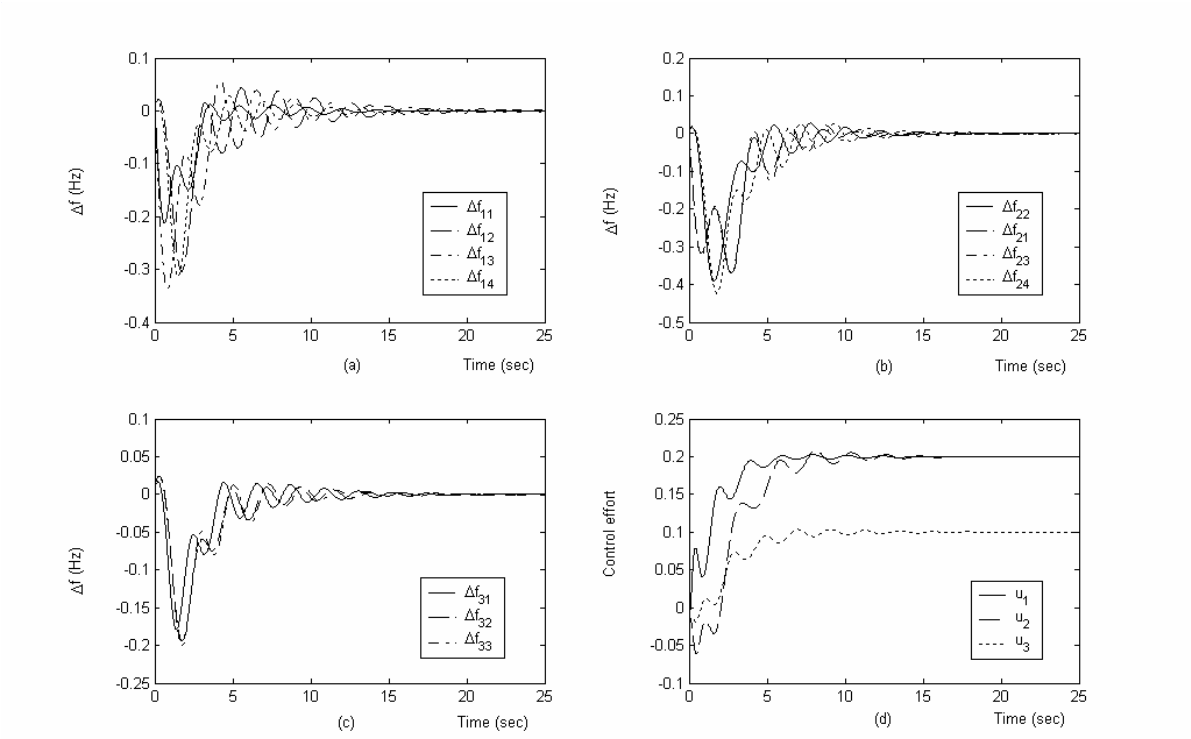

Figure 3.24: Frequency deviation in (a) area 1, (b) area 2, (c) area 3 and (d) control signals, following a step disturbance in interconnection lines and the worst case of uncertainties in each area

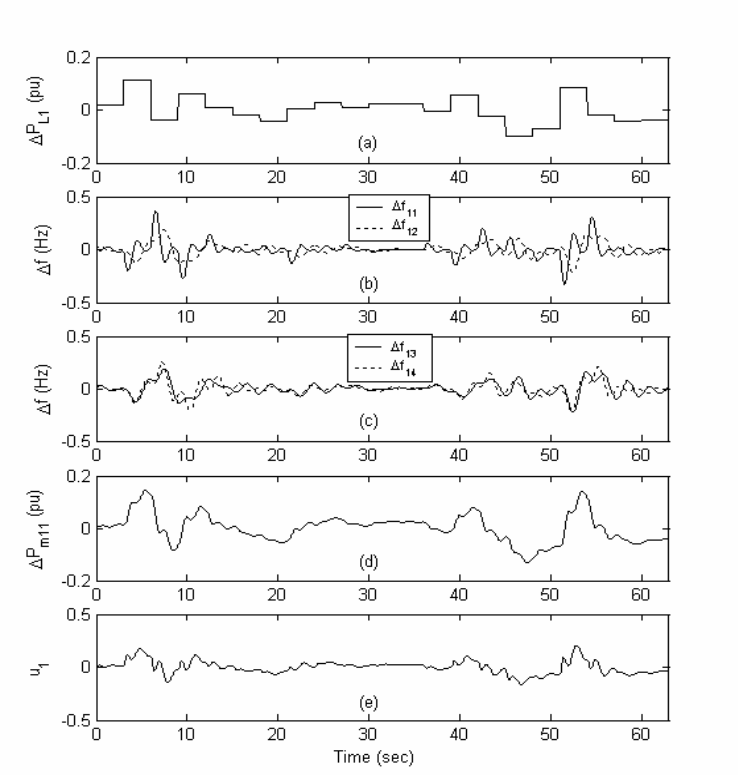

Figure 3.25: System response to random demand; a) Demand load, b) $\Delta f_{11}, \Delta f_{12}$, c) $\Delta f_{13}, \Delta f_{14}$, d) Power change at G_{11} and e) Control effort

Although in the proposed simulation, it seems that the frequency deviation and other signals have a fast behavior at startup time following a large step disturbance and/or parameter changes, they have started from zero. Here, academic examples (and data) have been used and the assumed parameters (in result dynamics of the simplified models) are not completely matched to the real ones and give the impression that the output of the models can be changed in a fast way (especially at startup time). In the LFC practice, rapidly varying components of system signals are almost unobservable due to filters involved in the process.

The proposed control strategies in the present chapter are flexible enough to set a desired level of performance to cover the practical constraint on a control action signal. It is easily carried out by tuning the considered fictitious weighting functions (W_{P1i} in Fig. 3.2 and W_{P1} in Fig. 3.15).

3.3 Summary

A new systematic method for robust sequential decentralized load frequency controllers using µ-synthesis in an interconnected multi-area power system has been proposed in the first section. In each design step, the information about the controllers designed in the previous steps is taken into account. Therefore, the method is less conservative than an independent decentralized design and more practical than the proposed simultaneous decentralized load frequency controller designs. The simulation results demonstrate the effectiveness of the proposed method for a solution to the LFC problem in the presence of uncertainties and load disturbances in multi-area power systems.

In the second section, a new method for robust LFC synthesis using structured singular value theory in a restructured power system has been proposed. The proposed method was applied to a 3-control area power system under the pluralistic LFC scheme. It was shown that the controllers that have been designed will guarantee the robust stability and robust performance under a wide range of parameter variation and area-load conditions.

3.4 References

[1] M. Chiu, Y. Arkun, “A methodology for sequential design of robust decentralized control systems,” *Automatica*, vol. 28, pp. 997-1001, 1992.

[2] J. C. Doyle, “Analysis of feedback systems with structured uncertainties,” *IEE Proc.*, Pt. D, vol. 129, pp. 242-250, 1982.

[3] M. Djukanovic, M. Khammash, V. Vittal, “Structured singular value theory based stability robustness of power systems,” in Proc. *IEEE Conf. on Decision & Control*, pp. 2702-2707, 1997.

[4] H. Bevrani, “Robust load frequency controller in a deregulated environment: A µ-synthesis approach,” in Proc. *IEEE Int. Conf. on Control applications*, pp. 616-621, 1999.

[5] S. Skogestad, I. Postlethwaite, “Multivariable feedback control,” John Wiley & Sins Inc., pp. 397-448, 2000.

[6] M. Hovd, S. Skogestad, “Sequential design of decentralised controllers,” *Automatica*, vol. 30, pp. 1610-1607, 1994.

[7] G. J. Balas, J. C. Doyle, K. Glover, A. Packard, R. Smith, “µ-Analysis and Synthesis Toolbox for use with MATLAB,” The MathWorks Inc., 1995.

[8] M. Djukanovic, M. Khammash, V. Vittal, "Sequential synthesis of structured singular value based decentralized controllers in power systems," *IEEE Trans. Power Systems*, vol. 14, pp. 635-641, 1999.

[9] T. Hiyama, "Design of decentralised load-frequency regulators for interconnected power systems," *IEE Proc.* Pt. C, vol. 129, pp. 17-23, 1982.

[10] T. C. Yang, H. Cimen, Q. M. Zhu, "Decentralised load frequency controller design based on structured singular values," *IEE Proc. Gener. Transm. Distrib.*, vol. 145, no. 1, pp. 7-14, 1998.

[11] T. C. Yang, Z. T. Ding, H. Yu, "Decentralized power system load frequency control beyond the limit of diagonal dominance," *Electrical power and Energy system*, vol. 24, pp. 173-184, 2002.

[12] H. Bevrani, Y. Mitani, K. Tsuji, "Robust load frequency regulation in a new distributed generation environment," in Proc. *2003 IEEE-PES General Meeting* (CD Record), Toronto, Canada, 2003.

Chapter 4

H_∞ based robust decentralized LFC design

There has been continuing interest in designing load-frequency controllers with better performance to maintain the frequency and to keep tie-line power flows within pre-specified values, using various robust and optimal control methods during the last two decades [1-8]. But most of them suggest complex state-feedback or high-order dynamic controllers, which are impractical for industry practices. Furthermore, some authors have used the new and untested LFC frameworks, which may have some difficulties in being implemented in real-world power systems. In practice, load-frequency control (LFC) systems use simple proportional-integral (PI) controllers. However, since the PI controller parameters are usually tuned based on experiences, classical, or trial-and-error approaches, they are incapable of obtaining good dynamical performance for a wide range of operating conditions and various load changes scenarios in a multi-area power system.

Recently, some control methods have been applied to the design of decentralized robust PI or low order controllers to solve the LFC problem [9-12]. A PI control design method has been reported in [9], which used a combination of H_∞ control and genetic algorithm techniques for tuning the PI parameters. The sequential decentralized method based on μ-synthesis and analysis has been used to obtain a set of low order robust controllers [10]. The decentralized LFC method has been used with the structured singular values [11]. The Kharitonov's theorem and its results have been used to solve the same problem [12].

In this chapter, the decentralized LFC synthesis is formulated as an H_∞-based static output feedback (SOF) control problem, and is solved using an iterative linear matrix inequalities (ILMI) algorithm to design robust PI controllers in the multi-area power systems. Two multi-area power system examples using both traditional and bilateral based LFC schemes with a wide range of load changes are given to illustrate the proposed approach. The obtained controllers are shown to minimize the effect of disturbances and maintain the robust performance.

This chapter is organized as follows. Technical background on H_∞-based SOF controller design using an ILMI approach is given in section 4.1. Section 4.2 presents the transformation from PI to SOF control design. The proposed methodology is applied to multi-area power system examples with traditional and bilateral configuration in sections 4.3 and 4.4.

4.1 H_∞-based SOF control design using an ILMI algorithm

This section gives a brief overview of H_∞-based SOF control design based on an ILMI approach. Consider a linear time invariant system *G(s)* with the following state-space realization.

$$\begin{aligned} \dot{x} &= Ax + B_1 w + B_2 u \\ z &= C_1 x + D_{12} u \\ y &= C_2 x \end{aligned} \tag{4.1}$$

where *x* is the state variable vector, *w* is the disturbance and other external input vector, *z* is the controlled output vector and *y* is the measured output vector.

The H_∞-based SOF control problem is to find a static output feedback law $u = Ky$, as shown in Fig. 4.1, such that the resulted closed-loop system is internally stable, and the H_∞ norm from *w* to *z* is smaller than γ, a specified positive number, i.e.

$$\left\| T_{zw}(s) \right\|_\infty < \gamma \tag{4.2}$$

<u>*Lemma 4.1*</u>: It is assumed that (A, B_2, C_2) is stabilizable and detectable. The matrix *K* is an H_∞ controller, if and only if there exists a symmetric matrix $X > 0$ such that

$$\begin{bmatrix} A_{cl}^T X + X A_{cl} & X B_{cl} & C_{cl}^T \\ B_{cl}^T X & -\gamma I & D_{cl}^T \\ C_{cl} & D_{cl} & -\gamma I \end{bmatrix} < 0 \tag{4.3}$$

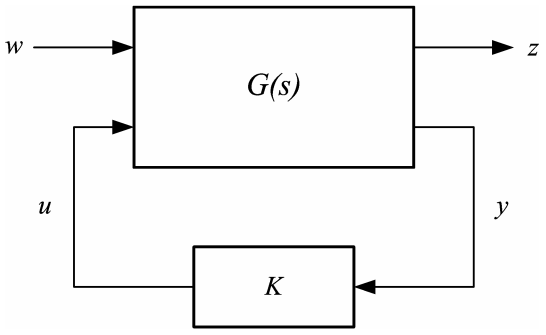

Figure 4.1: Closed-loop system via H_∞ control

where

$$A_{cl} = A + B_2 K C_2, \quad B_{cl} = B_1$$
$$C_{cl} = C_1 + D_{12} K C_2, \quad D_{cl} = 0$$

The proof is given in [13] and [14]. We can rewrite (4.3) as the following matrix inequality [15],

$$\overline{XB}K\overline{C} + (\overline{XB}K\overline{C})^T + \overline{A}^T\overline{X} + \overline{XA} < 0 \tag{4.4}$$

where

$$\overline{A} = \begin{bmatrix} A & B_1 & 0 \\ 0 & -\gamma I/2 & 0 \\ C_1 & 0 & -\gamma I/2 \end{bmatrix}, \quad \overline{B} = \begin{bmatrix} B_2 \\ 0 \\ D_{12} \end{bmatrix}, \quad \overline{C} = \begin{bmatrix} C_2 & 0 & 0 \end{bmatrix}, \quad \overline{X} = \begin{bmatrix} X & 0 & 0 \\ 0 & I & 0 \\ 0 & 0 & I \end{bmatrix} \tag{4.5}$$

Hence, the H_∞-based SOF control problem is reduced to find $X > 0$ and K such that matrix inequality (4.4) holds. It is a generalized static output feedback stabilization problem of the system $(\overline{A}, \overline{B}, \overline{C})$ which can be solved via lemma 4.2.

Lemma 4.2: The system (*A, B, C*) that may also be identified by the following representation:

$$\begin{aligned} \dot{x} &= Ax + Bu \\ y &= Cx \end{aligned} \tag{4.6}$$

is stabilizable via static output feedback if and only if there exist $P>0$, $X>0$ and K satisfying the following quadratic matrix inequality

$$\begin{bmatrix} A^T X + XA - PBB^T X - XBB^T P + PBB^T P & (B^T X + KC)^T \\ B^T X + KC & -I \end{bmatrix} < 0 \tag{4.7}$$

Proof. According to the Schur complement, the quadratic matrix inequality (4.7) is equivalent to the following matrix inequality

$$A^T X + XA - PBB^T X - XBB^T P + PBB^T P + (B^T X + KC)^T (B^T X + KC) < 0 \tag{4.8}$$

For this new inequality notation (4.8), the sufficiency and necessity of theorem are already proven [16].

A solution of the consequent non-convex optimization problem, introduced in lemma 4.2, cannot be directly achieved using the general LMI technique. On the other hand, the matrix inequality (4.7) points to an iterative approach to solve the matrix *K* and *X*, namely, if *P* is fixed, then it reduces to an LMI problem in the unknowns

K and *X*. For this purpose, we introduce an iterative LMI algorithm that is mainly based on the approach given in [16]. The key point is to formulate the H_∞ problem via a generalized static output stabilization feedback, such that all eigenvalues of (*A-BKC*) shift towards the left half-plane through the reduction of *a*, a real number, to close to feasibility of (4.7).

In summary, the H_∞-based SOF controller design based on ILMI approach for a given system consists of the following steps:

Step 1. Compute the new system $(\overline{A},\overline{B},\overline{C})$, according to (4.5). Set $i=1$ and $\Delta\gamma=\Delta\gamma_0$. Let $\gamma_i=\gamma_0$ a positive real number.

Step 2. Select $Q>0$, and solve $\overline{X}$ from the following algebraic Riccati equation:

$$\overline{A}^T\overline{X}+\overline{X}\overline{A}-\overline{X}\overline{B}\overline{B}^T\overline{X}+Q=0 \tag{4.9}$$

Set $P_1=\overline{X}$.

Step 3. Solve the following optimization problem for $\overline{X}_i$, K_i and a_i. Minimize a_i subject to the LMI constraints:

$$\begin{bmatrix} \overline{A}^T\overline{X}_i+\overline{X}_i\overline{A}-P_i\overline{B}\overline{B}^T\overline{X}_i-\overline{X}_i\overline{B}\overline{B}^TP_i+P_i\overline{B}\overline{B}^TP_i-a_i\overline{X}_i & (\overline{B}^T\overline{X}_i+K_i\overline{C})^T \\ \overline{B}^T\overline{X}_i+K_i\overline{C} & -I \end{bmatrix}<0 \tag{4.10}$$

$$\overline{X}_i=\overline{X}_i^T>0 \tag{4.11}$$

Denote a_i^* as the minimized value of a_i.

Step 4. If $a_i^*\le 0$, go to step 8.

Step 5. For $i>1$ if $a_{i-1}^*\le 0$, K_{i-1} is desired H_∞ controller and $\gamma^*=\gamma_i+\Delta\gamma$ indicates a lower bound such that the above system is H_∞ stabilizable via static output feedback.

Step 6. Solve the following optimization problem for $\overline{X}_i$ and K_i:

Minimize trace($\overline{X}_i$) subject to the above LMI constraints (4.10) and (4.11) with $a_i=a_i^*$. Denote $\overline{X}_i^*$ as the $\overline{X}_i$ that minimized trace($\overline{X}_i$).

Step 7. Set $i=i+1$ and $P_i=\overline{X}_{i-1}^*$, then go to step 3.

Step 8. Set $\gamma_i=\gamma_i-\Delta\gamma$, $i=i+1$. Then do steps 2 to 4.

The matrix inequalities (4.10) and (4.11) give a sufficient condition for the existence of the static output feedback controller.

4.2 Transformation from PI to SOF control problem

According to Fig. 2.1 and Fig. 2.3, in each control area the ACE acts as the input signal of the PI controller which is used by the LFC system. Therefore we have

$$u_i = \Delta Pci = k_{Pi} ACE_i + k_{Ii} \int ACE_i \tag{4.12}$$

Where k_{Pi} and k_{Ii} are constant real numbers. By augmenting the system description (4.1) to include the ACE signal and its integral as a measured output vector, the PI control problem becomes one of finding a static output feedback that satisfies prescribed performance requirements. Using this strategy, the PI-based LFC design can be reduced to an H_∞-based SOF control problem as shown in Fig. 4.2. To change (4.12) to a simple SOF control as

$$u_i = K_i y_i \tag{4.13}$$

We can rewrite (4.12) as follows,

$$u_i = [k_{Pi} \quad k_{Ii}] \begin{bmatrix} ACE_i \\ \int ACE_i \end{bmatrix} \tag{4.14}$$

Therefore, y_i in (4.13) can be augmented as given in (4.15).

$$y_i^T = [ACE_i \quad \int ACE_i] \tag{4.15}$$

In the next step, according to synthesis methodology described in the previous section and summarized in Fig. 4.3, a robust PI controller to be designed for the given area.

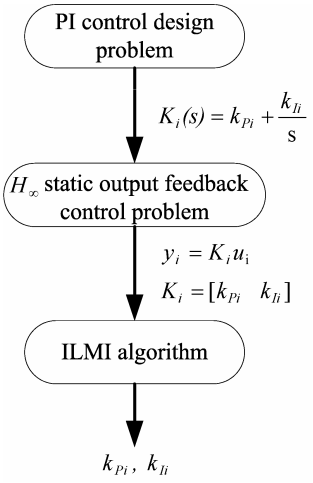

Figure 4.2: Problem formulation

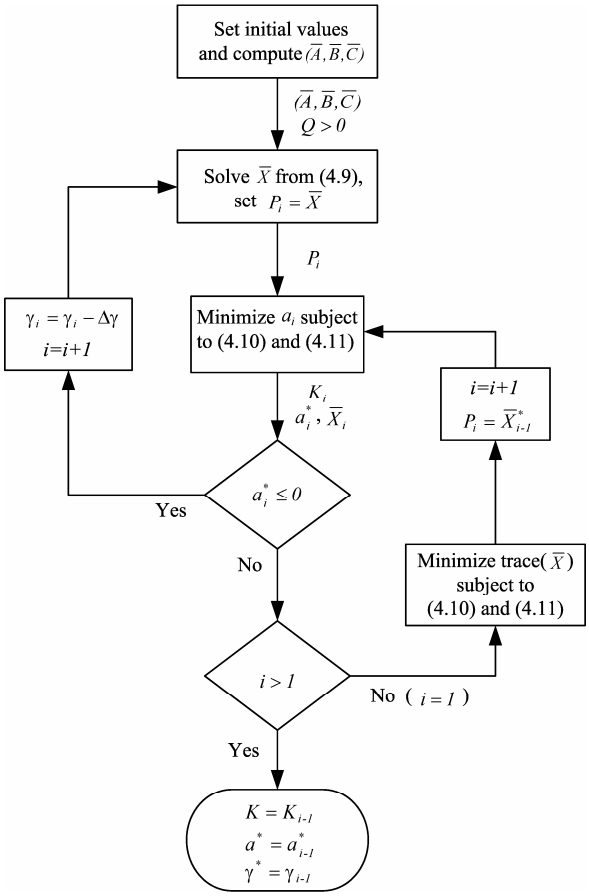

Figure 4.3: Proposed ILMI algorithm

4.3 Application to a traditional-based LFC scheme

4.3.1 Control framework

The main control framework to formulate the PI-based LFC via an H_∞-based SOF control design problem, for a given control area, is shown in Fig. 4.4. $G_i(s)$ denotes the dynamical model corresponds to the control area *i* shown in Fig. 2.1. According to Eq. (4.1), the state space model for each control area *i* can be obtained as

$$\begin{aligned} \dot{x}_i &= A_i x_i + B_{1_i} w_i + B_{2i} u_i \\ z_i &= C_{1i} x_i + D_{12i} u_i \\ y_i &= C_{2i} x_i \end{aligned} \tag{4.16}$$

where

$$x_i^T = [\Delta f_i \quad \Delta P_{tie-i} \quad \int ACE_i \quad x_{ti} \quad x_{gi}] \tag{4.17}$$

$$x_{ti} = \left[\Delta P_{t1i} \quad \Delta P_{t2i} \quad \cdots \quad \Delta P_{tni}\right], \quad x_{gi} = \left[\Delta P_{g1i} \quad \Delta P_{g2i} \quad \cdots \quad \Delta P_{gni}\right]$$

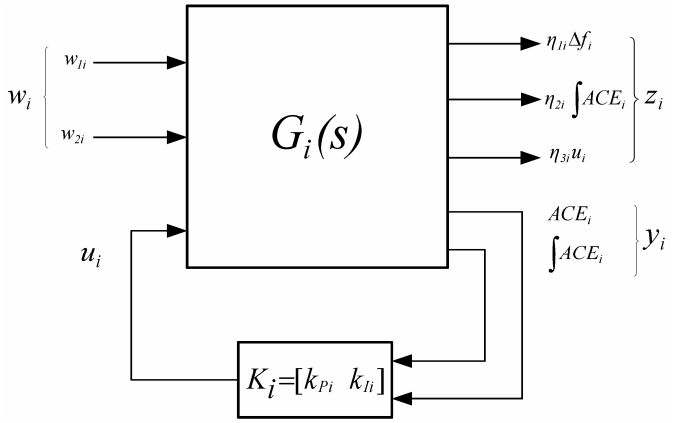

Figure 4.4: Proposed control framework

$$y_i^T = [ACE_i \quad \int ACE_i], \quad u_i = \Delta P_{Ci} \tag{4.18}$$

$$z_i^T = [\eta_{1i}\Delta f_i \quad \eta_{2i}\int ACE_i \quad \eta_{3i}u_i] \tag{4.19}$$

$$w_i^T = [w_{1i} \quad w_{2i}] \tag{4.20}$$

and,

$$A_i = \begin{bmatrix} A_{i11} & A_{i12} & A_{i13} \\ A_{i21} & A_{i22} & A_{i23} \\ A_{i31} & A_{i32} & A_{i33} \end{bmatrix}, \quad B_{1i} = \begin{bmatrix} B_{1i1} \\ B_{1i2} \\ B_{1i3} \end{bmatrix}, \quad B_{2i} = \begin{bmatrix} B_{2i1} \\ B_{2i2} \\ B_{2i3} \end{bmatrix}$$

$$C_{1i} = [c_{1i} \quad 0_{3\times n} \quad 0_{3\times n}], \quad c_{1i} = \begin{bmatrix} \eta_{1i} & 0 & 0 \\ 0 & 0 & \eta_{2i} \\ 0 & 0 & 0 \end{bmatrix}, \quad D_{12i} = \begin{bmatrix} 0 \\ 0 \\ \eta_{3i} \end{bmatrix}$$

$$C_{2i} = [c_{2i} \quad 0_{2\times n} \quad 0_{2\times n}], \quad c_{2i} = \begin{bmatrix} B_i & 1 & 0 \\ 0 & 0 & 1 \end{bmatrix}$$

$$A_{i11} = \begin{bmatrix} -D_i/M_i & -1/M_i & 0 \\ 2\pi\sum_{\substack{j=1 \\ j\neq i}}^{N} T_{ij} & 0 & 0 \\ B_i & 1 & 0 \end{bmatrix}, \quad A_{i12} = \begin{bmatrix} 1/M_i & \cdots & 1/M_i \\ 0 & \cdots & 0 \\ 0 & \cdots & 0 \end{bmatrix}_{3\times n}$$

$$A_{i22} = -A_{i23} = diag[-1/T_{t1i} \quad -1/T_{t2i} \quad \cdots \quad -1/T_{tni}]$$

$$A_{i33} = diag[-1/T_{g1i} \quad -1/T_{g2i} \quad \cdots \quad -1/T_{gni}]$$

$$A_{i31} = \begin{bmatrix} -1/(T_{g1i}R_{1i}) & 0 & 0 \\ \vdots & \vdots & \vdots \\ -1/(T_{gni}R_{ni}) & 0 & 0 \end{bmatrix}, \quad A_{i13} = A_{i21}{}^{\mathrm{T}} = 0_{3\times n}, \quad A_{i32} = 0_{n\times n}$$

$$B_{1i1} = \begin{bmatrix} -1/M_i & 0 \\ 0 & -2\pi \\ 0 & 0 \end{bmatrix}, \quad B_{1i2} = B_{1i3} = 0_{n\times 2}$$

$$B_{2i1} = 0_{3\times 1}, B_{2i2} = 0_{n\times 1}, \quad B_{2i3}{}^{T} = \begin{bmatrix} \alpha_{1i}/T_{g1i} & \alpha_{2i}/T_{g2i} & \cdots & \alpha_{ni}/T_{gni} \end{bmatrix}$$

Similar to [9], three constant weighting coefficients are considered for controlled output signals. η_{1i}, η_{2i}, and η_{3i} must be chosen by the designer to obtain the desired performance. In the next section, two types of robust controllers are developed for a power system example including three control areas. The first one is a dynamic controller based on general robust LMI-based H_∞ control design and the second controller is based on H_∞-based SOF control approach using developed ILMI algorithm (described in section 4.1) with the same assumed objectives to achieve robust performance.

4.3.2 Case study

To illustrate the effectiveness of the proposed control strategy, a 3-control area power system, shown in Fig. 4.5, is considered as a test system. It is assumed that each control area includes three Gencos. The power system parameters are considered to be the same as in [9].

For the sake of comparison, in addition to the proposed control strategy to obtain the robust PI controller, a robust H_∞ dynamic output feedback controller using the LMI control toolbox is designed for each control area. Specifically, based on general LMI, the control design is first reduced to an LMI formulation [9], and then the H_∞ control problem is solved using the function *hinflmi*, provided by the MATLAB LMI control toolbox [17]. This function gives an optimal H_∞ controller through minimizing the guaranteed robust performance index (γ) subject to the constraint given by the matrix inequality (4.3) and returns the controller *K(s)* with the optimal robust performance index. The resulted controllers using the *hinflmi* function are of dynamic type and have the following state-space form, whose orders are the same size as the plant model (9^{th} order in the present example).

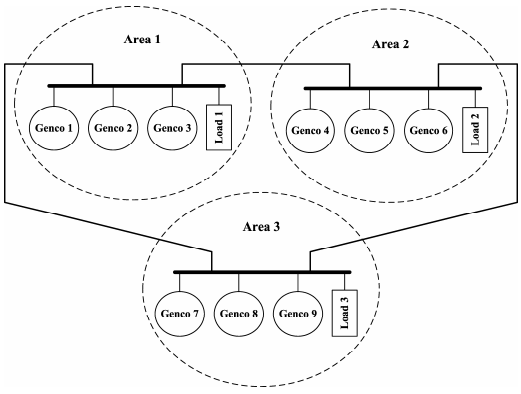

Figure 4.5: 3-control area power system

$$\begin{aligned} \dot{x}_{ki} &= A_{ki}x_{ki} + B_{ki}y_i \\ u_i &= C_{ki}x_{ki} + D_{ki}y_i \end{aligned} \tag{4.21}$$

In the next step, according to the described synthesis methodology summarized in Fig. 4.2, a set of three decentralized robust PI controllers are designed. As already mentioned, this control strategy is entirely suitable for LFC applications which usually employ the PI control, while most other robust and optimal control designs (such as the LMI approach) yield complex controllers whose size can be larger than real-world LFC systems. Using the ILMI approach, the controllers are obtained following several iterations. The control parameters are shown in Table 4.1.

A set of suitable values for constant weights [η_{1i} , η_{2i} , η_{3i}] can be chosen as [0.5, 1, 500], respectively. An important issue with regards to the selection of these weights is the degree to which they can guarantee the satisfaction of design performance objectives. The selection of these weights entails a trade-off among several performance requirements. The coefficients η_{1i} and η_{2i} at controlled outputs set the performance goals; e.g. tracking the load variation and disturbance attenuation. η_{3i} sets a limit on the allowed control signal to penalize fast change and large overshoot in the governor load set-point signal. The recent objective is very important to realize the designed controller in the real-world power systems. The large coefficient "500' for η_{3i} results in a smooth control action signal with reasonable changes in amplitude.

It is notable that the robust performance index given by the standard H_∞ control design can be used as a valid measure tool to analyze the robustness of the closed-loop system for the proposed control design. The resulting robust performance indices (γ^*) of both synthesis methods are close to each other and shown in Table 4.2. It shows that although the proposed ILMI approach gives a set of much simpler controllers (PI) than the LMI based dynamic H_∞ design, they also give a robust performance like the dynamic H_∞ controllers.

Table 4.1: Control parameters (ILMI design)

Parameter	*Area 1*	*Area 2*	*Area 3*
a^*	-0.3285	-0.2472	-0.3864
k_{Pi}	0.0371	0.0465	0.0380
k_{Ii}	-0.2339	-0.2672	-0.3092
η_{ji}	η_{1i} =0.5	η_{2i} =1	η_{3i} =500

Table 4.2: Robust performance index

Control design	*Control structure*	*Performance index*	*Area1*	*Area 2*	*Area 3*
H∞	9^{th} order	γ	500.0103	500.0045	500.0065
ILMI	PI	γ^*	500.0183	500.0140	500.0105

4.3.3 Simulation results

The proposed controllers were applied to the 3-control area power system described in Fig. 4.5. In this section, the performance of the closed-loop system using the robust PI controllers compared to the designed dynamic H_∞ controllers will be tested for the various load disturbances.

Case 1:

As the first test case, the following load disturbances (step increase in demand) are applied to three areas:

$$\Delta P_{d1} = 100\ MW,\ \Delta P_{d2} = 80\ MW,\ \Delta P_{d3} = 50\ MW$$

The frequency deviation (Δf), area control error (ACE), and control action (ΔPc) signals of the closed-loop system are shown in Fig. 4.6. Using the proposed method (ILMI), the area control error and frequency deviation of all areas are quickly driven back to zero as well as dynamic H_∞ control (LMI).

Case 2:

Consider larger demands by area 2 and area 3, i.e.

$$\Delta P_{d1} = 100\ MW,\ \Delta P_{d2} = 100\ MW,\ \Delta P_{d3} = 100\ MW$$

The closed-loop response for each control area is shown in Fig. 4.7.

Case 3:

As another severe condition, assume a bounded random load change shown in Fig. 4.8a is applied to all control areas simultaneously, where

$$-50\ MW \le \Delta P_d \le +50\ MW$$

The purpose of this scenario is to test the robustness of the proposed controllers against random large load disturbances. The control area responses are shown in Fig. 4.8b to Fig. 4.8d. This figure demonstrates that the designed controllers track the load fluctuations effectively. The simulation results show the proposed PI controllers perform as robustly as robust dynamic H_∞ controllers (with complex structures) for a wide range of load disturbances.

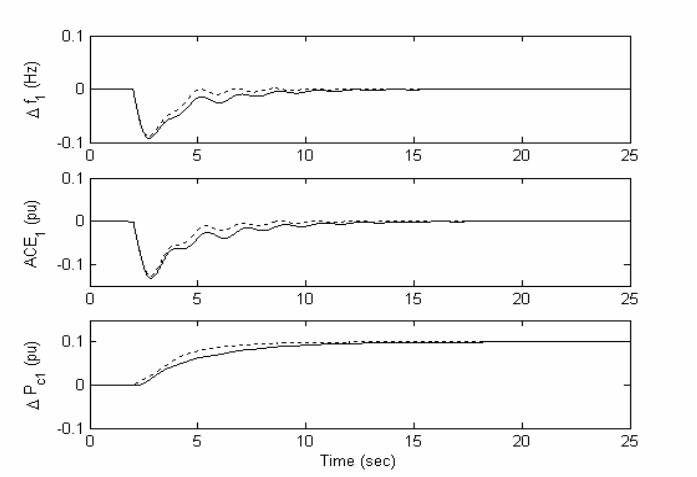

(a)

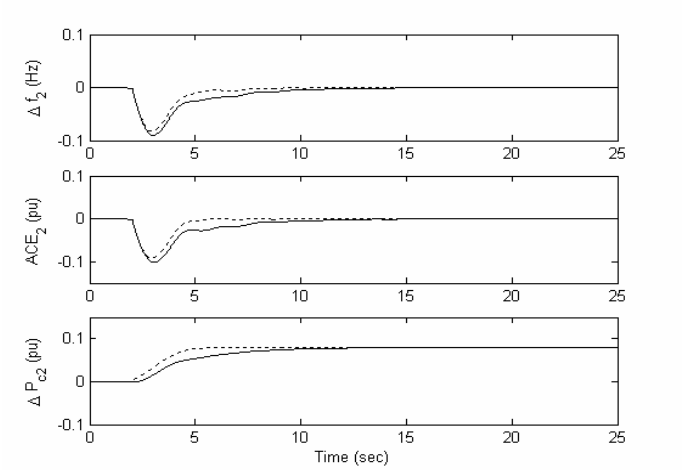

(b)

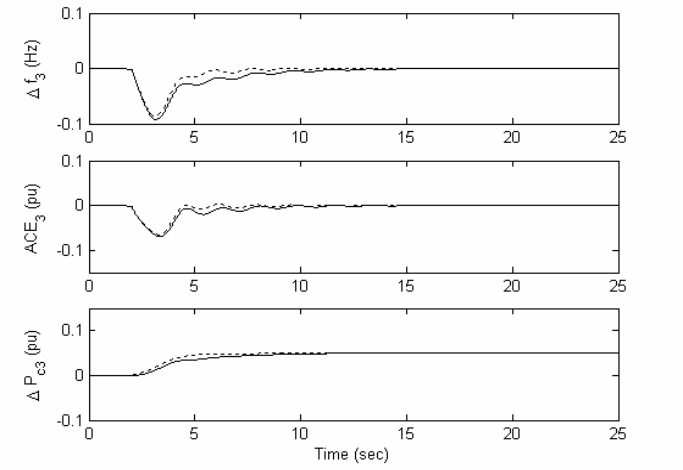

(c)

Figure 4.6: System response in case 1; (a) Area 1, (b) Area 2 and (c) Area 3. Solid (ILMI-based PI controller), dotted (dynamic H_∞ controller)

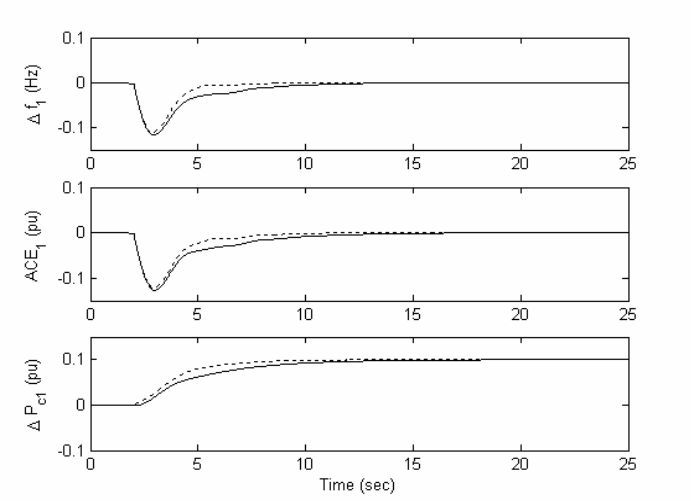

(a)

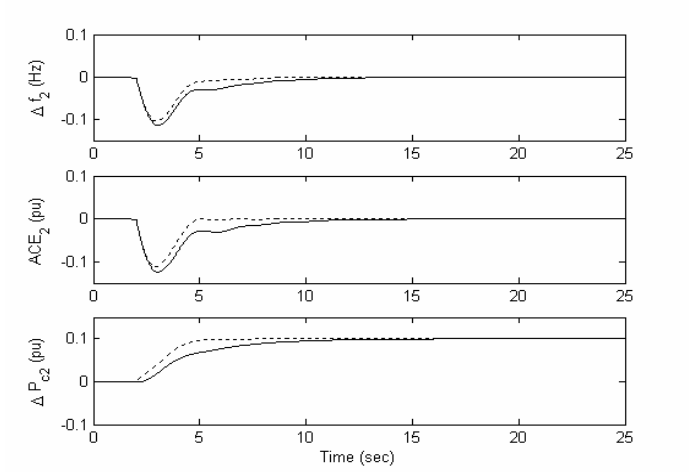

(b)

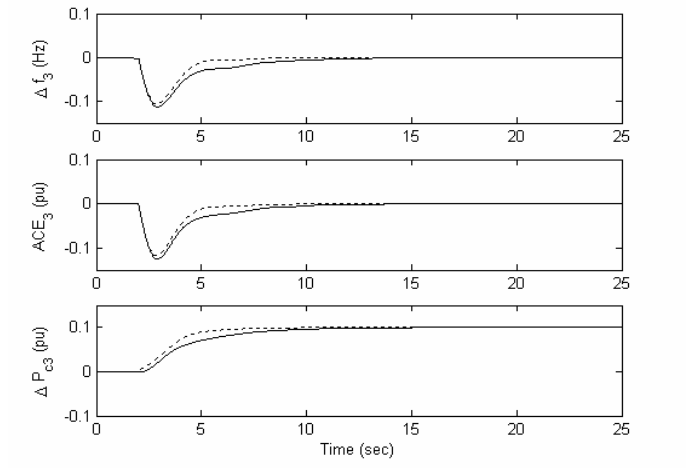

(c)

Figure 4.7: System response in case 2; (a) Area 1, (b) Area 2 and (c) Area 3. Solid (ILMI-based PI controller), dotted (dynamic H_∞ controller)

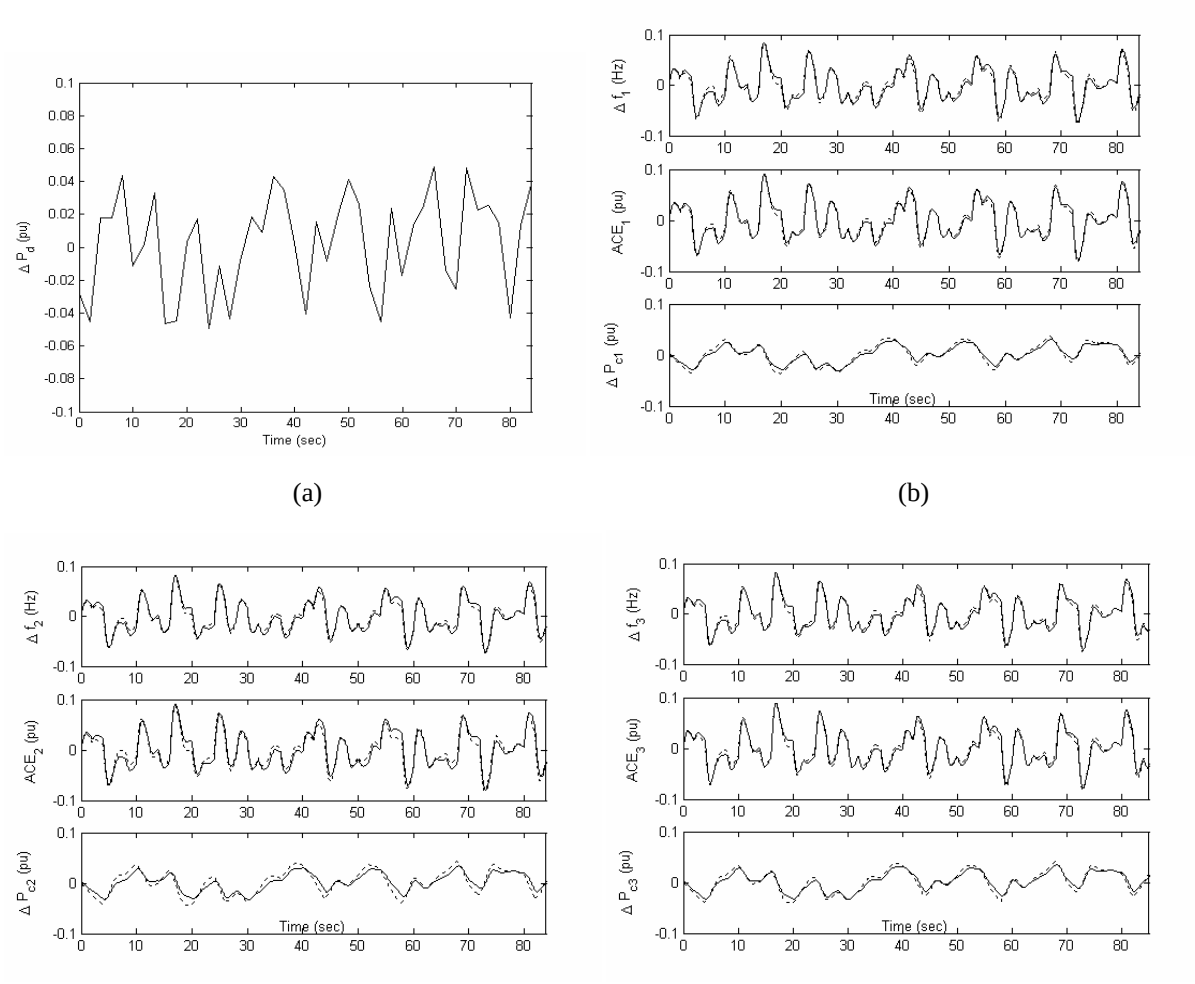

Figure 4.8: System response in case 3; (a) Random load demand signal, (b) Area 1, (c) Area 2 and (d) Area 3. Solid (ILMI-based PI controller), dotted (dynamic H_∞ controller)

4.3.4 Using a modified controlled output vector

In the proposed control framework (Fig. 4.4), it is expected the robust controller K_i to be able to minimize the fictitious output (z_i) in the presence of disturbance and external input (w_i). Therefore, the vector z_i must properly cover all signals which must be minimized to meet the LFC goals, e.g., frequency regulation, tracking the load changes, maintaining the tie-line power interchanges to specified values in the presence of generation constraints and minimizing the ACE signal. By considering the tie-line power flow changes in the proposed fictitious output vector, we can rewrite (4.19) as follows:

$$z_i^T = \begin{bmatrix} \eta_{1i}\Delta f & \eta_{2i}\int ACE_i & \eta_{3i}\Delta P_{tie\text{-}i} & \eta_{4i}u_i \end{bmatrix} \tag{4.22}$$

The new fictitious output $\eta_{3i}\Delta P_{tie\text{-}i}$ is used to minimize the effects of input disturbances on tie-line power flow signal. Referring to Eq. (4.16), the related coefficients to the fictitious output vector (z_i) in the proposed state-space model can be obtained as,

$$C_{1i} = \begin{bmatrix} c_{1i} & 0_{4\times n} & 0_{4\times n} \end{bmatrix}, \quad c_{1i} = \begin{bmatrix} \eta_{1i} & 0 & 0 \\ 0 & 0 & \eta_{2i} \\ 0 & 0 & 0 \\ 0 & \eta_{3i} & 0 \end{bmatrix}, \quad D_{12i} = \begin{bmatrix} 0 \\ 0 \\ \eta_{4i} \\ 0 \end{bmatrix}$$

A set of suitable values for constant weights according to the new control framework for the present power system example (Fig. 4.5) is considered as follows:

η_{1i} =0.4, η_{2i} =1.075, η_{3i} =0.39, η_{4i} =333

Using the ILMI approach, the controllers are obtained following several iterations. For example, for control area 3, the final result is obtained after 29 iterations (Table 4.3). The control parameters for three control areas are shown in Table 4.4. The resulting robust performance indices of both synthesis methods are shown in Table 4.5.

Table 4.3: ILMI algorithm result for design of K_3

Iteration	γ	k_{P3}	k_{I3}
1	449.3934	-0.0043	-0.0036
5	419.1064	-0.0009	-0.0042
11	352.6694	0.1022	-0.2812
14	340.2224	-0.0006	-0.0154
19	333.0816	-0.0071	-0.1459
22	333.0332	0.0847	-0.2285
24	333.0306	0.0879	-0.2382
26	333.0270	0.0956	-0.2537
28	333.0265	0.0958	-0.2560
29	333.0238	-0.0038	-0.2700

Table 4.4: Control parameters (ILMI design)

Parameter	*Area 1*	*Area 2*	*Area 3*
a^*	-0.0246	-0.3909	-0.2615
k_{Pi}	-9.8e-03	-2.6e-03	-3.8e-03
k_{Ii}	-0.5945	-0.3432	-0.2700

Table 4.5: Robust performance index

Control design	*Control structure*	*Performance index*	*Area1*	*Area 2*	*Area 3*
H∞	9^{th} order	γ	333.0084	333.0083	333.0080
ILMI	PI	γ^*	333.0261	333.0147	333.0238

The proposed controllers are applied to the 3-control area power system described in Fig. 4.5. The performance of the closed-loop system using the robust PI controllers compared to the designed dynamic H_∞ controllers and proposed control design in [9] is tested for some serious load disturbances.

Case 1:

As the first test scenario, the following large load disturbances (step increase in demand) are applied to the three areas. The system response is shown in Fig. 4.9 and Fig. 4.10.

$$\Delta P_{d1} = 105\ MW,\ \Delta P_{d2} = 105\ MW,\ \Delta P_{d3} = 105\ MW$$

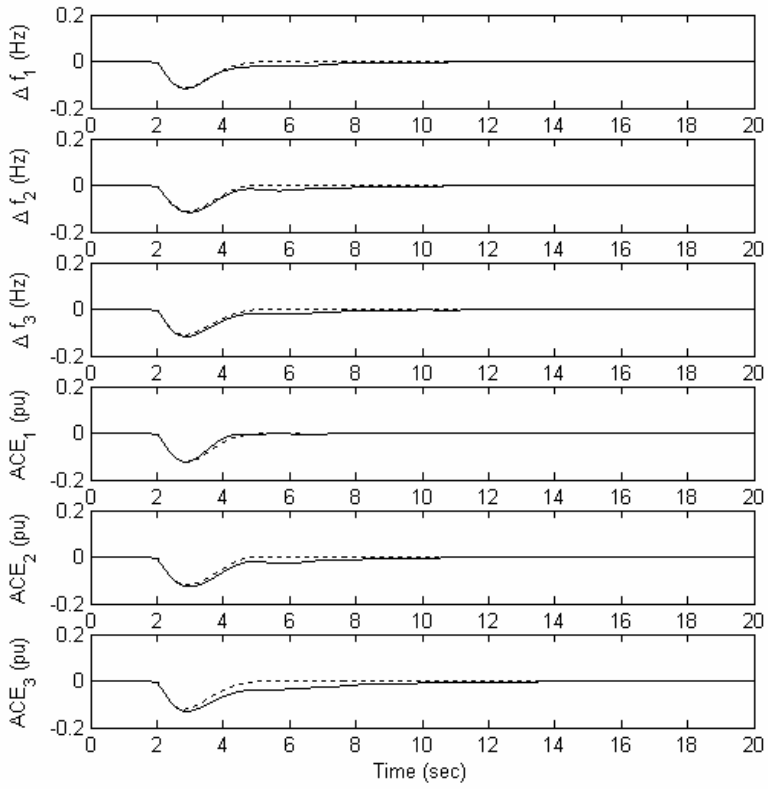

Figure 4.9: Frequency deviation and ACE signals following a large step load demand (105 MW) in each area. Solid (ILMI-based PI controller), dotted (dynamic H_∞ controller)

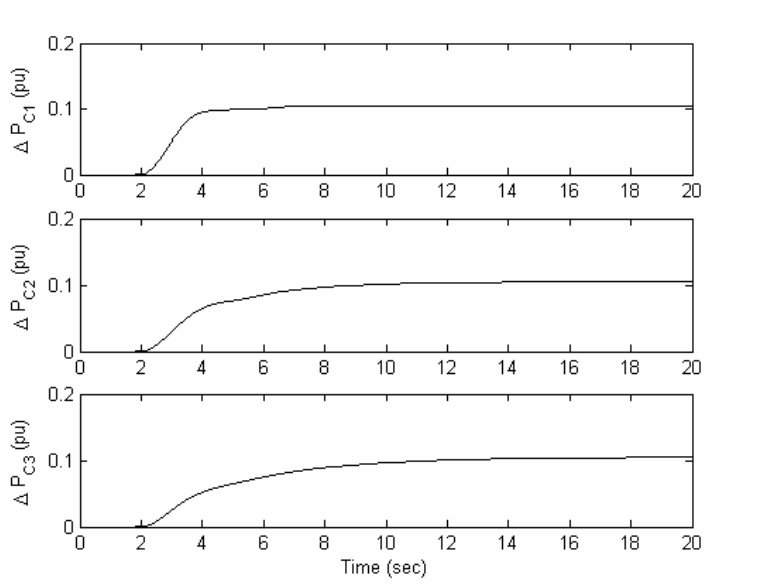

Figure 4.10: Control signals following a large step load demand (105 MW) in each area

Case 2:

As another severe condition, assume a bounded random load change ($-50\,MW \le \Delta P_d \le +50\,MW$) is applied to all control areas simultaneously. The system response is shown in Fig. 4.11 and Fig. 4.12. These figures demonstrate that the designed controllers track the load fluctuations effectively. The simulation results show the proposed PI controllers perform robustness as well as robust dynamic H_∞ controllers (with complex structures) for a wide range of load disturbances.

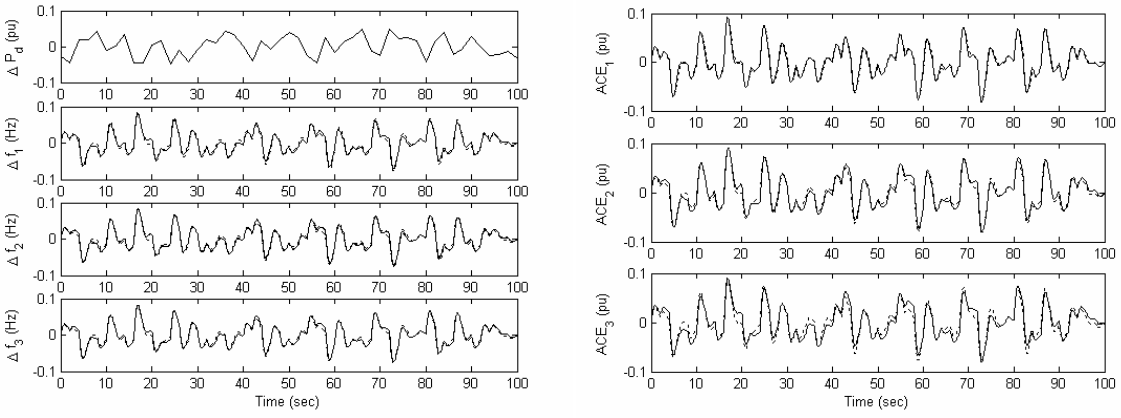

(a) (b)

Figure 4.11: a) Random load pattern and frequency deviation, b) ACE signals in each area. Solid (ILMI-based PI controller), dotted (dynamic H_∞ controller)

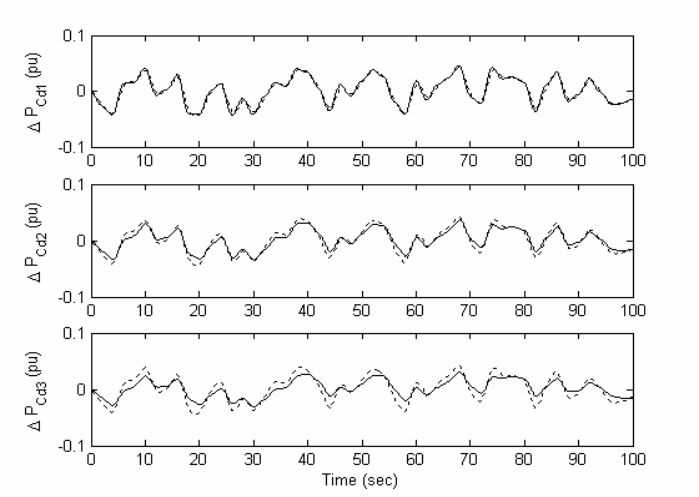

Figure 4.12: Control action signals in each area, following a random load demand. Solid (ILMI-based PI controller), dotted (dynamic H_∞ controller)

Case 3:

Fig. 4.13 compares the frequency deviation (Δf) and governor load set-point (ΔPc) signals for the proposed method and the recent published design technique [9], following 100 MW step load increase in each control area. A combination of genetic algorithm (GA) and LMI-based H_∞ control (GALMI) has been used in [9]. As seen from Fig. 4.13, the proposed controllers track the load changes and meet the robust performance as well as reported results for the same simulation case in [9]. Consider the tie-line power change as the fictitious controlled output in the H_∞ control framework adds enough flexibility to set the desired level of performance. Moreover, the proposed control design uses a simpler algorithm that takes a short time (few seconds) for tuning the controller parameters in comparison of [9].

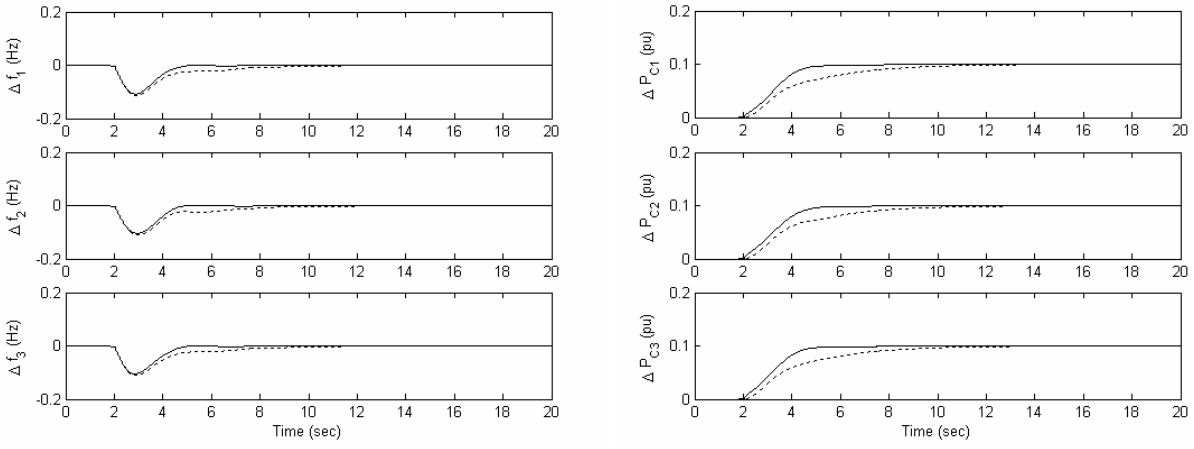

(a) (b)

Figure 4.13: a) Frequency deviation and b) Control action signals, following a +100 MW step load in each area. Solid (ILMI), Dotted ([9])

4. 4 Application to a bilateral-based LFC scheme

4.4.1 Control framework

The proposed control framework to the design of PI controller, via the H_∞-based SOF control problem for a given control area in a deregulated environment, is shown in Fig. 4.14. $G_i(s)$ denotes the dynamic model corresponds to the shown control area in Fig. 2.3. Assume the same variables as given in (4.17), (4.18), and (4.19). According to (4.16), we can write

$$w_i^{\mathrm{T}} = \begin{bmatrix} v_{1i} & v_{2i} & v_{3i} & v_{4i} \end{bmatrix},\ v_{4i}^{\mathrm{T}} = \begin{bmatrix} v_{4i\text{-}1} & v_{4i\text{-}2} & \cdots & v_{4i\text{-}n} \end{bmatrix} \tag{4.23}$$

and,

$$B_{1i} = \begin{bmatrix} B_{1i11} & B_{1i12} \\ B_{1i21} & B_{1i22} \\ B_{1i31} & B_{1i32} \end{bmatrix},\ B_{1i11} = \begin{bmatrix} -1/M_i & 0 & 0 \\ 0 & -2\pi & 0 \\ 0 & 0 & -1 \end{bmatrix}$$

$$B_{1i21} = B_{1i31} = 0_{n\times 3},\ B_{1i12} = 0_{3\times n},\ B_{1i22} = 0_{n\times n}$$

$$B_{1i32} = diag\begin{bmatrix} 1/T_{g1i} & 1/T_{g2i} & \cdots & 1/T_{gni} \end{bmatrix}$$

The other coefficient matrices and vectors can be defined the same as those given in section 4.3.1.

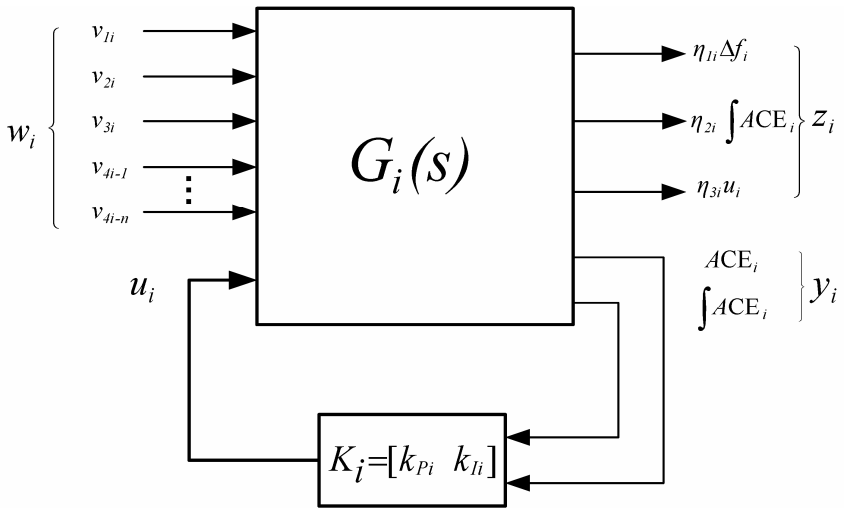

Figure 4.14: Proposed control framework for the bilateral based LFC scheme

4.4.2 Case study

A 3-control area power system shown in Fig. 4.15 is considered as a test system. It is assumed that each control area includes two Gencos and one Disco. The power system parameters are tabulated in Table 4.6 and Table 4.7. For the sake of comparison, for each area, in addition to the proposed control strategy to obtain the robust PI controller, a robust H_∞ dynamic output feedback controller is designed using LMI control toolbox [17].

The selection of constant weights η_{1i}, η_{2i} and η_{3i} is dependent on the specified performance objectives and must be chosen by the designer. For the present example, a set of suitable values for constant weights are chosen as *5*, *0.5* and *300*, respectively. The resulted controllers using the *hinflmi* function are dynamic type and have the state-space form, whose orders are the same as the size of plant model (7^{th} order in the present example).

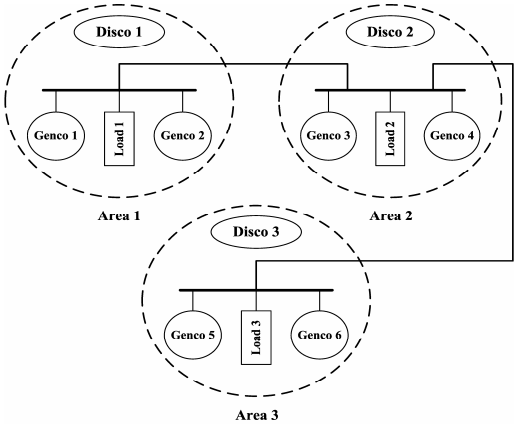

Figure 4.15: 3-control area power system

Table 4.6: Applied data for Gencos

Quantity	*Genco 1*	*Genco 2*	*Genco 3*	*Genco 4*	*Genco 5*	*Genco 6*
Rating (MW)	800	1000	1100	1200	1000	1000
R (Hz/pu)	2.4	3.3	2.5	2.4	3	2.4
T_t (sec)	0.36	0.42	0.44	0.4	0. 36	0.4
T_g (sec)	0.06	0.07	0.06	0.08	0.07	0.08
α	0.5	0.5	0.5	0.5	0.5	0.5

Table 4.7: Applied control area parameters

Quantity	*Area 1*	*Area 2*	*Area 3*
D (pu/Hz)	0.0084	0.014	0.011
M (pu.sec)	0.1667	0.2	0.1667
B (pu/Hz)	0.8675	0.795	0.870
T_{ij} (pu/Hz)	0.545		

Using ILMI approach, a set of three decentralized robust PI controllers is obtained following several iterations. For example, for control area 3 the final result is obtained after 32 iterations. Some iterations are listed in Table 4.8. The proposed control parameters for three control areas are shown in Table 4.9. The resulted robust performance indices of both synthesis methods (γ^* and γ) are very close to each other and given in Table 4.10. It shows that although the proposed ILMI approach gives a set of much simpler controllers (PI) than the dynamic H_∞ design, however they hold robust performance as well as dynamic H_∞ controllers.

Table 4.8: ILMI algorithm result for design of K_3

Iteration	γ	k_{P3}	k_{I3}
1	863.3337	-0.4471	-0.5365
2	863.2084	-0.4456	-0.5363
15	826.0470	-0.2915	-0.0053
22	804.7513	-0.0079	-0.0127
25	800.9137	-0.0672	-0.1236
26	800.8829	-0.1205	-0.2400
27	800.8783	-0.1823	-0.3146
29	800.8770	-0.2095	-0.3525
31	800.8763	-0.2275	-0.3787
32	800.8762	-0.2319	-0.3796

Table 4.9: Control parameters from ILMI design

Parameters	*Area 1*	*Area 2*	*Area 3*
a^*	-0.3901	-0.2610	-0.0407
k_{Pi}	-0.2695	-0.0418	-0.2319
k_{Ii}	-0.3788	-0.1806	-0.3796

Table 4.10: Robust performance index

Control design	*Control structure*	*Perf. index*	*Area 1*	*Area 2*	*Area 3*
H_∞	7^{th} order	γ	803.0393	801.0699	800.2284
ILMI	PI	γ^*	803.0396	801.0306	800.8762

4.4.3 Simulation results

In order to demonstrate the effectiveness of the proposed control strategy, some simulations were carried out. The performance of the closed-loop system using the robust PI controllers in comparison of designed dynamic H_∞ controllers is tested for the various possible scenarios of bilateral contracts and load disturbances.

Scenario 1:

It is assumed that a step increase in demand as $\Delta P_{L1} = 100\ MW$, $\Delta P_{L2} = 70\ MW$ and $\Delta P_{L3} = 60\ MW$ are applied to the control areas and each Disco demand is sent to its local Gencos only, based on the following GPM.

$$GPM = \begin{bmatrix} 0.5 & 0 & 0 \\ 0.5 & 0 & 0 \\ 0 & 0.5 & 0 \\ 0 & 0.5 & 0 \\ 0 & 0 & 0.5 \\ 0 & 0 & 0.5 \end{bmatrix}$$

The frequency deviation (Δf), tie-line power flow (ΔP_{tie}), power changes (ΔP_m), area control error (ACE) and its integral are shown in Fig. 4.16 and Fig. 4.17 for the closed-loop system. Using the proposed method (ILMI), the area control error and frequency deviation of all areas are quickly driven back to zero, the generated power and tie-line power are properly convergence to specified values, like the dynamic H_∞ control (LMI).

Since there are no contracts between areas, the scheduled steady state power flows over the tie lines are zero. The actual tie-line powers are shown in Fig. 4.16. As is seen from Fig. 4.17a, the actual generated powers of Gencos, according to (2.24), reach the desired values in the steady state.

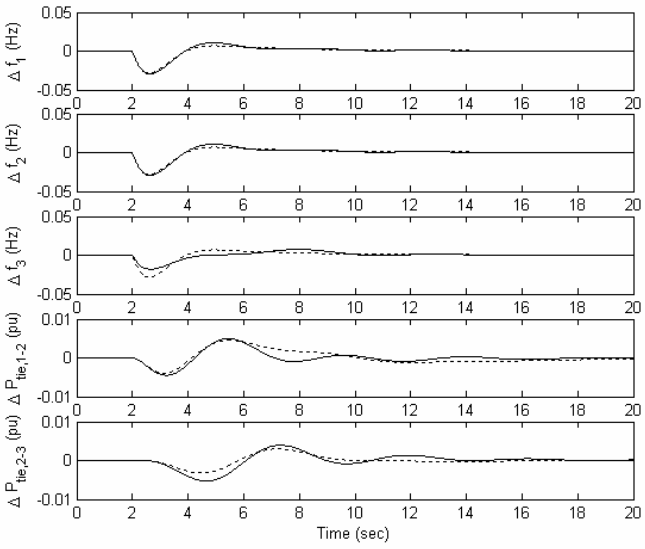

Figure 4.16: Frequency deviation and tie-line power changes; Solid (ILMI-based PI controller), dotted (dynamic H_∞ controller)

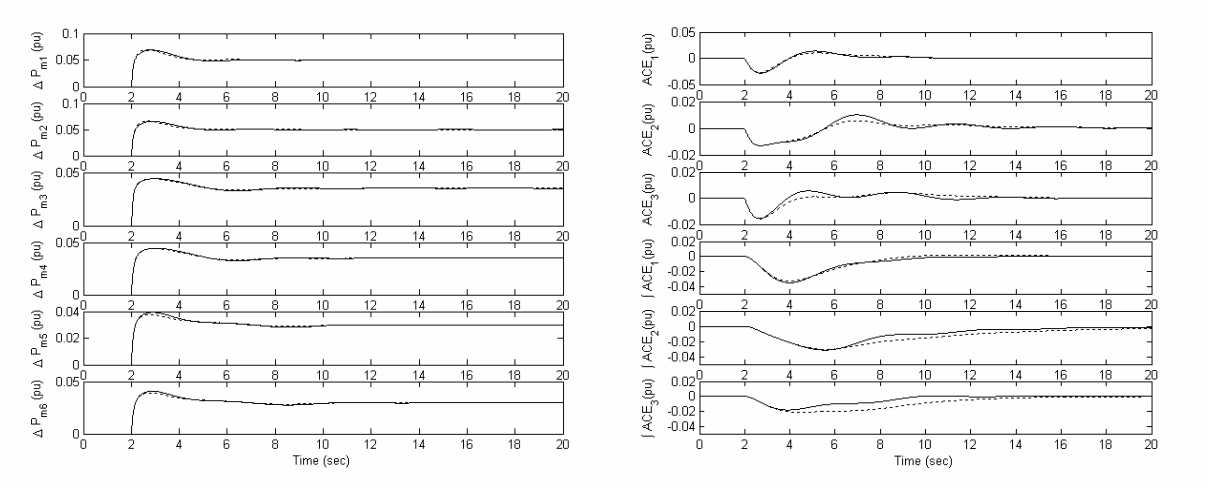

(a) (b)

Figure 4.17: a) Mechanical power changes, b) ACE and its integral; Solid (ILMI-based PI controller), dotted (dynamic H_∞ controller)

$$\Delta P_{m1} = gpf_{11}\Delta P_{L1} + gpf_{12}\Delta P_{L2} + gpf_{13}\Delta P_{L3} = 0.5(0.1) + 0 + 0 = 0.05\ pu$$

and,

$$\Delta P_{m2} = 0.05\ pu, \Delta P_{m3} = \Delta P_{m4} = 0.035\ pu, \quad \Delta P_{m5} = \Delta P_{m6} = 0.03\ pu.$$

Scenario 2:

Consider larger demands by Disco 2 and Disco 3, i.e. $\Delta P_{L1} = 100\ MW$, $\Delta P_{L2} = 100\ MW$ and $\Delta P_{L3} = 100\ MW$, and assume Discos contract with the available Gencos in other areas, according to the following GPM,

$$GPM = \begin{bmatrix} 0.25 & 0.25 & 0 \\ 0.5 & 0 & 0 \\ 0 & 0.25 & 0.75 \\ 0.25 & 0.25 & 0 \\ 0 & 0.25 & 0 \\ 0 & 0 & 0.25 \end{bmatrix}$$

The closed-loop response is shown in Fig. 4.18 and Fig. 4.19. According to Eq. (2.24), the actual generated powers of Gencos for this scenario can be obtained as

$$\Delta P_{m1} = 0.25(0.1) + 0.25(0.1) + 0 = 0.05\ pu$$

and, $\Delta P_{m2} = 0.05\ pu, \Delta P_{m3} = 0.1\ pu, \quad \Delta P_{m4} = 0.05\ pu, \Delta P_{m5} = \Delta P_{m6} = 0.025\ pu.$

The simulation results show the same values in steady state. The scheduled tie-line powers in the directions from area 1 to area 2, and area 2 to area 3 are obtained as follows using Eq. (2.20). Fig. 4.19a shows actual tie-line powers and they reach to above values at steady state.

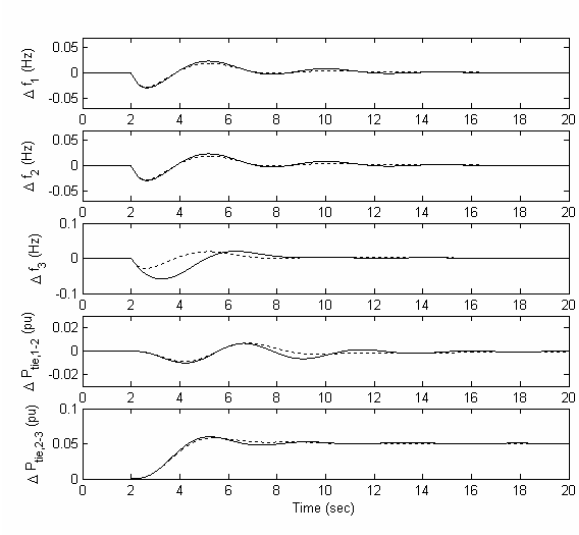

Figure 4.18: Frequency deviation and tie-line power changes; Solid (ILMI-based PI controller), dotted (dynamic H_∞ controller)

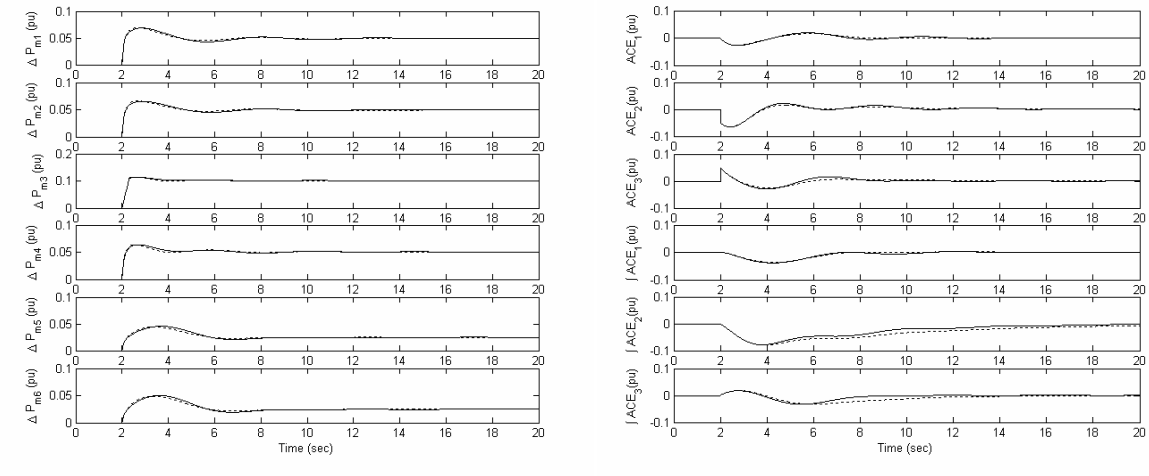

(a) (b)

Figure 4.19: a) Mechanical power changes , b) ACE and its integral; Solid (ILMI-based PI controller), dotted (dynamic H_∞ controller)

$$\Delta P_{tie,1\text{-}2} = (gpf_{12} + gpf_{22})\Delta P_{L2} - (gpf_{31} + gpf_{41})\Delta P_{L1} = (0.25+0)0.1 - (0+0.25)0.1 = 0 \ pu$$

and,

$$\Delta P_{tie,2\text{-}3} = (0.75+0)0.1 - (0.25+0)0.1 = 0.05 \ pu$$

Scenario 3:

In this scenario, the effect of the contract violation problem is simulated. Consider the scenario 2 again, but assume the Disco 1 demands 50 MW more power than that specified in the contract. As has been mentioned in

section 2.3, this excess power must be reflected as an uncontracted local demand of area 1 and must be supplied by local Gencos, only. Simulation result is shown in Fig. 4.20.

Fig. 4.20 shows that the excess load is only taken up by Genco 1 and Genco 2, according to their LFC participation factors, and Gencos in other distribution areas do not participate to compensate it. Since GPM is the same as in scenario 2, the generated power of Gencos in area 2 and area 3 is the same as in scenario 2 in steady state.

Scenario 4:

Consider the conditions of scenario 2 again. In addition to specified contracted demand (100 MW), assume a bounded random load changes (Fig. 4.21a) as an uncontracted local demand,

$$-50\ MW \le \Delta P_{di} \le +50\ MW$$

is applied to each control area. The contract step demands as in previous simulation tests are started from 2 sec. The purpose of this scenario is to test the performance of proposed controllers against large contracted demands and random load disturbances. The corresponded power changes, frequency deviations and tie-line power flows are shown in Fig. 4.21b and 4.21c. Finally, Fig. 4.21d shows ACE and control effort signals for the proposed controllers. These figures demonstrate that the designed controllers track the load fluctuations, effectively.

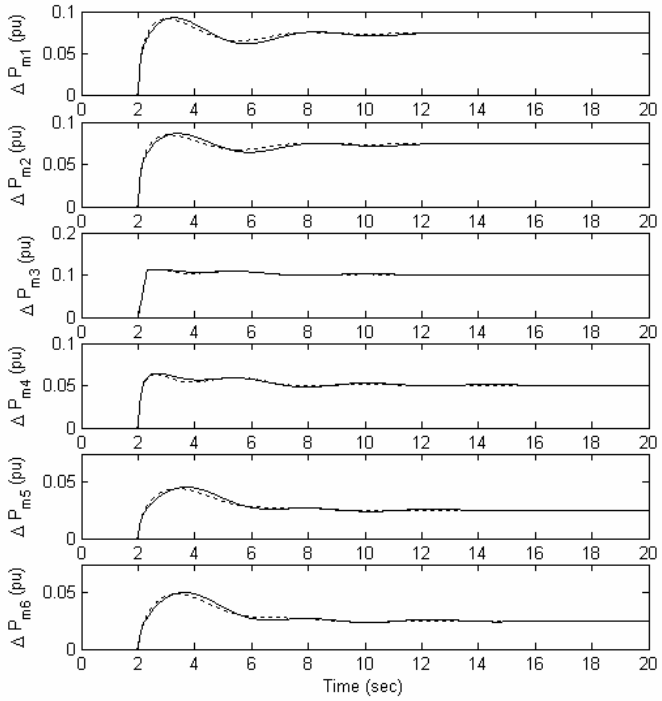

Figure 4.20: Generated power in responses to contract violation; Solid (ILMI-based PI controller), dotted (dynamic H_∞ controller)

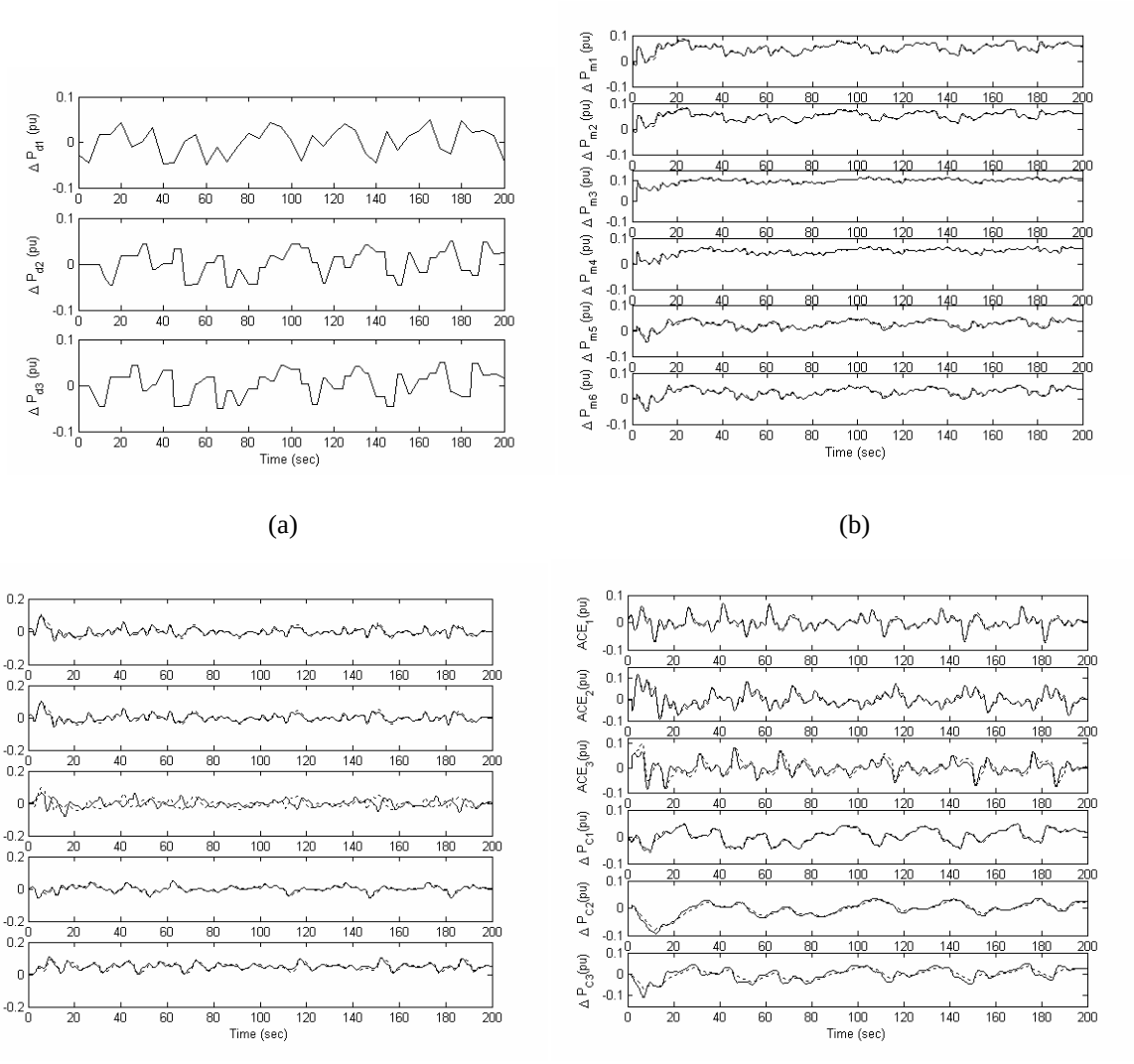

Figure 4.21: a) Random load changes, b) Generated power, c) Frequency deviation and tie-line power flow, d) ACE and control action signals for scenario 4; Solid (ILMI-based PI controller), dotted (dynamic H_∞ controller)

The simulation results demonstrate that the proposed PI controllers perform robust performance as well as full order dynamic H_∞ controllers in a deregulated environment for a wide range of load disturbances and possible bilateral contract scenarios.

4.5 Summary

In this chapter, a new decentralized method to design robust LFC using a developed ILMI algorithm has been provided for a large scale power system. The proposed design control strategy gives a set of simple PI controllers via the H_∞-based SOF control design, which are commonly useful in real-world power systems. The proposed method was applied to multi-area power system examples with different LFC schemes and the closed-loop system was tested under serious load change scenarios. The results were compared with the results

of applied full dynamic H_∞ controllers. It was shown that the designed controllers can guarantee the robust performance under a wide range of area-load disturbances.

4. 6 References

[1] T. Hiyama, "Design of decentralised load-frequency regulators for interconnected power systems," *IEE Proc.*, Pt. C, vol. 129, pp. 17-23, 1982.

[2] A. Feliachi, "Optimal decentralized load frequency control," *IEEE Trans. Power System*, vol. PWRS-2, pp. 379-384, 1987.

[3] C. M. Liaw, K. H. Chao, "On the design of an optimal automatic generation controller for interconnected power systems," *Int. J. Control*, vol. 58, pp. 113-127, 1993.

[4] Y. Wang, R. Zhou, C. wen, "Robust load-frequency controller design for power systems," *IEE Proc.* Pt. C, vol. 140, no. 1, pp. 11-16, 1993.

[5] K. Y. Lim, Y. Wang, R. Zhou, "Robust decentralized load-frequency control of multi-area power systems," *IEE Proc. Gener. Transm. Distrib.*, vol. 143, no. 5, pp. 377-386, 1996.

[6] T. Ishi, G. Shirai, G. Fujita, "Decentralized load frequency based on H_∞ control," *Electrical Engineering in Japan*, vol. 136, no. 3, pp. 28-38, 2001.

[7] M. H. Kazemi, M. Karrari, M. B. Menhaj, "Decentralized robust adaptive-output feedback controller for power system load frequency control," *Electrical Engineering Journal*, no. 84, pp. 75-83, 2002.

[8] M. K. El-Sherbiny, G. El-Saady, A. M. Yousef, "Efficient fuzzy logic load-frequency controller," *Energy Conversion & Management*, vol. 43, pp. 1853-1863, 2002.

[9] D. Rerkpreedapong, A. Hasanovic, A. Feliachi, "Robust load frequency control using genetic algorithms and linear matrix inequalities," *IEEE Trans. Power Systems*, vol. 18, no. 2, pp. 855-861, 2003.

[10] H. Bevrani, Y. Mitani, K. Tsuji, "Sequential design of decentralized load-frequency controllers using μ-synthesis and analysis," *Energy Conversion & Management*, vol. 45, no. 6, pp. 865-881, 2004.

[11] T. C. Yang, H. Cimen, Q. M. ZHU, "Decentralised load frequency controller design based on structured singular values," *IEE Proc. Gener. Transm. Distrib.*, vol. 145, no. 1, pp. 7-14, 1998.

[12] H. Bevrani, "Application of Kharitonov's theorem and its results in load-frequency control design," *J. Electr. Sci. Technol.-BARGH* (in Persian), no. 24, pp. 82-95, 1998.

[13] R. E. Skelton, J. Stoustrup, T. Iwasaki, "The H_∞ control problem using static output feedback," *Int. J. of Robust and Nonlinear Control*, no. 4, pp. 449-455, 1994.

[14] P. Gahinet, P. Apkarian, "A linear matrix inequality approach to H_∞ control," *Int. J. of Robust and Nonlinear Control*, no. 4, pp. 421-448, 1994.

[15] Y. Y. Cao, Y. X. Sun, W. J. Mao, "Output feedback decentralized stabilization: ILMI approach," *Systems & Control Letters*, vol. 35, pp. 183-194, 1998.

[16] Y. Y. Cao, Y. X. Sun, W. J. Mao, "Static output feedback stabilization: an ILMI approach," *Automatica*, vol. 34, no. 12, pp. 1641-1645, 1998.

[17] P. Gahinet, A. Nemirovski, A. J. Laub, M. Chilali, "LMI Control Toolbox," The MathWorks, Inc., 1995.

Chapter 5

Multi-objective control based robust decentralized LFC design

LFC goals, i.e., frequency regulation and tracking the load changes, maintaining the tie-line power interchanges to specified values in the presence of generation constraints and model uncertainties, identifies the LFC synthesis as a multi-objective control problem. On the other hand, the proportional-integral (PI) based load-frequency controllers which are usually used in the real-world power systems and tuned based on experiences, classical, or trial-and-error approaches, are incapable of obtaining good dynamical performance to meet all of the specified objectives.

In section 5.1, the LFC problem is formulated as a multi-objective control problem and the mixed H_2/H_∞ control technique is used to synthesis the desired robust controllers for LFC system in a multi-area power system. A 3-control area power system example with possible contract scenarios and a wide range of load changes is given to illustrate the proposed approach. The results of the proposed control strategy are compared with the pure H_∞ method.

In section 5.2, first with regard to model uncertainties, the multi-objective LFC problem is reformulated via a mixed H_2/H_∞ control technique and then in order to design a robust PI controller, the control problem is reduced to a static output feedback control synthesis. Finally, it is easily carried out using a developed iterative linear matrix inequalities (ILMI) algorithm. The proposed method is applied to multi-area power system examples with traditional and bilateral-based LFC schemes. The results are compared with the designed mixed H_2/H_∞ dynamic controllers.

5.1 Robust LFC synthesis using a mixed H_2/H_∞ control technique

In most reported robust LFC approaches, only one single norm is used to capture design specifications. It is clear that meeting all LFC design objectives by a single norm-based control approach with regard to increasing the complexity and changing of power system structure is difficult. Furthermore, each robust method is mainly useful for capturing a set of special specifications. For instance, the regulation against random disturbances more naturally can be addressed by Linear Quadratic Gaussian (LQG) or H_2 synthesis, while H_∞ approach is more useful for holding closed-loop stability and formulation of physical control constraints. It is shown that using the combination of H_2 and H_∞ (mixed H_2/H_∞) allows better performance for a control design problem including both sets of the above objectives [1-3].

In this section, the LFC problem is formulated as a multi-objective control problem and is solved by a mixed H_2/H_∞ control approach to obtain the desired robust decentralized controllers. The proposed strategy is applied to a 3-control area example in a deregulated environment. The results show that the controllers guarantee the robust performance for a wide range of operating conditions. The results of the proposed multi-objective control approach are compared with pure H_∞ controllers using general LMI technique.

5.1.1 Mixed H_2/H_∞: technical background

In many real-world control problems, we follow several objectives such as stability, disturbance attenuation, reference tracking, and considering the practical constraints, simultaneously. Pure H_∞ synthesis cannot adequately capture all design specifications. For example, H_∞ synthesis mainly enforces closed-loop stability and meets some constraints and limitations, while noise attenuation or regulation against random disturbances is more naturally expressed in LQG terms (H_2 synthesis). The mixed H_2/H_∞ control synthesis gives a powerful multi-objective control design addressed by the LMI techniques. This section gives a brief overview of the mixed H_2/H_∞ output feedback control design.

The general synthesis control scheme is shown in Fig. 5.1. *G(s)* is a linear time invariant system with the following state-space realization:

$$\begin{aligned} \dot{x} &= Ax + B_1 w + B_2 u \\ z_\infty &= C_\infty x + D_{\infty 1} w + D_{\infty 2} u \\ z_2 &= C_2 x + D_{21} w + D_{22} u \\ y &= C_y x + D_{y1} w \end{aligned} \tag{5.1}$$

Where *x* is the state variable vector, *w* is the disturbance and other external input vector, and *y* is the measured output vector. The output channel z_2 is associated with the LQG aspects (H_2 performance) while the output channel z_∞ is associated with the H_∞ performance. Assume $T_\infty(s)$ and $T_2(s)$ are transfer functions from *w* to z_∞ and z_2 respectively, and consider the following state-space realization for the closed-loop system.

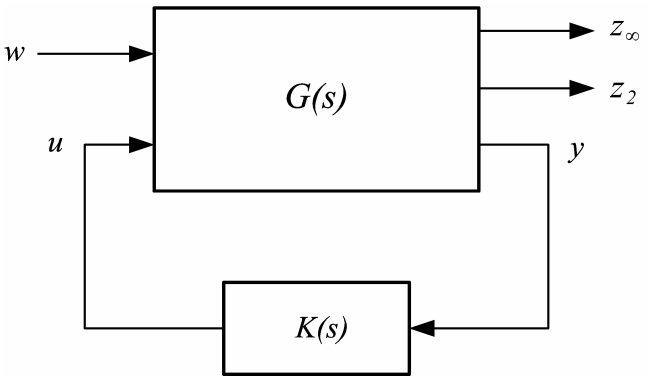

Figure 5.1: Closed-loop system via the mixed H_2/H_∞ control

$$\begin{aligned} \dot{x}_{cl} &= A_{cl}x_{cl} + B_{cl}w \\ z_\infty &= C_{cl1}x_{cl} + D_{cl1}w \\ z_2 &= C_{cl2}x_{cl} + D_{cl2}w \end{aligned} \tag{5.2}$$

The following lemmas express the design objectives in term of LMIs [4]. The details are available in [1-3].

Lemma 5.1 (H_∞ performance): The closed-loop RMS gain for $T_\infty(s)$ does not exceed γ_∞ if and only if there exists a symmetric matrix $X_\infty > 0$, such that

$$\begin{bmatrix} A_{cl}X_\infty + X_\infty A_{cl}^T & B_{cl} & X_\infty C_{cl1}^T \\ B_{cl}^T & -I & D_{cl1}^T \\ C_{cl1}X_\infty & D_{cl1} & -\gamma_\infty^2 I \end{bmatrix} < 0 \tag{5.3}$$

Lemma 5.2 (H_2 performance): The H_2 norm of $T_2(s)$ does not exceed γ_2 if and only if $D_{cl2} = 0$ and there exist two symmetric matrices X_2 and Q such that

$$\begin{bmatrix} A_{cl}X_2 + X_2A_{cl}^T & B_{cl} \\ B_{cl}^T & -I \end{bmatrix} < 0, \quad \begin{bmatrix} Q & C_{cl2}X_2 \\ X_2C_{cl2}^T & X_2 \end{bmatrix} > 0, \quad \text{Trace}(Q) < \gamma_2^2 \tag{5.4}$$

The mixed H_2/H_∞ control design method uses both lemmas and gives us an output feedback controller $K(s)$ that minimizes the following trade-off criterion:

$$k_1\|T_\infty(s)\|_\infty^2 + k_2\|T_2(s)\|_2^2, \qquad (k_1 \geq 0,\ k_2 \geq 0) \tag{5.5}$$

An efficient algorithm to solve this problem is available in function *hinfmix* of the LMI control toolbox for

Matlab [4].

5.1.2 Control framework

Consider a large scale power system which consists of a number of interconnected distribution control areas and each control area may have several Gencos. For example, assume the power system is under a bilateral policy scheme (Fig. 2.3). In this case, a useful control framework to formulate the LFC problem via a mixed H_2/H_∞ control design can be introduced as shown in Fig. 5.2. Here, $G_i(s)$ denotes the dynamical model which corresponds to the modified control area (Fig. 2.3). According to (5.1), the state space model for control area *i* can be obtained as;

$$\begin{aligned} \dot{x}_i &= A_i x_i + B_{1i} w_i + B_{2i} u_i \\ z_{\infty i} &= C_{\infty i} x_i + D_{\infty 1i} w_i + D_{\infty 2i} u_i \\ z_{2i} &= C_{2i} x_i + D_{21i} w_i + D_{22i} u_i \\ y_i &= C_{yi} x_i + D_{y1_i} w_i \end{aligned} \tag{5.6}$$

where

$$x_i^T = \begin{bmatrix} \Delta f_i & \Delta P_{tie-i} & x_{ti} & x_{gi} \end{bmatrix} \tag{5.7}$$

$$x_{ti} = \begin{bmatrix} \Delta P_{t1i} & \Delta P_{t2i} & \cdots & \Delta P_{tni} \end{bmatrix}, \quad x_{gi} = \begin{bmatrix} \Delta P_{g1i} & \Delta P_{g2i} & \cdots & \Delta P_{gni} \end{bmatrix}$$

$$u_i = \Delta P_{Ci}, \quad y_i = \beta_i \Delta f_i + \Delta P_{tie\text{-}i} - v_{3i} \tag{5.8}$$

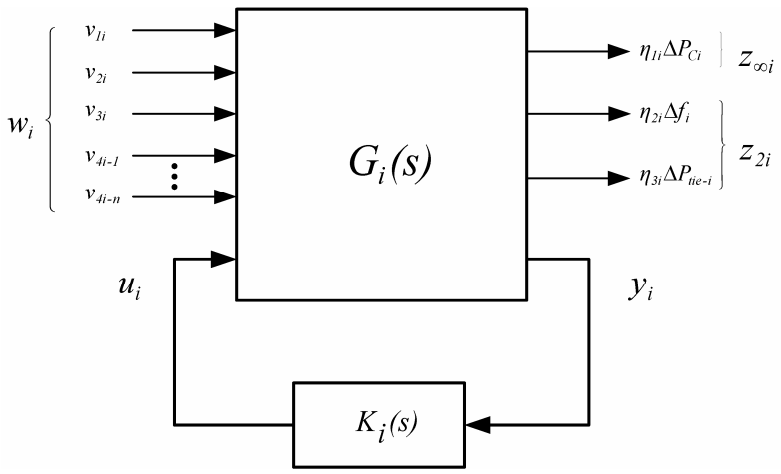

Figure 5.2: The proposed control framework

$$z_{\infty i} = \eta_{1i}\Delta P_{Ci} = \eta_{1i}u_i, \quad z_{2i}^T = \begin{bmatrix}\eta_{2i}\Delta f_i & \eta_{3i}\Delta P_{tie\text{-}i}\end{bmatrix} \tag{5.9}$$

$$w_i^{\mathrm{T}} = \begin{bmatrix}v_{1i} & v_{2i} & v_{3i} & v_{4i}\end{bmatrix}, \quad v_{4i}{}^{\mathrm{T}} = \begin{bmatrix}v_{4i\text{-}1} & v_{4i\text{-}2} & \cdots & v_{4i\text{-}n}\end{bmatrix} \tag{5.10}$$

and,

$$A_i = \begin{bmatrix}A_{i11} & A_{i12} & A_{i13}\\ A_{i21} & A_{i22} & A_{i23}\\ A_{i31} & A_{i32} & A_{i33}\end{bmatrix}, \quad B_{1i} = \begin{bmatrix}B_{1i11} & B_{1i12}\\ B_{1i21} & B_{1i22}\\ B_{1i31} & B_{1i32}\end{bmatrix}, \quad B_{2i} = \begin{bmatrix}B_{2i1}\\ B_{2i2}\\ B_{2i3}\end{bmatrix}$$

$$c_{2i} = \begin{bmatrix}\eta_{1i} & 0 & 0_{1\times 2n}\\ 0 & \eta_{2i} & 0_{1\times 2n}\end{bmatrix}, \quad D_{21i} = 0_{2\times(n+3)}, \quad D_{22i} = 0_{2\times 1}$$

$$C_{\infty i} = 0_{1\times(2n+2)}, \quad D_{\infty 1i} = 0_{1\times(n+3)}, \quad D_{\infty 2i} = \eta_{3i}$$

$$c_{yi} = \begin{bmatrix}\beta_i & 1 & 0_{1\times 2n}\end{bmatrix}, \quad D_{y1i} = \begin{bmatrix}0 & 0 & -1 & 0_{1\times n}\end{bmatrix}$$

$$A_{i11} = \begin{bmatrix}-D_i/M_i & -1/M_i\\ 2\pi\sum_{\substack{j=1\\ j\neq i}}^{N} T_{ij} & 0\end{bmatrix}, \quad A_{i12} = \begin{bmatrix}1/M_i & \cdots & 1/M_i\\ 0 & \cdots & 0\end{bmatrix}_{2\times n}$$

$$A_{i22} = -A_{i23} = diag\begin{bmatrix}-1/T_{t1i} & -1/T_{t2i} & \cdots & -1/T_{tni}\end{bmatrix}$$

$$A_{i33} = diag\begin{bmatrix}-1/T_{g1i} & -1/T_{g2i} & \cdots & -1/T_{gni}\end{bmatrix}$$

$$A_{i31} = \begin{bmatrix}-1/(T_{g1i}R_{1i}) & 0\\ \vdots & \vdots\\ -1/(T_{gni}R_{ni}) & 0\end{bmatrix}, \quad A_{i13} = A_{i21}{}^{\mathrm{T}} = 0_{2\times n}, \quad A_{i32} = 0_{n\times n}$$

$$B_{1i11} = \begin{bmatrix}-1/M_i & 0 & 0\\ 0 & -2\pi & 0\end{bmatrix}, \quad B_{1i21} = B_{1i31} = 0_{n\times 3}, \; B_{1i12} = 0_{2\times n}, \; B_{1i22} = 0_{n\times n}$$

$$B_{1i32} = diag\begin{bmatrix}1/T_{g1i} & 1/T_{g2i} & \cdots & 1/T_{gni}\end{bmatrix}, \quad B_{2i1} = 0_{2\times 1}, B_{2i2} = 0_{n\times 1}, \quad B_{2i3}{}^{T} = \begin{bmatrix}\alpha_{1i}/T_{g1i} & \alpha_{2i}/T_{g2i} & \cdots & \alpha_{ni}/T_{gni}\end{bmatrix}$$

The H_∞ performance is used to set a limit on the control set-point to penalize the fast change and large overshoot in the control action signal. The H_2 performance is used to minimize the effects of disturbances on control area frequency and tie-line flow signals. Therefore, it is expected that the proposed strategy satisfy the main objectives of LFC system under load change and bilateral contracts variation. The coefficients η_{1i}, η_{2i} and η_{3i} in Fig. 5.2 and Eq. (5.9) are constant weights that must be chosen by the designer to get the desired performance. In the next section, two sets of robust controllers are designed for a power system example

including three control areas. The first one includes pure H_∞ controllers based on the general LMI technique and the second one contains designed low-order controllers based on the proposed mixed H_2/H_∞ approach with the same assumed objectives to achieve desired robust performance.

5.1.3 Application to a 3-control area power system

The 3-control area power system example given in section 4.4.2 (Fig. 4.15) is considered as a test system. The power system parameters are assumed to be the same as in Table 4.6 and Table 4.7.

5.1.3.1 Pure H_∞ control design For the sake of comparison, for each area, in addition to the proposed control strategy, a pure H_∞ dynamic output feedback controller is developed using lemma 5.1. Specifically, the control design is reduced to an LMI formulation, and then the H_∞ control problem is solved using the function *hinflmi*, provided by the MATLAB LMI control toolbox [4]. This function gives an optimal H_∞ controller through the minimizing guaranteed robust performance index subject to the specified constraints, and returns the controller *K(s)* with the optimal robust performance index.

The control framework, which is shown in Fig. 5.2, is used for the pure H_∞ control design also, but using only one fictitious output channel (z_∞) as:

$$z_\infty{}^T = \left[\eta_{1i}\Delta P_{Ci} \quad \eta_{2i}\Delta f_i \quad \eta_{3i}\Delta P_{tie\text{-}i}\right] \tag{5.11}$$

A set of suitable constant weights (η_{1i} , η_{2i} and η_{3i}) for the present example is chosen as (*2.5*, *1*, and *1*) respectively. The resulting controllers are dynamic types as follow, whose orders are the same as the size of area model (6^{th} order).

$$K_{1\infty}(s) = \frac{-4.3183\,s^5 - 151.5977\,s^4 - 1591.4874\,s^3 - 4630.9097\,s^2 - 3529.211\,s + 596.585}{s^6 + 42.6561\,s^5 + 645.1347\,s^4 + 4262.8509\,s^3 + 13116.3347\,s^2 + 16735.9031\,s + 5105.7057}$$

$$K_{2\infty}(s) = \frac{-2.7694\,s^5 - 90.4397\,s^4 - 858.9605\,s^3 - 2067.3481\,s^2 - 668.8242\,s + 1214.4936}{s^6 + 39.4468\,s^5 + 545.6694\,s^4 + 3313.9408\,s^3 + 9898.8032\,s^2 + 14038.0905\,s + 7342.4697} \tag{5.12}$$

$$K_{3\infty} = \frac{-4.5755\,s^5 - 141.8668\,s^4 - 1343.0582\,s^3 - 3781.6026\,s^2 - 2851.0296\,s + 366.7874}{s^6 + 38.9744\,s^5 + 552.8201\,s^4 + 3547.385\,s^3 + 10743.1064\,s^2 + 13506.6111\,s + 3887.5418}$$

5.1.3.2 Mixed H_2/H_∞ control design In the next step, according to the described synthesis methodology (mixed H_2/H_∞), a set of three decentralized robust controllers are designed. The constant weights are chosen the same as pure H_∞ design. The coefficients k_1 and k_2 in (5.5) are fixed in unity.

The order of the resulting controllers is 6. Using the standard Hankel norm approximation, the order is reduced to 3 for each controller, with no performance degradation. The Bode plot of the full-order and reduced order controllers for area 1 and area 2 are shown in Fig. 5.3.

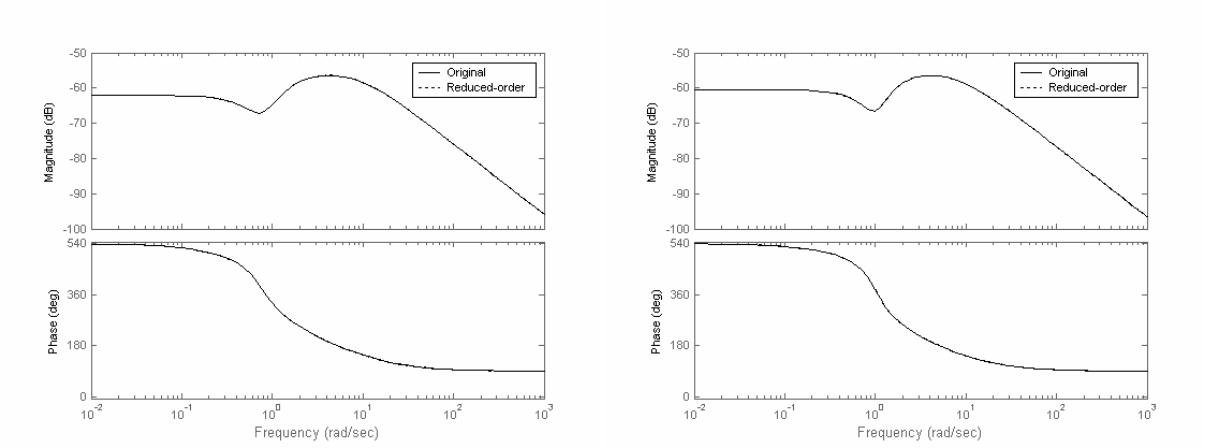

(a) (b)

Figure 5.3: Bode plots comparison of full-order (original) and reduced controllers: a) $K_{1mix}(s)$, b) $K_{2mix}(s)$

This figure presents the same frequency response for both original and reduced-order controllers. The transfer functions of the resulting reduced controllers with simple structures are

$$K_{1mix}(s) = \frac{-0.0161\,s^2 + 0.0099\,s - 0.0097}{s^3 + 10.9846\,s^2 + 21.5941\,s + 12.1933}$$

$$K_{2mix}(s) = \frac{-0.0147\,s^2 + 0.0092\,s - 0.0148}{s^3 + 10.17\,s^2 + 19.6734\,s + 15.478} \qquad (5.13)$$

$$K_{3mix}(s) = \frac{-0.0167\,s^2 + 0.0107\,s - 0.0101}{s^3 + 12.1815\,s^2 + 24.9846\,s + 14.4173}$$

5.1.3.3 Simulation results The proposed low-order controllers (5.13) were applied to the 3-control area power system described in Fig. 4.15. The performance of the closed-loop system using the proposed controllers compared to the designed full-order pure H_∞ controllers (5.12) will be tested for the various scenarios of bilateral contracts and load disturbances. Following, the system responses are shown for scenarios 1 and 2 which are explained in section 4.4.3. These scenarios present different bilateral contracts (GPM) with large load disturbances.

The frequency deviation (Δf), power changes (ΔP_m), area control error (*ACE*), and tie-line power flows (ΔP_{tie}) of the closed-loop system for scenario 1 are shown in Fig. 5.4. Using the proposed method, the area control error and frequency deviation of all areas are quickly driven back to zero, and the generated powers and tie-line powers are properly converged to specified values. As shown in these figures, the actual generated powers of Gencos, according to Eq. (2.24), reach the desired values in the steady state. Since there are no contracts between areas, the scheduled steady state power flows (2.20) over the tie lines are zero.

The difference between the mixed H_2/H_∞ and pure H_∞ controllers will be more clear in case of the application of a set of larger step disturbances under a complex bilateral contract such as scenario 2 (section 4.4.3). The closed-loop response for this scenario is shown in Fig. 5.5. It is seen that the proposed low-order controllers perform robustness better than the full-order H_∞ controllers for a wide range of load disturbances and possible bilateral contract scenarios.

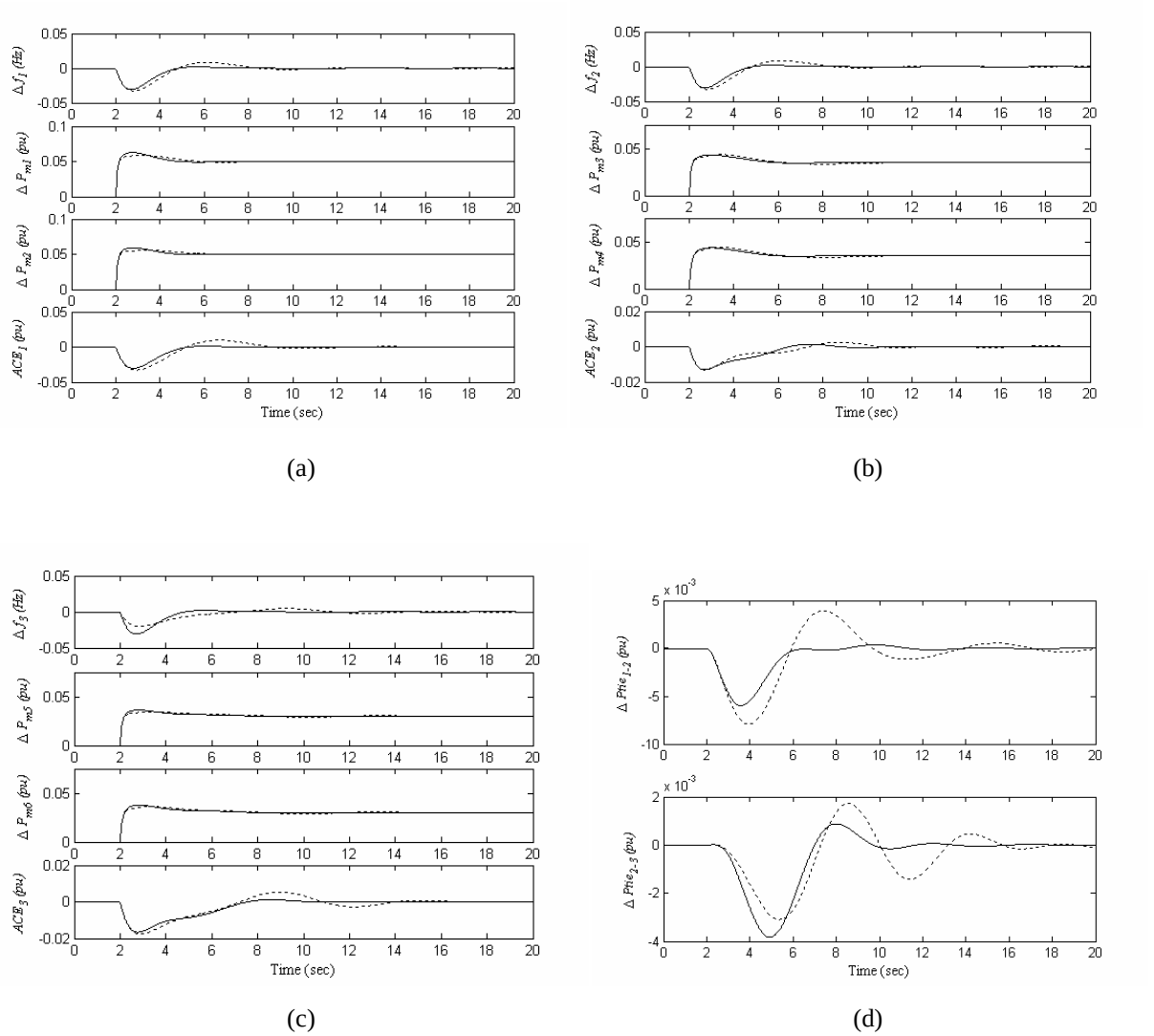

Figure 5.4: Power system response for scenario 1. Solid (Mixed H_2/H_∞), dotted (H_∞);
a) Area-1, b) Area-2, c) Area-3 and d) Tie-line powers

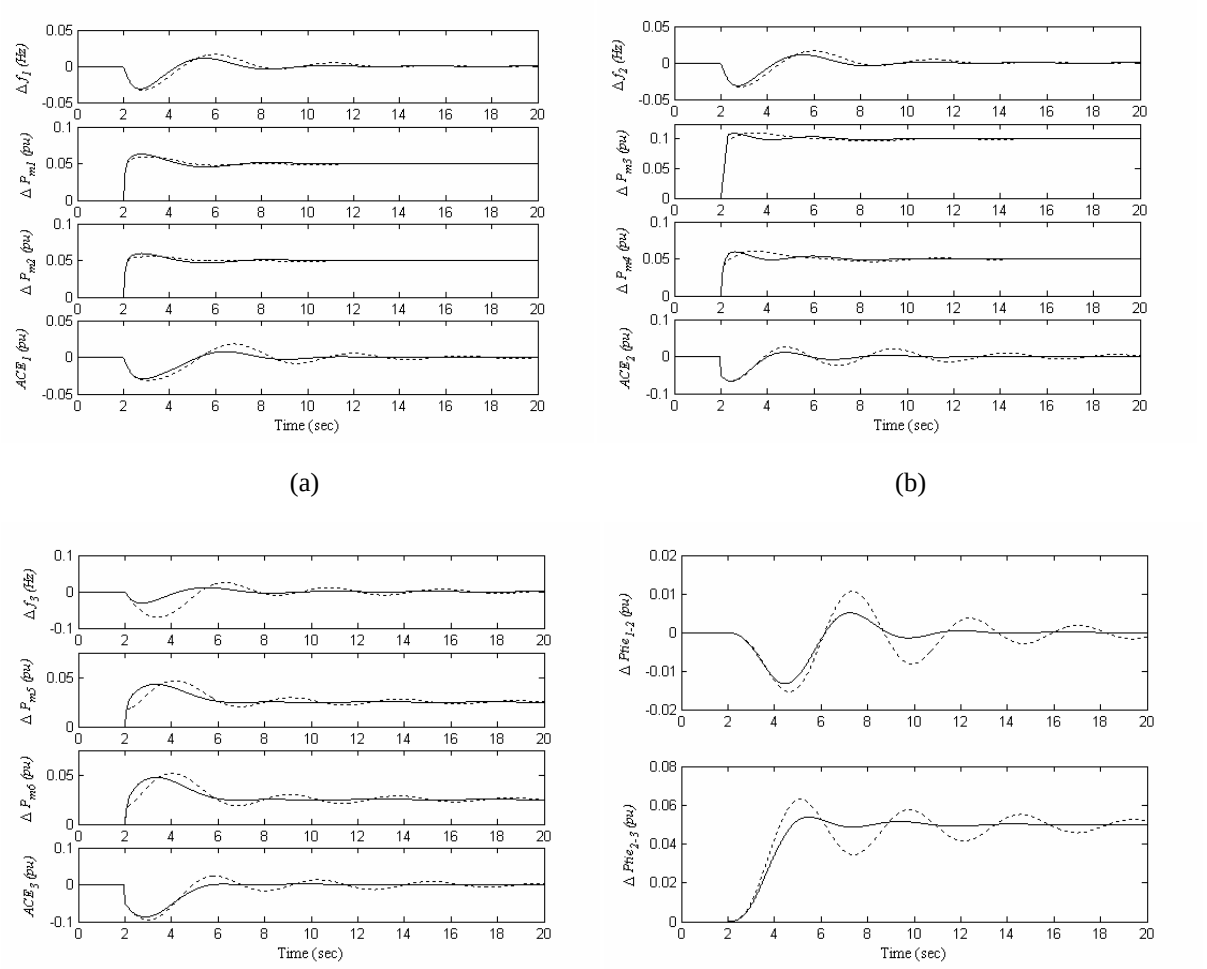

(a) (b)

(c) (d)

Figure 5.5: Power system response for scenario 2. Solid (Mixed H_2/H_∞), dotted (H_∞);
a) Area-1, b) Area-2, c) Area-3 and d) Tie-line powers

5.2 PI based multi-objective robust LFC design

In this section, the LFC synthesis is formulated as a mixed H_2/H_∞-static output feedback (SOF) control problem to obtain a desired PI controller. An iterative linear matrix inequalities (ILMI) algorithm is developed to compute the PI parameters. It is assumed that in each control area the power system model has uncertain parameters and the uncertainties are covered by an unstructured multiplicative uncertainty block. The proposed strategy is applied to multi-area power system examples with traditional and bilateral based LFC schemes. The designed robust PI controllers, which are practical for industry, are compared with the mixed H_2/H_∞ dynamic output feedback controllers (using general LMI technique [4]). The results show that the PI controllers guarantee the robust performance for a wide range of operating conditions as well as H_2/H_∞ dynamic controllers. The proposed control strategy and developed ILMI algorithm are given in sections 5.2.1 and 5.2.2. Problem formulation and control framework is presented in section 5.2.3. The proposed methodology is applied to multi-area power systems with traditional and bilateral LFC schemes in sections 5.2.4 and 5.2.5.

5.2.1 H_2/H_∞-based SOF design

The general control scheme using the mixed H_2/H_∞ control technique (Fig. 5.1) is redrawn in Fig. 5.6. $G_i(s)$ is a linear time invariant system with the given state-space realization in Eq. 5.6. Where x_i is the state variable vector, w_i is the disturbance and the other external input vector, y_i is the measured output vector and K_i is the controller. The output channel z_{2i} is associated with the LQG aspects (H_2 performance) while the output channel $z_{\infty i}$ is associated with the H_∞ performance. With $T_{z_{\infty i}\, w1i}$ and $T_{z2i\, w2i}$ defined as transfer functions from $w_i = [w_{1i} \;\; w_{2i}]^T$ to $z_{\infty i}$ and z_{2i} respectively, consider the following state-space realization for closed-loop system.

$$\begin{aligned} \dot{x}_i &= A_{ic}x_i + B_{1_{ic}}w_i \\ z_{\infty i} &= C_{\infty ic}x_i + D_{\infty_{ic}}w_i \\ z_{2i} &= C_{2ic}x_i + D_{2_{ic}}w_i \\ y_i &= C_{yic}x_i + D_{yic}w_i \end{aligned} \tag{5.14}$$

A mixed H_2/H_∞-SOF control design can be expressed as the following optimization problem.

Optimization problem: Determine an admissible SOF law K_i which belongs to a family of internally stabilizing SOF gains K_{sof},

$$u_i = K_i y_i \;\;,\;\; K_i \in K_{sof} \tag{5.15}$$

such that

$$\inf_{K_i \in K_{sof}} \left\| T_{z2i\, w2i} \right\|_2 \;\; \textit{subject to} \;\; \left\| T_{z_{\infty i}\, w1i} \right\|_\infty < 1 \tag{5.16}$$

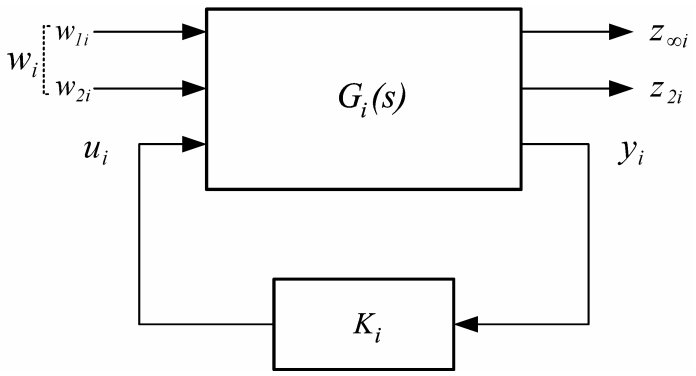

Figure 5.6: The closed-loop system via the mixed H_2/H_∞ control

This problem defines a robust performance synthesis problem where the H_2 norm is chosen as a performance measure. Recently, several methods are proposed to obtain a suboptimal solution for the H_2, H_∞, and H_2/H_∞-SOF control problems [5-9].

Here, a new ILMI algorithm is introduced to get a suboptimal solution for the mentioned optimization problem. Specifically, the proposed algorithm formulates the H_2/H_∞-SOF control through a general SOF stabilization problem using lemma 4.2 (general stabilizing SOF, [7]) and the following lemma.

Lemma 5.3 (H_2 Suboptimal SOF), [9]:

For fixed $(A_i, B_{1i}, B_{2i}, C_{yi}, K_i)$, there exists a positive definite matrix X which solves inequality

$$(A_i + B_{2i}K_iC_{yi})X + X(A_i + B_{2i}K_iC_{yi})^T + B_{1i}B_{1i}^T < 0,\ X > L_C \tag{5.17}$$

to satisfy $\left\|T_{z_{2i}w_{2i}}\right\|_2 < \gamma$, if and only if the following inequality has a positive definite matrix solution,

$$A_iX + XA_i^T + XC_{yi}^TC_{yi}X + (B_{2i}K_i + XC_{yi}^T)(B_{2i}K_i + XC_{yi}^T)^T + B_{1i}B_{1i}^T < 0 \tag{5.18}$$

where L_C in (5.17) denotes the controllability Gramian of the pair (A_{ic}, B_{1ic}) and can be presented as follows.

$$\left\|T_{z_{2i}w_{2i}}\right\|_2^2 = trace(C_{2ic}L_CC_{2ic}^T) \tag{5.19}$$

The proposed algorithm searches the desired suboptimal H_2/H_∞-SOF controller K_i within a family of H_2 stabilizing controllers K_{sof}, such that

$$\left|\gamma_2^* - \gamma_2\right| < \varepsilon,\quad \gamma_\infty = \left\|T_{z_{\infty i}w_{1i}}\right\|_\infty < 1 \tag{5.20}$$

where ε is a small real positive number, γ_2^* is H_2 performance corresponded to H_2/H_∞-SOF controller K_i and γ_2 is optimal H_2 performance index, which can result from the application of standard H_2/H_∞ dynamic output feedback control.

5.2.2 Developed ILMI algorithm

Developed ILMI algorithm, which uses the ideas given in lemma 4.2 and lemma 5.3, provides a suboptimal solution to obtain an H_2/H_∞-SOF controller for a given power system control area and includes the following steps:

Step 1. Compute the state-space model for the given control area, according to Eq. 5.6.

Step 2. Compute the optimal H_2 performance index γ_2 using function *hinfmix* in MATLAB based LMI control toolbox [4] to design standard H_2/H_∞ dynamic output controller for the performed system in Step 1.

Step 3. Set $i=1$, $\Delta\gamma_2 = \Delta\gamma_0$ and let $\gamma_{2i} = \gamma_0 > \gamma_2$. $\Delta\gamma_0$ is a small positive real number.

Step 4. Select $Q = Q_0 > 0$, and solve X from the following algebraic Riccati equation:

$$A_i X + X A_i^T - X C_{yi}^T C_{yi} X + Q = 0, \quad X > 0 \tag{5.21}$$

Set $P_1 = X$.

Step 5. Solve the following optimization problem for X_i, K_i and a_i.

Minimize a_i subject to the LMI constraints:

$$\begin{bmatrix} A_i X_i + X_i A_i^T + B_{1i} B_{1i}^T + \sum_i & B_{2i} K_i + X_i C_{yi}^T \\ (B_{2i} K_i + X_i C_{yi}^T)^T & -I \end{bmatrix} < 0 \tag{5.22}$$

$$trace(C_{2ic} L_C C_{2ic}^T) < \gamma_{2i} \tag{5.23}$$

$$X_i = X_i^T > 0 \tag{5.24}$$

where,

$$\sum_i = P_i C_{yi}^T C_{yi} X_i - X_i C_{yi}^T C_{yi} P_i + P_i C_{yi}^T C_{yi} P_i - a_i X_i .$$

Denote a_i^* as a minimized value of a_i.

Step 6. If $a_i^* \le 0$, go to Step 10.

Step 7. For $i > 1$ if $a_{i-1}^* \le 0$, $K_{i-1} \in K_{sof}$ and go to step 11. Otherwise go to Step 8.

Step 8. Solve the following optimization problem for X_i and K_i:

Minimize $trace(X_i)$ subject to LMI constraints (5.22), (5.23) and (5.24) with $a_i = a_i^*$. Denote X_i^* as X_i that minimized $trace(X_i)$.

Step 9. Set $i = i+1$ and $P_i = X_{i-1}^*$, then go to Step 5.

Step 10. Set $\gamma_{2i} = \gamma_{2i} - \Delta\gamma_2$, $i = i+1$. Then do Steps 4 to 6.

Step 11. If

$$\gamma_{\infty,i-1} = \left\| T_{z_{\infty i} w_{1i}} \right\|_\infty \le 1 \tag{5.25}$$

K_{i-1} is a suboptimal H_2/H_∞-SOF controller and $\gamma_2^* = \gamma_{2i} - \Delta\gamma_2$ indicates a lower H_2 bound such that the obtained controller satisfies (5.20). Otherwise set $\gamma_{2i} = \gamma_{2i} + \Delta\gamma_2$, $i = i+1$, then do Steps 4 to 6.

The developed ILMI algorithm is summarized in Fig. 5.7.

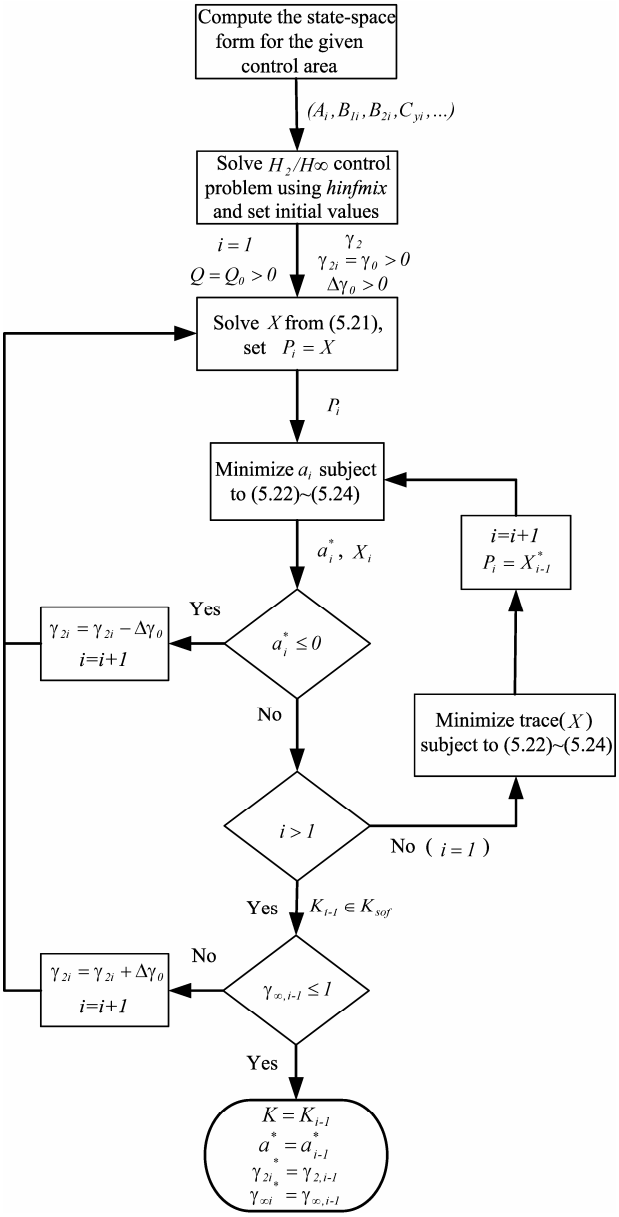

Figure 5.7: Developed ILMI algorithm

5.2.3 Problem formulation and control framework

By augmenting the system description (5.6) to include the ACE signal and its integral as a measured output vector, the PI control problem becomes finding a static output feedback that satisfies the prescribed performance requirements. Using this strategy, the PI-based LFC design can be reduced to an H_2/H_∞-SOF control problem as shown in Fig. 5.8.

The main control framework in order to formulate the LFC problem via a mixed H_2/H_∞ control design for a

given control area is shown in Fig. 5.9. The model uncertainties in a power system can be considered as multiplicative and/or additive uncertainties [10-11]. Here, Δ_i block models the structured uncertainty set in the form of multiplicative type and W_i includes the associated weighting function, as presented in Fig. 5.10. The output channel $z_{\infty i}$ is associated with the H_∞ performance while the fictitious output vector z_{2i} is associated with LQG aspects or H_2 performance.

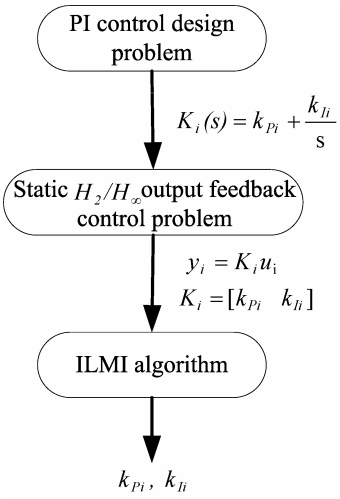

Figure 5.8: Problem formulation

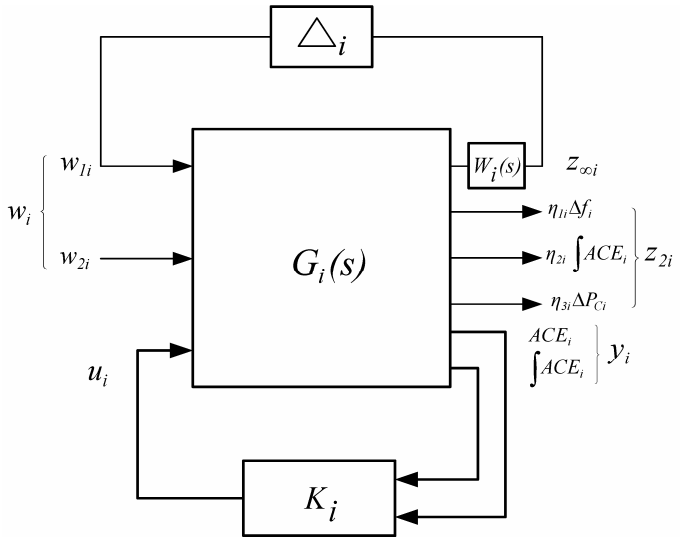

Figure 5.9: H_2/H_∞-SOF control framework

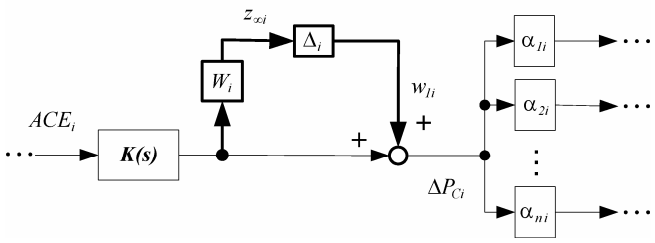

Figure 5.10: Modeling of uncertainties

Constant weights must be chosen by the designer to get a desired closed-loop performance. Experience suggests that one can fix the weights η_{1i}, η_{2i} and η_{3i} to unity and use the method with the regional pole placement technique for performance tuning [12]. $G_i(s)$ and K_i correspond to the nominal dynamic model of the given control area and controller, respectively. Also, y_i is the augmented measured output vector (performed by ACE and its integral), u_i is the control input, and w_i includes the perturbed and disturbance signals in the given control area.

The proposed control framework covers all mentioned LFC objectives. The H_2 performance is used to minimize the effects of disturbances on the area frequency and area control error by introducing fictitious controlled outputs $\eta_{1i}\Delta f_i$ and $\eta_{2i}\int ACE_i$. As a result, the tie-line power flow which can be described as a linear combination of frequency deviation and ACE signals,

$$\Delta P_{tie\text{-}i} = ACE_i - B_i\Delta f_i \tag{5.26}$$

is controlled. Furthermore, fictitious output $\eta_{3i}\Delta P_{Ci}$ sets a limit on the allowed control signal to penalize fast changes and large overshoot in the governor load set-point with regard to practical constraint on power generation by generator units. Also, in LFC design, it is important to keep up the frequency regulation and desired performance in the face of uncertainties affecting the control area. The H_∞ performance is used to meet the robustness against specified uncertainties and reduction of its impact on closed-loop system performance. Therefore, it is expected that the proposed strategy satisfy the main objectives of LFC system in the presence of load disturbance and model uncertainties.

For the following multi-area power system examples, two types of designed robust controllers are tested. The first one is the H_2/H_∞ dynamic controller using the general robust LMI design and the second controller is based on the proposed H_2/H_∞-SOF using the ILMI algorithm with the same assumed objectives and initializations to achieve desired robust performance.

5.2.4 Application to a traditional-based LFC scheme

A 3-control area power system, shown in Fig. 5.11, is considered as a test system. It is assumed that each control area includes three Gencos. The power system parameters are considered to be the same as in [13].

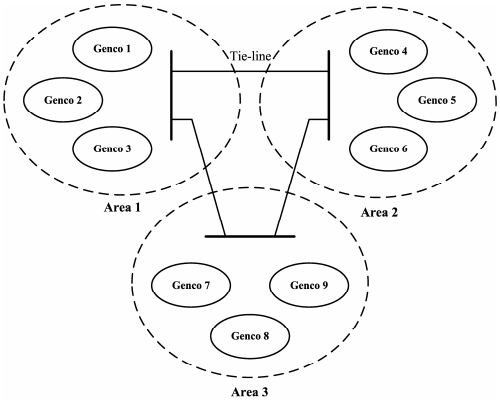

Figure 5.11: 3-control area power system

5.2.4.1 Uncertainty and performance weights selection In this example, it is assumed that the power system (rotating mass and load) model parameters have uncertain values. The variation range for D_i and M_i parameters in each control area is assumed $\pm 20\%$ of nominal values. It is notable that there is no obligation to consider uncertainty in two parameters, only. As already mentioned, considering a more complete model by including additional uncertainties in the model of other units is possible and causes less conservatism in the synthesis. However, the complexity of computations and the order of the resulting dynamic controller will increase. As a result, finding a tighter control solution by a simple PI structure will be difficult. In the next step, these uncertainties are modeled as an unstructured multiplicative uncertainty block W_i that contains all the information available about D_i and M_i variations.

Using the described method in section 3.1.3.1, some sample uncertainties due to D_i and M_i variations for area 1 are obtained, as shown in Fig. 5.12. To keep the complexity of the obtained controller low, uncertainties from both parameter variations can be modeled by using a norm bonded multiplicative uncertainty (W_1) to cover all possible plants. Using the mentioned method, the uncertainties weighting functions are determined for the 3-control area example as follows.

$$W_1(s)=\frac{0.3619s+0.1613}{s+1.6242},\quad W_2(s)=\frac{0.2950s+0.1073}{s+1.6814},\quad W_3(s)=\frac{0.3497s+0.3515}{s+3.4815} \tag{5.27}$$

Fig. 5.12 clearly shows that attempting to cover the uncertainties at all frequencies by finding a tighter fit (around 4 rad/sec) using higher order transfer function will result in high-order controller. The weight W_1 in our design provides a conservative design at some frequencies but it gives a good trade-off between robustness and controller complexity.

The selection of performance constant weights η_{1i}, η_{2i}, and η_{3i} is dependent on the specified performance objectives. An important issue with regard to selection of the weights is the degree to which they can guarantee the satisfaction of design performance objectives. For the present example, a set of suitable values for constant weights is chosen as follows.

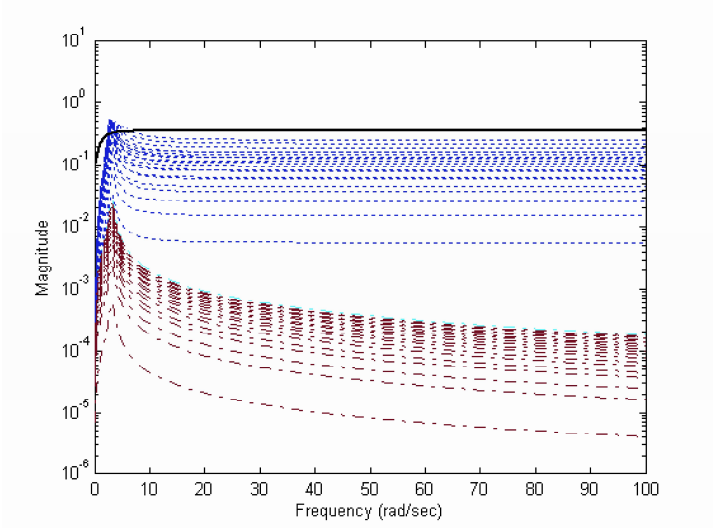

Figure 5.12: Uncertainty plots due to parameters changes in area 1; D_i (dotted), M_i (dash-dotted) and W_1 (solid)

$$\eta_{1i} = 0.12, \quad \eta_{2i} = 0.35, \quad \eta_{3i} = 0.42 \tag{5.28}$$

5.2.4.2 Mixed H_2/H_∞ dynamic and SOF control design For the sake of comparison, in addition to the proposed control strategy to synthesize the robust PI controller, a mixed H_2/H_∞ dynamic controller is designed for each control area, using *hinfmix* function in the LMI control toolbox. This function results in an optimal H_2/H_∞ controller *K(s)* with optimal H_2 performance index γ_2 through the solution of the optimization problem given in Eq. (5.16). The resulting controller is dynamic type and has the following state-space form, whose order is the same as the size of a generalized plant model (10^{th} order in the present example).

$$\begin{aligned} \dot{x}_{ki} &= A_{ki} x_{ki} + B_{ki} y_i \\ u_i &= C_{ki} x_{ki} + D_{ki} y_i \end{aligned} \tag{5.29}$$

In the next step, according to the synthesis methodology described in sections 5.2.2 and 5.2.3, a set of three decentralized robust PI controllers are designed. This control strategy is fully suitable for LFC applications which usually employ the PI control, while most other robust and optimal control designs (such as LMI approach) yield complex controllers whose size is larger than real-world LFC systems. Using the developed ILMI algorithm, the controllers are obtained following several iterations. The proposed control parameters for three control areas are shown in Table 5.1. The guaranteed optimal H_2 and H_∞ indices for dynamic and PI controllers are listed in Table 5.2.

Table 5.1: PI control parameters from ILMI design

Parameters	*Area 1*	*Area 2*	*Area 3*
k_{Pi}	-2.00E-04	-4.80E-03	-2.50E-03
k_{Ii}	-0.3908	-0.4406	-0.4207

Table 5.2: Guaranteed H_2 and H_∞ indices

Indices	*Area 1*	*Area 2*	*Area 3*
γ_{2i} (Dynamic)	1.0700	1.0300	1.0310
$\gamma_{\infty i}$ (Dynamic)	0.3919	0.2950	0.3497
γ_{2i}^* (PI)	1.0976	1.0345	1.0336
$\gamma_{\infty i}^*$ (PI)	0.3920	0.2950	0.3498

The resulting robust H_∞ indices ($\gamma_{\infty i}$ and $\gamma_{\infty i}^*$) and guaranteed H_2 performance indices (γ_{2i} and γ_{2i}^*) in both synthesis methods are very close to each other. This shows that although the proposed ILMI approach gives a set of much simpler controllers (PI) than the dynamic H_2/H_∞ design, they hold robustness as well as dynamic H_2/H_∞ controllers.

5.2.4.3 Simulation results The proposed PI controllers were applied to a 3-control area power system described in Fig. 5.11. The performance of the closed-loop system using the designed PI controllers in comparison of the full-order H_2/H_∞ dynamic controllers will be tested in the presence of load disturbances and uncertainties.

Case 1:

In this case, the closed-loop performance is tested in the face of both step load demand and uncertainties. It is assumed that a large step load disturbance 100 MW (0.1 pu) is applied to each control area, following a 20% decrease in uncertain parameters D_i and M_i. The power system response is shown in Fig. 5.13.

Using the proposed ILMI-based PI controllers, the area control error and frequency deviation of all areas reach zero quickly, and the generated powers convergence to the specified values according to assumed ACE participation factor α_i in each Genco, as well as H_2/H_∞ dynamic controllers. The results show that the power initially comes from all Gencos to respond to the load increase which will result in a frequency drop that is sensed by the governors of all machines, but at steady state the necessary powers come from participating Gencos in the LFC task.

Case 2:

Assume in addition to a 20% decrease in D_i and M_i, a bounded random step load changes shown in Fig. 5.14a appear in control areas, where $-0.05\ pu \le \Delta P_{di} \le +0.05\ pu$.

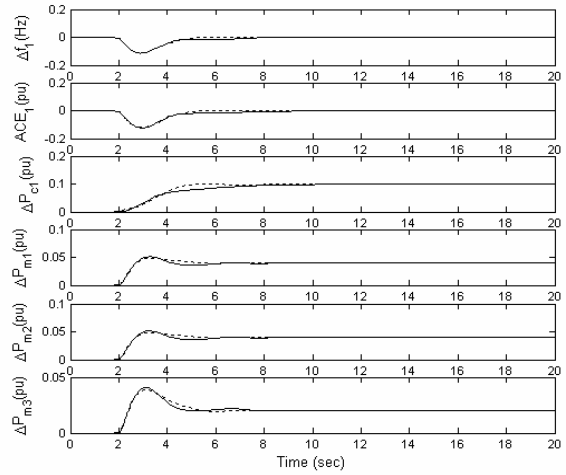

(a)

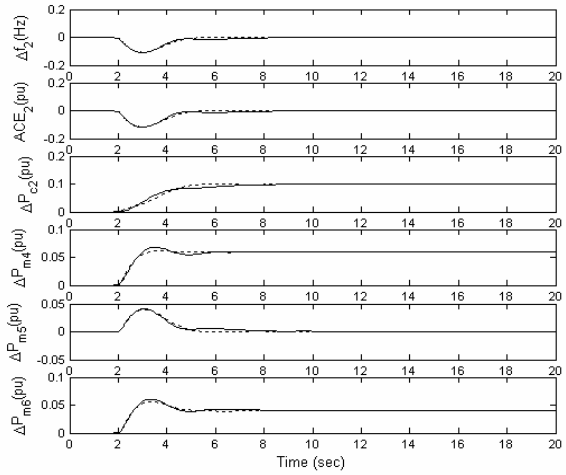

(b)

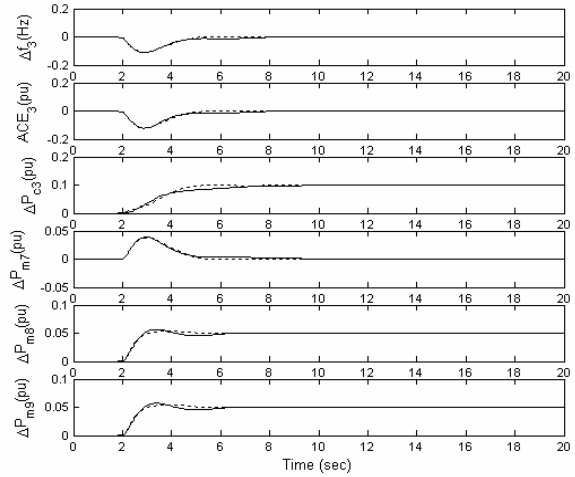

(c)

Figure 5.13: Power system response for case 1; a) Area 1, b) Area 2 and c) Area 3. Solid (ILMI-based PI controller), dotted (dynamic H_2/H_∞ controller)

The purpose of this scenario is to test the closed-loop performance against uncertainties and random large load disturbances. The power system closed-loop response is shown in Fig. 5.14b to Fig. 5.14d.

Although the applied load disturbance patterns include fast changes in amplitude, it is seen that the proposed controllers penalize the fast changes and large overshoot in the governor set-point (control action) signals ΔP_{ci}, effectively. The simulation results demonstrate that the proposed ILMI-based PI controllers track the load fluctuations and meet robustness for a wide range of load disturbances like the mixed H_2/H_∞ dynamic controllers.

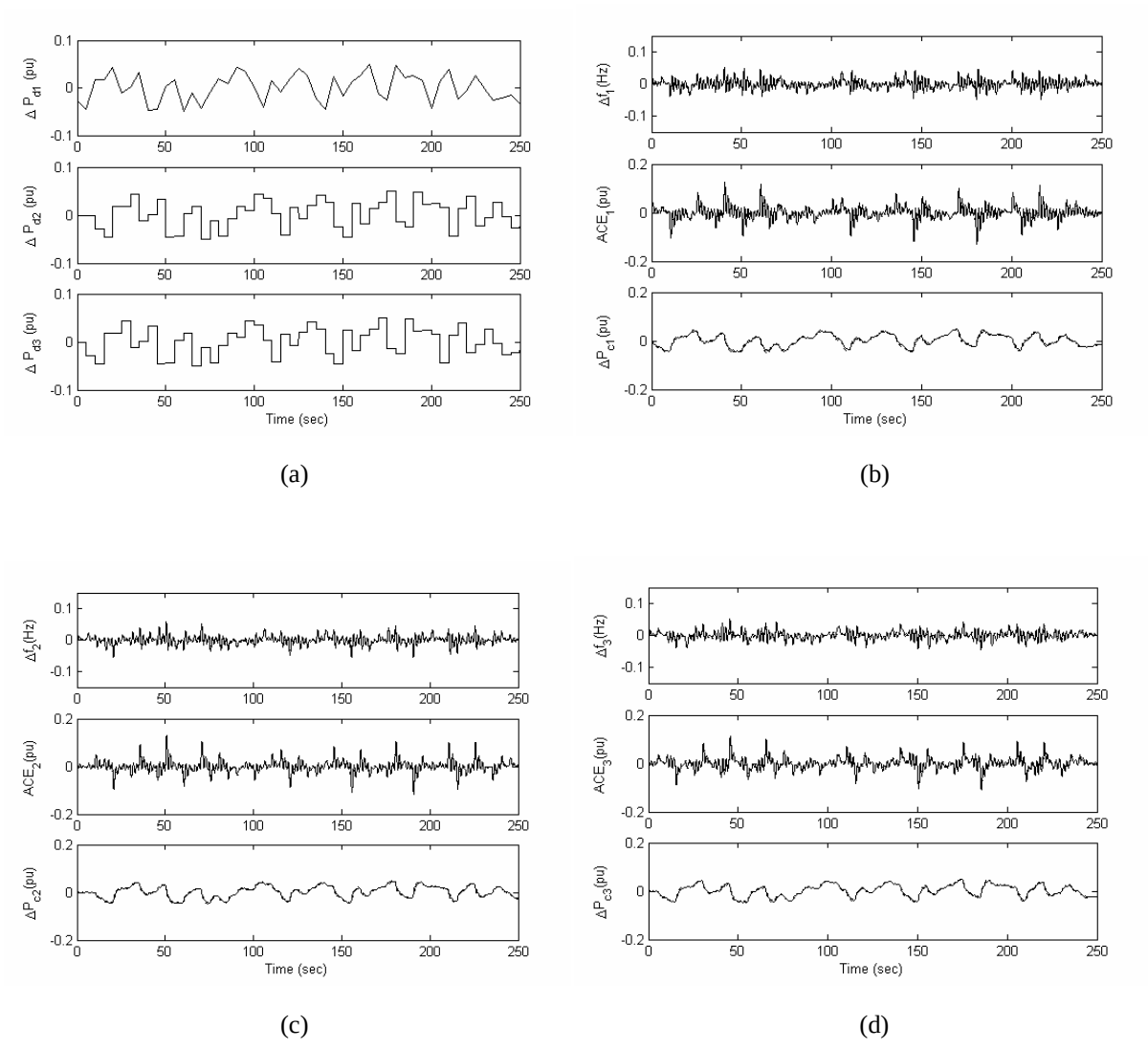

(a) (b)

(c) (d)

Figure 5.14: Power system response for case 2; a) Random load patterns, b) Area 1, c) Area 2 and d) Area 3. Solid (ILMI-based PI controller), dotted (dynamic H_2/H_∞ controller)

5.2.5 Application to a bilateral-based LFC scheme

As a second test case, the proposed control strategy is applied to a 3-control area power system with bilateral transaction given in section 4.4.2 (Fig. 4.15).

5.2.5.1 Uncertainty and performance weights selection Similar to section 5.4.2, it is assumed that the rotating mass and load pattern parameters have uncertain values in each control area. The variation range for D_i and M_i parameters in each control area is assumed $\pm 20\%$. Using the described method to determine uncertainties and performance weighting functions in previous sections, a set of suitable weights is properly chosen as follows.

$$W_1(s)=\frac{0.3986s+0.0786}{s+0.6888},\quad W_2(s)=\frac{0.3088s+0.0487}{s+0.6351},\quad W_3(s)=\frac{0.3483s+0.0751}{s+0.7826} \tag{5.30}$$

$$\eta_{1i} = 1.25,\quad \eta_{2i} = 0.001,\quad \eta_{3i} = 1.5 \tag{5.31}$$

5.2.5.2 Mixed H_2/H_∞ dynamic and SOF control design In addition to the proposed control strategy to synthesize the robust PI controller, a mixed H_2/H_∞ dynamic output feedback controller is designed for each control area, using the *hinfmix* function [4]. The resulting controllers are a dynamic type and have the same state-space form as Eq. (5.29), whose orders are the same as the size of the generalized plant model (8^{th} order in the present example).

Using the proposed ILMI approach, the control parameters for three control areas are obtained as shown in Table 5.3. The optimal performance indices for dynamic and PI controllers are listed in Table 5.4. The resulting robust performance indices of both synthesis methods (γ_{2i} and γ_{2i}^{*}) are close to each other. This shows that although the proposed ILMI approach gives a set of much simpler controllers (PI) than the dynamic H_2/H_∞ design, they also give a robust performance like the dynamic H_2/H_∞ controllers.

Table 5.3: PI control parameters from ILMI design

Parameters	*Area1*	*Area 2*	*Area 3*
k_{Pi}	-0.1250	-0.0015	-0.4278
k_{Ii}	-5.00E-04	-5.14E-04	-5.30E-04

Table 5.4: Robust performance indices

Perf. index	*Area1*	*Area 2*	*Area 3*
γ_{2i} (Dynamic)	2.1835	1.7319	2.1402
γ_{2i}^{*} (PI)	2.2900	1.8321	2.2370
$\gamma_{\infty i}$ (Dynamic)	0.4177	0.3339	0.3536
$\gamma_{\infty i}^{*}$ (PI)	0.3986	0.3088	0.3483

5.2.5.3 Simulation results The performance of the closed-loop system using the designed PI controllers in comparison of full-order H_2/H_∞ dynamic controllers is tested in the presence of load demands, disturbances, and uncertainties for the given 3-control area power system example.

Scenario 1:

In this scenario, the closed-loop performance is tested in the face of both step contracted load demand and uncertainties. It is assumed that a large load demand 100 MW (0.1 pu) is requested by each Disco, following a 20% decrease in uncertain parameters D_i and M_i. Furthermore, assume Discos contract with the available Gencos according to the following GPM,

$$GPM^T = \begin{bmatrix} 0.25 & 0.5 & 0 & 0.25 & 0 & 0 \\ 0.25 & 0 & 0.25 & 0.25 & 0.25 & 0 \\ 0 & 0 & 0.75 & 0 & 0 & 0.25 \end{bmatrix} \tag{5.32}$$

All Gencos participate in the LFC task. Gencos 2 and 6 only participate to perform the LFC in their areas, while other Gencos track the load demand in their areas and/or others. The frequency deviation, area control error (ACE 1 and ACE 2), and tie-line power changes are shown in Fig. 5.15. It is seen that the area control error and frequency deviation of all areas are driven back to zero. The tie-line power flows are properly converged to the specified values. The generated powers are shown in Fig. 5.16. The actual generated powers of Gencos reach to the desired values in the steady state as given in Table 5.5.

Table 5.5: Generated power in response to case 1

Genco	*1*	*2*	*3*	*4*	*5*	*6*
ΔP_{mi} (*pu*)	0.05	0.05	0.1	0.05	0.025	0.025

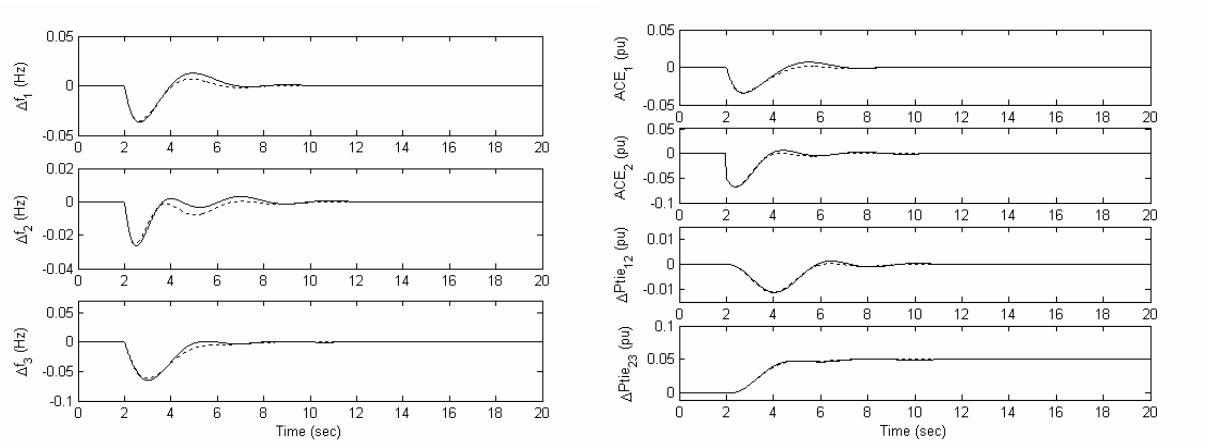

(a) (b)

Figure 5.15: a) Frequency deviation; b) area control error and tie-line powers. Solid (ILMI-based PI controller), dotted (dynamic H_2/H_∞ controller)

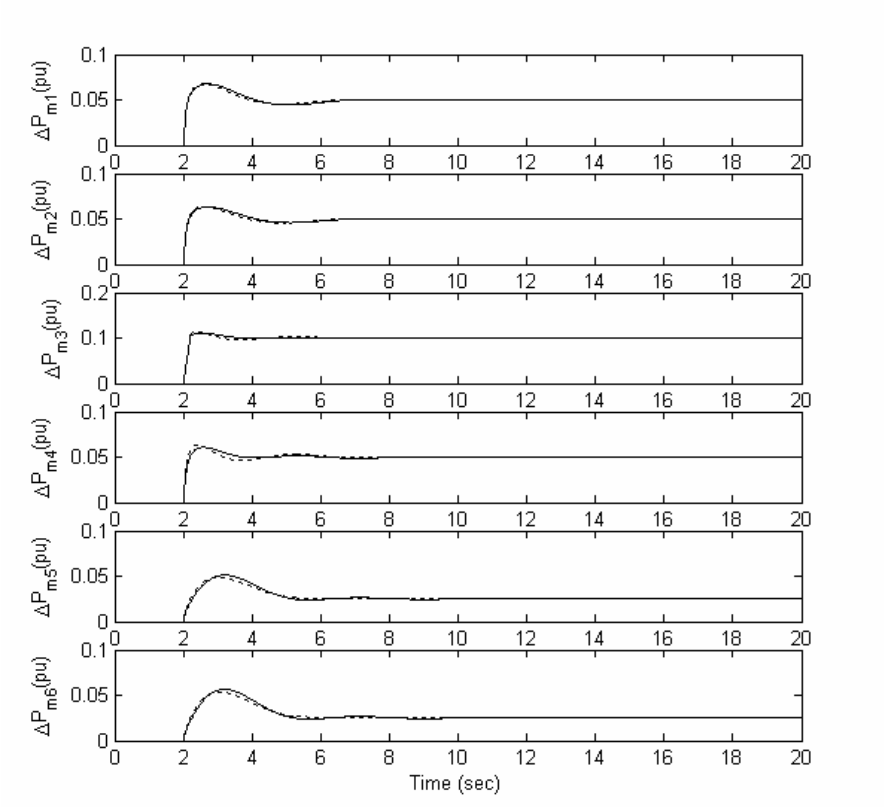

Figure 5.16: Mechanical power changes. Solid (ILMI-based PI controller), dotted (dynamic H_2/H_∞ controller)

Scenario 2:

Consider scenario 1 again. Assume, in addition to the specified contracted load demands (0.1 pu) and 20% decrease in D_i and M_i, a bounded random step load change as a large uncontracted demand (shown in Fig. 5.17a) appears in each control area, where $-50\,MW\,(-0.05\,pu) \le \Delta P_{di} \le +50\,MW\,(+0.05\,pu)$. The purpose of this scenario is to test the robustness of the proposed controllers against uncertainties and random large load disturbances. The closed-loop response for areas 1 and 3 are shown in Fig. 5.17b and Fig. 5.17c. Fig. 5.17d shows the tie-line power flows.

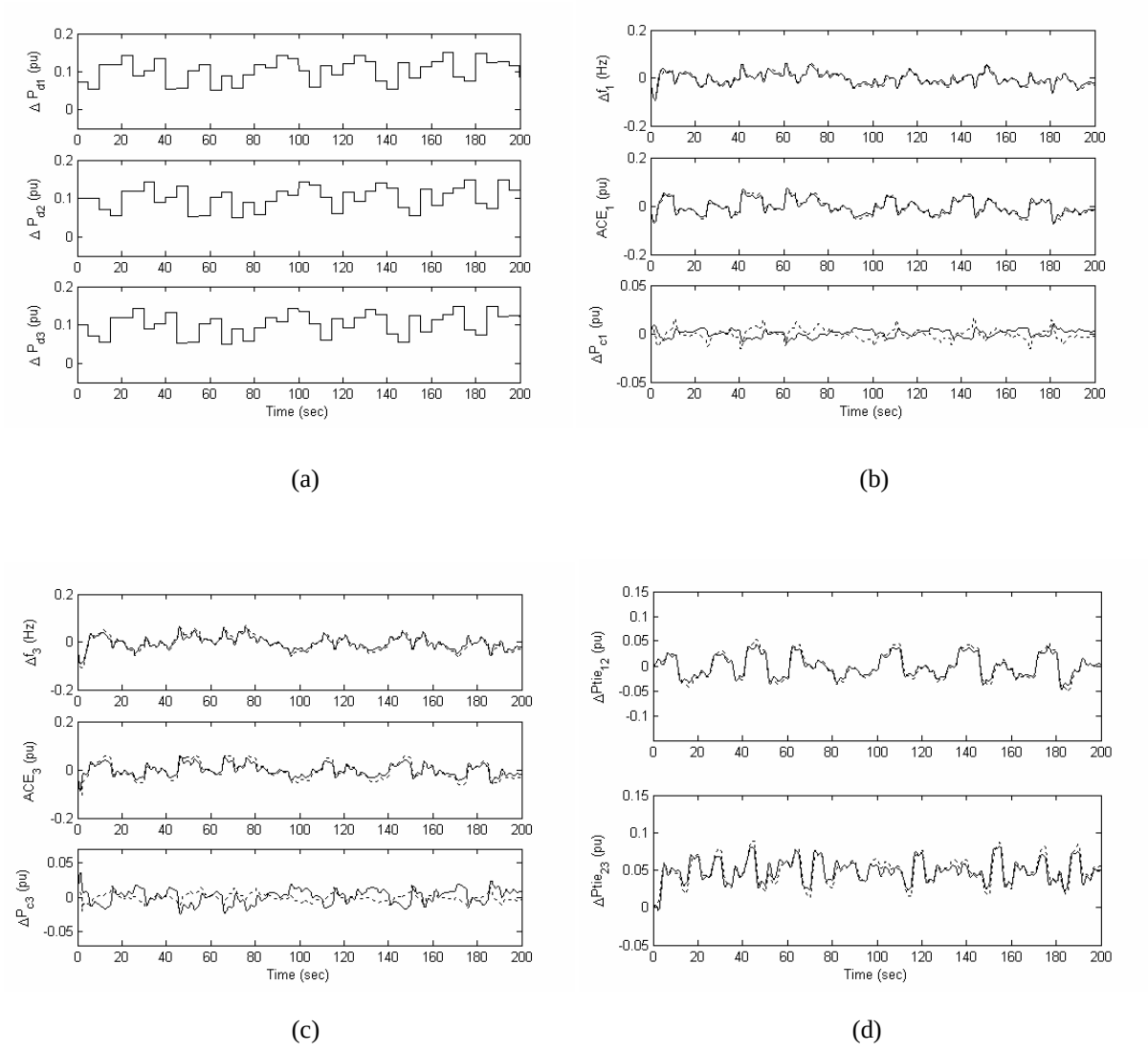

(a) (b)

(c) (d)

Figure 5.17: Power system response for case 2; (a) random load patterns b) Area-1,c) Area-3, d) tie-line powers. Solid (ILMI-based PI controller), dotted (dynamic H_2/H_∞ controller)

The simulation results demonstrate that the proposed ILMI-based PI controllers track the load fluctuations and meet robustness for a wide range of load disturbances and possible bilateral contract scenarios as well as H_2/H_∞ dynamic controllers.

5.3 Summary

In this chapter, the LFC is considered as a multi-objective control problem and a new method has been proposed for robust decentralized LFC design using the mixed H_2/H_∞ approach. In section 5.1, the proposed method was applied to a 3-control area power system and it is tested under various contract scenarios. The results are compared with the results of applied pure H_∞ controllers.

In section 5.2, an ILMI algorithm is developed to design a mixed H_2/H_∞-SOF based PI controllers. The proposed method was applied to multi-area power system examples with traditional and bilateral-based LFC schemes under serious operating conditions. The results are compared with the results of the H_2/H_∞ dynamic controllers. It was shown that the proposed simple PI controllers are capable of setting the desired level of performance under a wide range of area-load disturbances and specified uncertainties like the H_2/H_∞ dynamic controllers.

5.4 References

[1] P. P. Khargonekar, M. A. Rotea, "Mixed H_2/H_∞ control: a convex optimization approach," *IEEE Trans. Automatic Control*, vol. 39, pp. 824-837, 1991.

[2] C. W. Scherer, "Multiobjective H_2/H_∞ control," *IEEE Trans. Automatic Control*, vol. 40, pp. 1054-1062, 1995.

[3] C. W. Scherer, P. Gahinet, M. Chilali, "Multiobjective output-feedback control via LMI optimization," *IEEE Trans. Automatic Control*, vol. 42, no. 7, pp. 896-911. 1997.

[4] P. Gahinet, A. Nemirovski, A. J. Laub, M. Chilali, "LMI Control Toolbox," The MathWorks, Inc., 1995.

[5] R. E. Skelton, J. Stoustrup, T. Iwasaki, "The H_∞ control problem using static output feedback," *Int. J. of Robust and Nonlinear Control*, vol. 4, pp. 449-455, 1994.

[6] I. Yaesh, U. Shaked, "Minimum entropy static output-feedback control with an H_∞-norm performance bound," *IEEE Trans. Automatic Control*, vol. 42, no. 6, pp. 853-858, 1997.

[7] Y. Y. Cao, J. Lam, Y. X. Sun, W. J. Mao, "Static output feedback stabilization: an ILMI approach," *Automatica*, vol. 34, no. 12, pp. 1641-1645, 1998.

[8] F. Leibfritz, "An LMI-based algorithm for designing suboptimal static H_2/H_∞ output feedback controllers," *SIAM J. Control Optim.* vol. 39, no. 6, pp. 1711-1735, 2001.

[9] F. Zheng, QG. Wang, HT. Lee, "On the design of multivariable PID controllers via LMI approach," *Automatica*, vol. 38, pp. 517-526, 2002.

[10] M. Djukanovic, M. Khammash, V. Vittal, "Sequential synthesis of structured singular value based decentralized controllers in power systems," *IEEE Trans. Power Systems*, vol. 4, no. 2, pp. 635-641, 1999.

[11] H. Bevrani, Y. Mitani, K. Tsuji, "Sequential design of decentralized load-frequency controllers using μ-synthesis and analysis," *Energy Conversion & Management*, vol. 45, no. 6, pp. 865-881, 2004.

[12] P. Gahinet, M. Chilali, "H_∞-design with pole placement constraints," *IEEE Trans. Automat. Control*, vol. 41, no. 3, pp. 358-367, 1996.

[13] D. Rerkpreedapong, A. Hasanovic, A. Feliachi, "Robust load frequency control using genetic algorithms and linear matrix inequalities," *IEEE Trans. Power Systems*, vol. 18, no. 2, pp. 855-861, 2003.

Chapter 6

Conclusions

The present dissertation is mainly focused on technical issues associated with the load-frequency control (LFC) in restructured power systems and addresses new generalized dynamic models and decentralized robust control methodologies for the interconnected electric power systems with possible structures in a competitive environment.

In a deregulated environment, LFC as an ancillary service acquires a fundamental role to maintain the electrical system reliability at an adequate level. That is why there has been increasing interest for designing load frequency controllers with better performance according to the changing environment of power system operation under deregulation. In an open energy market, generation companies may or may not participate in the LFC problem. Technically, this problem will be more important as the independent power producers (IPPs) penetrate the electric power markets. Therefore, the control strategies for new structure with a number of LFC participators are not as straight as those for vertically integrated utility structure. In a control area including numerous distributed generators with an open access policy, the need arises for novel control strategies based on modified dynamical models to maintain the reliability and eliminate the frequency error.

The proposed research can be summarized in two main topics: (1) proposing generalized dynamic LFC model for LFC analysis and synthesis purposes in a deregulated environment, and (2) developing new decentralized robust load-frequency control approaches for a multi-area power system in a deregulated environment. The following points are the important outcomes of the present dissertation under the above mentioned topics:

- **Generalized LFC models for restructured power system**

Generalized dynamical models are introduced to adapt the well-tested classical LFC scheme to the changing environment of power system operation under deregulation. The main advantage of the proposed models is the use of basic concepts in the traditional framework and avoiding the use of the impractical or untested LFC schemes. It is shown that the introduced models are useful for both LFC synthesis and analysis. The details are given in Chapter 2.

- **Robust sequential decentralized LFC design**

Simultaneous design for a fixed controller structure is used in all reported decentralized LFC scenarios. This is numerically difficult for a large scale power system, and it does not provide some of the advantages that are usually the reason for using decentralized control in the first place, such as the ability to bring the system into service by closing one loop at a time, and the guarantee of stability and performance in the case of failures. In addition, some proposed methods might not work properly and do not guarantee performance, when the operating points vary.

In this work, a new systematic approach to the sequential decentralized LFC design in a multi-area power system based on the structured singular value theory (μ) is described. The sequential control design, because of its advantages, is the most common design procedure in real applications of decentralized synthesis methods. Sequential design involves closing and tuning one loop at a time. This method is less conservative than independent decentralized design, because, in each design step, one utilizes the information about the controller specified in the previous step, and it is more practical in comparison with common decentralized methods. The details are reported in Chapter 3.

- **Robust decentralized LFC design using μ-synthesis**

The μ theory is successfully used for the design of decentralized robust load frequency controller in response to new technical control demand for large scale power systems in a deregulated environment. In this approach, the power system, as a collection of different control areas, is considered under a pluralistic LFC scheme.

Each control area can buy electric power from some generation companies to supply the area-load. The control area is responsible for performing its own LFC by buying enough power from pre-specified generation companies equipped with a robust load frequency controller. The design methodology is explained in Chapter 3.

- **Robust decentralized PI-based LFC design**

In practice, LFC systems use the simple proportional-integral (PI) controllers. However, since the PI parameters are usually tuned based on classical or trial-and-error approaches, they are incapable of obtaining good dynamical performance for a wide range of operating conditions and various scenarios in a deregulated environment. Regarding this problem, LFC synthesis is formulated as a robust static output feedback (SOF)

control problem and is solved using a developed iterative linear matrix inequalities (ILMI) algorithm to the design of robust PI controllers in restructured control areas. The details are reported in Chapters 4 and 5.

- **Multi-objective control based robust decentralized LFC synthesis**

The LFC goals, i.e., frequency regulation and tracking the load changes, maintaining the tie-line power interchanges to specified values in the presence of generation constraints and model uncertainties, identifies the LFC synthesis as a multi-objective control problem. On the other hand, the low-order and proportional-integral based load-frequency controllers which are usually used in real-world power systems and tuned based on classical or trial-and-error approaches, are incapable of obtaining good dynamical performance to meet all specified objectives. In this work, to cover the above aspects, the LFC is formulated to a multi-objective control problem via a mixed H_2/H_∞ control technique. The model uncertainty in each control area is covered by an unstructured multiplicative uncertainty block. A standard model reduction method is used to provide the low-order robust load-frequency controllers. In order to design a robust PI controller, the control problem is reduced to a SOF control synthesis. Finally, it is easily carried out using a developed ILMI algorithm. The results are compared with the pure H_∞ and mixed H_2/H_∞ dynamic control designs. The methodology is explained in Chapter 5.

In response to new technical demands in load-frequency control area, the present dissertation addresses several useful modeling and control methodologies. The following points can be suggested to continue this research:

1. Implement the proposed load-frequency controllers for the real-world power systems.
2. Develop a more complete LFC model to couple system dynamics, deregulation policies, economical issues, and the other variables of interest for both analysis and synthesis purposes.
3. Generalize the study to other aspects of power system control with regard to new uncertainties in the liberalized electricity markets, and coupling between performance objectives and market dynamics to obtain a good trade off between efficiency and robustness.

Publications

1. In transactions and journals

[1] H. Bevrani, Y. Mitani, K. Tsuji, "Sequential design of decentralized load-frequency controllers using μ-synthesis and analysis," *Energy Conversion & Management*, vol. 45, no. 6, pp. 865-881, Feb. 2004.

[2] H. Bevrani, Y. Mitani, K. Tsuji, "On robust load-frequency regulation in a restructured power system," *IEEJ Trans. on Power and Energy*, vol. 124, no. 2, pp. 190-198, Feb. 2004.

[3] H. Bevrani, Y. Mitani, K. Tsuji, "Robust AGC: Traditional structure versus restructured scheme," *IEEJ Trans. on Power and Energy*, vol. 124, no. 5, pp. 751-761, May 2004.

[4] H. Bevrani, Y. Mitani, K. Tsuji, "Robust decentralized AGC in a restructured power system," *Energy Conversion & Management*, vol. 45, no. 15-16, pp. 2297-2312, June 2004.

[5] H. Bevrani, T. Ise, Y. Mitani, K. Tsuji, "A robust approach to controller design for DC-DC quasi-resonant converters," *IEEJ Trans. on Industry Applications*, vol. 124, no. 1, pp. 91-100, Jan. 2004.

[6] H. Bevrani, Y. Mitani, K. Tsuji, "Robust decentralized load-frequency control using an iterative linear matrix inequalities algorithm," *IEE Proc. Generation, Transmission and Distribution*, vol. 151, no. 3, pp. 347-354, May 2004.

[7] H. Bevrani, Y. Mitani, K. Tsuji, H. Bevrani, "Bilateral-based robust load-frequency control," Accepted to publish in *Energy Conversion & Management*.

[8] H. Bevrani, Y. Mitani, K. Tsuji, "Robust LFC in a deregulated environment: multi-objective control approch," Accepted to publish in *IEEJ Trans. on Power and Energy*.

2. In proceedings of international and domestic conferences

[9] H. Bevrani, Y. Mitani, K. Tsuji, "Robust decentralized LFC design in a deregulation environment," In Proc. of *2nd Int. Conf. on Electric Utility Deregulation, Restructuring and Power Technologies-DRPT*, CD ROM, Hong Kong, April 2004.

[10] H. Bevrani, T. Ise, Y. Mitani, K. Tsuji, "DC-DC quasi-resonant converters: Linear robust control," In Proc. of *IEEE Int. Symposium on Industrial Electronics (ISIE 2004)*, vol. 2, pp. 863-868, Ajaccio, France, May 2004.

[11] H. Bevrani, Y. Mitani, K. Tsuji, "An LFC model for competitive power system markets," In Proc. of *2004 National Convention Record IEE Japan*, vol. 6, pp. 39-40, Yokohama, Japan, March 2004.

[12] H. Bevrani, Y. Mitani, K. Tsuji, "Robust LFC design using mixed H2/Hinf technique," In Proc. of *Int. Conf. on Electrical Eng.* (ICEE), vol. 2, pp. 172-177, Sapporo, Japan, July 2004.

[13] H. Bevrani, Y. Mitani, K. Tsuji, "PI-based multi-objective load-frequency control in a restructured Power System," To be published in Proc. of *SICE Annual Conference*, Sapporo, Japan, Aug. 2004.

[14] H. Bevrani, Y. Mitani, K. Tsuji, "Decentralized robust load-frequency control: A PI-based approach," In Proc. of *Int. Conf. on Electrical Eng. (ICEE)*, vil. 2, pp. 166-171, Sapporo, Japan, July 2004.

[15] H. Bevrani, Y. Mitani, K. Tsuji, "Robust LFC in a deregulated environment: Multi-objective control approach," To be published in Proc. of *Annual Conf. of Power & Energy Society*, Nagoya, Japan, Aug. 2004.

[16] H. Bevrani, Y. Mitani, K. Tsuji, "Robust AGC in a competitive environment," To be published in Proc. of *39th Int. Univ. Power Eng. Conf (UPEC)*, Bristol, UK, Sept. 2004.

[17] H. Bevrani, Y. Mitani, K. Tsuji, "Sequential decentralized design of load frequency controllers in multiarea power systems," In Proc. of *IFAC Symposium on Power Plants and Power Systems Control*, vol. 1, pp. 65-70, Seoul, Korea, Sep. 2003.

[18] H. Bevrani, Y. Mitani, K. Tsuji, "A scenario on load-frequency controller design in a deregulated power system," In Proc. of *SICE Annual Conference*, pp. 144-149, Fukui, Japan, Aug. 2003.

[19] H. Bevrani, Y. Mitani, K. Tsuji, "On robust load frequency regulation in a new multi-machine power system structure," In Proc. of *2003 National Convention Record IEE Japan*, vol. 6, pp. 288-289, Sendai, Japan, March 2003.

[20] H. Bevrani, Y. Mitani, K. Tsuji, "On robust load-frequency regulation in a restructured power system," In Proc. of *Annual Conf. of Power & Energy Society*, vol. A, pp. 14-19, Tokyo, Japan, Aug. 2003.

[21] H. Bevrani, Y. Mitani, K. Tsuji, "Robust load frequency regulation in a new distributed generation environment," In Proc. of *IEEE-PES General Meeting*, CD ROM, Toronto, Canada, July 2003.

[22] H. Bevrani, "A novel approach for power system load frequency controller design," In Proc. of *IEEE/PES T&D 2002 Asia Pacific*, vol. 1, pp. 184-189, Yokohama, Japan, 2002.

[23] H. Bevrani, Y. Mitani, K. Tsuji, "Robust control design for a ZCS converter," In Proc. of *28th Annual Conf. of the IEEE Industrial Electronics Society (IECON)*, Spain, Nov. 2002.

[24] H. Bevrani, T. Ise, Y. Mitani, K. Tsuji, "Robust controller design for a DC-DC ZCS converter using μ-synthesis and analysis," In Proc. of *IEEJ Technical Meeting*, IPC-02-96/IEA-02-37, pp. 111-116, Nagona, Japan, Nov. 2002.

[25] H. Bevrani, Y. Mitani, K. Tsuji, "Robust low-order load frequency controller in a deregulated environment," In Proc. of *5th Asia-Pacific Conf. on Control and Measurement (APC CM)*, Dali, China, July 2002.

Publications

I) Journal Papers

[1] Bevrani, Hassan and Hiyama, Takashi and Mitani, Yasunori and Tsuji, Kiichiro and Teshnehlab, Mohammad (2006) Load-frequency regulation under a bilateral LFC scheme using flexible neural networks. *Engineering Intelligent Systems* 14(2):pp. 109-117.

[2] Bevrani, Hassan and Mitani, Yasunori and Tsuji, Kiichiro and Bevrani, Hossein (2005) Bilateral based robust load frequency control. *Energy Conversion and Management* 46(7-8):pp. 1129-1146.

[3] Bevrani, Hassan and Mitani, Yasunori and Tsuji, Kiichiro (2004) Robust decentralized load-frequency control using an iterative linear matrix inequalities algorithm. *IEE Proceedings - Generation, Transmission and Distribution* 151(3):pp. 347-354.

[4] Bevrani, Hassan and Ise, Toshifumi and Mitani, Yasunori and Tsuji, Kiichiro (2004) A robust approach to controller design for DC-DC quasi-resonant converters . *IEEJ Transactions on Industry Applications* 124(5):pp. 91-100.

[5] Bevrani, Hassan and Mitani, Yasunori and Tsuji, Kiichiro (2004) Sequential design of decentralized load frequency controllers using mu synthesis and analysis. *Energy Conversion & Management* 45(6):pp. 865-881.

[6] Bevrani, Hassan and Mitani, Yasunori and Tsuji, Kiichiro (2004) Robust decentralized AGC in a restructured power system. *Energy Conversion and Management* 45(15-16):pp. 2297-2312.

[7] Bevrani, Hassan and Mitani, Yasunori and Tsuji, Kiichiro (2004) On robust load-frequency regulation in a restructured power system. *IEEJ Transactions on Power and Energy* 124(2):pp. 190-198.

[8] Bevrani, Hassan and Mitani, Yasunori and Tsuji, Kiichiro (2004) Robust AGC: Traditional structure versus restructured scheme. *IEEJ Transactions on Power and Energy* 124(5):pp. 751-761.

[9] Bevrani, Hassan and Mitani, Yasunori and Tsuji, Kiichiro (2004) LFC in a deregulated environment: Multi-objective control approach. *IEEJ Transactions on Power and Energy* 124(12):pp. 1409-1416.

II) Conference Papers

[10] Bevrani, Hassan and Hiyama, Takashi and Mitani, Yasunori and Tsuji, Kiichiro (2005) A bridge between robustness and simplicity: practical control design for complex systems. In *Proceedings 1st ASIJ Scientific Seminar*, Tokyo, Japan.

[11] Bevrani, Hassan and Hiyama, Takashi (2005) Bilateral-based LFC analysis using a modified conventional model. In *Proceedings 13th Iranian Conference on Electrical Engineering (ICEE)*, Zanjan, Iran.

[12] Bevrani, Hassan and Hiyama, Takashi (2005) On market-based robust load-frequency control. In *Proceedings 20th International Power System Conference (PSC)*, Tehran, Iran.

[13] Bevrani, Hassan and Ise, Toshifumi and Mitani, Yasunori and Tsuji, Kiichiro (2004) DC-DC Quasi-Resonant Converters: Linear Robust Control. In *Proceedings 2004 IEEE International Symposium on Industrial Electronics (ISIE 2004)* 2, pages pp. 863-868, France.

[14] Bevrani, Hassan and Mitani, Yasunori and Tsuji, Kiichiro (2004) PI-based multi-objective load-frequency control in a restructured power system. In *Proceedings SICE 2004 Annual Conference* 2, pages pp. 1745-1750, Japan.

[15] Bevrani, Hassan and Mitani, Yasunori and Tsuji, Kiichiro (2004) Robust Decentralized LFC Design In a Deregulated Environment. In *Proceedings 2004 IEEE International Conference on Electric Utility Deregulation, Restructuring and Power Technologies, 2004. (DRPT 2004)*, pages pp. 326-331, Hong Kong.

[16] Bevrani, Hassan and Mitani, Yasunori and Tsuji, Kiichiro (2004) Robust AGC in a competitive environment. In *Proceedings 39th Universities Power Engineering Conference-UPEC 2004* 2, pages pp. 722-726, UK.

[17] Bevrani, Hassan and Mitani, Yasunori and Tsuji, Kiichiro (2004) An LFC model for competitive power system markets. In *Proceedings National Convention Record IEE Japan 2004* 6, pages pp. 39-40, Yokohama, Japan.

[18] Bevrani, Hassan and Mitani, Yasunori and Tsuji, Kiichiro (2004) Robust LFC design using mixed H2/Hinf technique. In *Proceedings International Conference on Electrical Engineering (ICEE) 2004*, Sapporo, Japan.

[19] Bevrani, Hassan and Mitani, Yasunori and Tsuji, Kiichiro (2004) Decentralized robust load-frequency control: A PI-based approach. In *Proceedings International Conference on Electrical Engineering (ICEE) 2004*, Sapporo, Japan.

[20] Bevrani, Hassan and Mitani, Yasunori and Tsuji, Kiichiro (2004) Robust LFC in a deregulated environment: Multi-objective control approach. In *Proceedings Annual Conference of Power & Energy Society 2004*, pages pp. 11-16, Nagoya.

[21] Bevrani, Hassan and Mitani, Yasunori and Tsuji, Kiichiro (2003) Robust Load Frequency Regulation In a New Distributed Generation Environment. In *Proceedings IEEE Power Engineering Society General Meeting, 2003* 2, Toronto, Canada.

[22] Bevrani, Hassan and Mitani, Yasunori and Tsuji, Kiichiro (2003) A scenario on load-frequency controller design in a deregulated power system . In *Proceedings SICE 2003 Annual Conference* 3, pages pp. 3148-3153, Fukui, Japan.

[23] Bevrani, Hassan and Mitani, Yasunori and Tsuji, Kiichiro (2003) Sequential decentralized design of load frequency controllers in multiarea power systems. In *Proceedings 2003 IFAC Symposium on Power Plants and Power Systems Control* 1, pages pp. 65-70, Korea.

[24 Bevrani, Hassan and Mitani, Yasunori and Tsuji, Kiichiro (2003) On robust load frequency regulation in a new multi-machine power system structure. In *Proceedings 2003 National Convention Record IEE Japan* 6, pages pp. 2888-289, Sendai, Japan.

[25] Bevrani, Hassan and Mitani, Yasunori and Tsuji, Kiichiro (2003) On robust load-frequency regulation in a restructured power system. In *Proceedings 2003 IEEJ Annual Conference of Power & Energy Society* A, pages pp. 14-16, Japan.

[26] Bevrani, Hassan and Mitani, Yasunori and Tsuji, Kiichiro (2002) Robust Control Design for a ZCS Converter. In *Proceedings 28th Annual Conference of the Industrial Electronics Society (IECON 02),* pages pp. 609-614, Spain.

[27] Bevrani, Hassan and Mitani, Yasunori and Tsuji, Kiichiro (2002) Robust low-order load frequency controller in a deregulated environment. In *Proceedings 5th Asia-Pacific Conference on Control and Measurement (APCCM),* Dali, China.

[28] Bevrani, Hassan and Ise, Toshifumi and Mitani, Yasunori and Tsuji, Kiichiro (2002) Robust controller design for a DC-DC ZCS converter using μ-synthesis and analysis. In *Proceedings 2002 IEEJ Technical Meeting* SPC-02-96/IEA-02-37, pages pp. 111-116, Nagona, Japan.

[29] Bevrani, Hassan and Mitani, Yasunori and Tsuji, Kiichiro (2002) Sequential decentralized design of robust load frequency controllers in a multi-area power system. In *Proceedings Universities Student Meeting,* Awaji Island, Japan.